UNIVERSITY OF CAPE TOWN

AMBIENT VIBRATION TESTING OF CONCRETE DAMS

By

BUKENYA PATRICK

Submitted in partial fulfillment of the requirements for the degree

MSc Eng

in the

DEPARTMENT OF CIVIL ENGINEERING

FACULTY OF ENGINEERING AND THE BUILT ENVIRONMENT

Supervisor: A/Prof Pilate Moyo

Co-Supervisor: Dr. Hans Beushausen

DECLARATION

I know the meaning of plagiarism and declare that work in this document is may own otherwise references have been made. I also affirm that this work has not been submitted in this or any other university for examination or for any other purposes.

Signature……

Date……..

DEDICATION

This work is dedicated to my mother Ms Nakidde Regina (RIP), you are the reason why I have come this far

ACKNOWLEDGEMENTS

This thesis has been completed under the supervision of A/Prof Pilate Moyo and Dr Hans Beushausen both of the University of Cape Town. I express my gratitude to A/Prof Moyo for his valuable advice, interest, and encouragement throughout this project. My co-supervisor Dr Beushausen is specially acknowledged for the advice given to me during the thesis write-up. I also thank Prof. Chris Oosthuizen from Department of Water Affairs for his insightful advice and support.

This project made possible by funding from the Water Research Commission (WRC) of South Africa and support from the Department of Water Affairs for which I am grateful.

The author wishes to acknowledge the opportunity granted to him by the Concrete Materials and Structural Integrity Research Unit (CoMSIRU) to do research under their group.

The author is also grateful to the following people for their constructive ideas throughout the study: Dr. Denis Kalumba for the encouragement and prayers; Ms Elly Yelverton for the motherly support she has always provided; Tony Meri and Mike Otieno for all the things you have done for me.

May God bless you all

Kulwa Katonda ne Ensi yange

ABSTRACT

The dynamic behavior of civil engineering infrastructure is an essential factor in determining their structural stability, life span and reliability. Therefore, in many engineering applications it has become an important issue to identify dynamic characteristics of such structures and also monitor the structure in operation. Operational Modal Analysis (OMA) is a procedure which allows for the extraction of modal parameters of a structure in service.

There are different modal parameter estimation techniques that have been developed for the last 20 years in operational modal analysis either in the time domain, frequency domain or time-frequency domain. The effectiveness of these techniques has been studied on flexible structures such as bridges, building and but not on rigid structures like concrete dams. The objective of this study is to fill the gap by studying the performance of different OMA techniques when applied to ambient test data from two concrete arch dams.

In this thesis, seven techniques namely; rational fractional polynomial, complex exponential, frequency domain decomposition (FDD) based techniques which include; frequency domain decomposition (FDD), enhanced frequency domain decomposition (EFDD), curve fitting frequency domain decomposition (CFDD) and stochastic subspace identification (SSI) methods namely; unweighted principal component (UPC), principal component (PC) and canonical variant analysis (CVA)) have been applied to data from ambient vibration testing of two concrete dams namely; Roode Elsberg and Kouga dams. Using commercial software, i.e. ME'Scope Ves 5.0 and ARTeMIS Extractor 2010, modal parameters from ambient data of the two dams were extracted. Using MS Excel, analysis of variance of the data was done to find out if there were any differences in the natural frequencies determined by the different methods.

Six modes of natural frequencies between 3.7 and 8.9 Hz were determined from Kouga dam with frequency domain decomposition based procedures estimating all the modes. Rational fractional polynomial method and complex exponential method did not pick mode 3 while the stochastic subspace based procedures did not pick modes 3 and 6. Five modes ranging in the natural frequencies of 3.38 and 8.6 Hz for Roode Elsberg dam were estimated with rational fractional

polynomial method and complex exponential method not picking mode 2. Stochastic subspace based procedures did not pick mode 4 and 6. The modes which were not picked up by SSI based methods were weak modes and did not appear in all measurements (local modes).

Using Kurtosis and Short time Fourier transform, it was observed that there were no harmonics on the dams during the time of testing

Using MS Excel, analysis of variance showed with a P value of 0.979 that there were no significant differences between the natural frequencies of the modes which were detected by all techniques for Kouga dam.

A comparative study between the natural frequencies obtained from the different methods and finite element (FE) model of Roode Elsberg dam indicates that FDD- based methods perform better than the rest of the methods that have been used in this piece of work. This is because they correlated well with all the modes from the FE- model.

NOMENCLATURE

Acronyms

AF- Poly	**A**lias **F**ree **P**olynomial
ARMA	**A**uto **R**egressive **M**oving **A**verage
ARTeMIS	**A**mbient **R**esponse-**T**esting and **M**odal **I**dentification **S**oftware
AVT	**A**mbient **V**ibration **T**esting
CFDD	**C**urve **F**itting **F**requency **D**omain **D**ecomposition
EFDD	**E**nhanced **F**requency **D**omain **D**ecomposition
EMA	**E**xperimental **M**odal **A**nalysis
ERA	**E**igensystem **R**ealization **A**lgorithm
FDD	**F**requency **D**omain **D**ecomposition
FFT	**F**ast **F**ourier **T**ransform
FVT	**F**orced **V**ibration **T**esting
IRF	**I**mpulse **R**esponse **F**unction
LSCE	**L**east **S**quares **C**omplex **E**xponential
MAC	**M**odal **A**ssurance **C**riterion
MDOF	**M**ultiple **D**egrees **O**f **F**reedom
MIMO	**M**ulti **I**nput **M**ulti **O**utput
OMA	**O**perational **M**odal **A**nalysis

PDF	**P**robability **D**ensity **F**unction
PP	**P**eak **P**icking
PSD	**P**ower **S**pectral **D**ensity
RFP	**R**ational **F**ractional **P**olynomial
SDOF	**S**ingle **D**egree **O**f **F**reedom
SIMO	**S**ingle **I**nput **M**ulti **O**utput
SSI	**S**tochastic **S**ubspace **I**dentification
SVD	**S**ingular **V**alue **D**ecomposition

TABLE OF CONTENTS

LIST OF FIGURES

LIST OF TABLES

1 INTRODUCTION

1.1 Background

Identification of the global dynamic properties of civil engineering structures using vibration responses is a necessary pre-requisite in several types of analyses including, model updating and structural health monitoring, detecting and locating possible damage in structures and the safety evaluation of structures against severe events like earthquakes, wind load (Wei-Xin and Zong, 2004). In addition, the design of complaint structures which have become increasingly lighter, more flexible and yet strong, the increasing demands of safety defined by the government regulations especially where dynamic loads are involved have created new challenges to the scientific understanding of the behavior of engineering structures subjected to vibrations.

Dynamic properties offer an in-depth understanding of the structural behavior and performances of structures. These dynamic properties, also known as modal parameters (natural frequencies, mode shapes and damping ratios) are determined by a process called modal analysis. Modal analysis refers to the study of the dynamic characteristics or modal parameters of a structure under vibration. It simplifies the vibration response of a complex structure by reducing the data to a set of modal parameters that can be analyzed. Furthermore, the set of modal parameters are used to characterize the structural properties (mass and stiffness) of a structure. Under modal analysis, there are two ways of estimating modal parameters, i.e. analytical and experimental methods. In the analytical modal analysis, a finite element model of the structure is developed, and then modal analysis is performed to obtain the dynamic characteristics. However, the dynamic properties obtained analytically are not exactly true because of the uncertainties in design parameters such as material properties and boundary conditions. This makes the experimental method an alternative option where measurable or immeasurable input forces vibrate the structures and then modal parameters can be obtained from the structural responses. In literature, the experimental method is also known as modal testing (Ewins, 1984).

Modal testing is divided into two methods available in the identification of dynamic properties of structures. These methods include; experimental modal analysis and operational modal analysis (He and Fu, 2001).

Experimental modal analysis (EMA) is a conventional or traditional way of doing modal analysis where the structure is excited by one or several measured forces and then responses at selected positions on the structure are recorded. There are a number of methods of applying artificial excitations using equipments such as servo hydraulic shaker (Figure. 1.1) and eccentric mass vibrators (Figure. 1.2). For small structures that can be tested in the laboratory, or larger structures such as short span bridges that can be excited artificially without significant problems, this approach should be preferred as these structures can be easily excited.

Figure 1.1: Servo-hydraulic shaker (Cantieni, 2004)

Figure 1.2: Eccentric mass vibrator (Cunha et al, 2006)

In case of very large structures such as concrete dams, EMA is often difficult to implement as it might be difficult to artificially excite the structure to a level where the response from the background loading like wind or other non-controllable loading is small compared to the response from artificial loading. Even in cases where it is possible to vibrate such large structures, problems may arise from non-linearity introduced by exciting the structure to a higher response level. EMA is also an expensive method to conduct, for example the cost of hiring mechanical exciters and the personnel to operate the equipment can raise the overall budget by approximately 50 per cent (Danielle and Taylor, 1999).

Thus, to avoid such expenses and non-linearity problems, the solution is to measure responses while the structure is in operation. The methodology which utilizes natural responses or ambient responses in determining modal parameters is known as operational modal analysis or ambient vibration testing. The information obtained from these responses is the same as that obtained from by experimental modal analysis (Duron et al, 2007). Instead of loading the structure artificially and dealing with the natural loading as unwanted noise source, the natural loading is used as the loading source. Also, as it is hard to simulate the real operating conditions during laboratory modal tests, the need to identify modal models under operational conditions often arises.

Ambient vibration testing (Luz, 1991) is a vibration testing and analysis technique targeted towards large civil engineering structures such as concrete dams. This method requires no artificial excitation to be used on the structure being tested. It relies on the ambient and operating forces on the structure at the time of testing. Ambient vibration testing gained popularity since 1990 due to some of its advantages as compared to EMA (Zhang et al., 2005). These advantages include:

i). Relatively cheap and fast to conduct as no elaborate excitation equipment and boundary condition simulation are needed.

ii). The model characteristics under real loading are linearlized due to broad band random excitation.

iii). All or part of the measurement coordinates can be used as references making the identification algorithm a MIMO-type. As a result, closed-spaced or even repeated modes can easily be handled making OMA suitable for complex civil engineering structures.

iv). Operational modal identification with output-only measurements can be utilized not only for dynamic design, structural control, but also for vibration based health monitoring and damage detection of the structures.

Recent experiences with ambient vibration testing on large concrete dams have shown that excellent agreement can be achieved with forced vibration test results. For example, dynamic testing conducted on Folsom Dam in California, United States of America (Duron et al., 2005), a large concrete gravity Dam, reported results in which ambient and forced derived resonances matched to within 4%. Furthermore, tests conducted on Big Creek Dam in the United States of America (Scheulen et al., 2009) indicated a match between ambient and forced vibration results of within 6%. Comparisons of corresponding response shapes have also indicated good agreement. The ambient vibration testing of Folsom Dam, Big Creek Dam and San Vicente Dam (Duron et al, 2007) suggest that ambient vibration testing is a viable option for identifying dynamic response and behavior of dams. The justification and technology exists for ambient vibration testing and analysis of dams. Therefore, ambient vibration analysis method presents a potentially inexpensive form for this thesis.

In the last two decades, a number of modal parameter estimation techniques classified into time domain, frequency domain and time-frequency domain have been developed by several researchers in the field of ambient vibration testing. The performance of these techniques which use output only responses have been studied and their applications to civil engineering structures such as bridges have been published. Lew et al. (1993) compared the techniques derived from the eigenvalue realization algorithm (ERA) for flexible structures, Brinker et al. (1996) presented a first comparison of different techniques using ambient data from bridges, He et al. (2006) made a comparative study of system identification. Other comparative studies have been published by Kinkegaard and Andersen (1997), Abdeghani et al. (1998) and Peeters and Ventura (2003). The knowledge of the relative advantages and disadvantages of each of these modal parameter estimation techniques as applied to concrete dams remains limited and therefore there is a need to explore them.

1.2 Problem statement

Modal analysis is a method for obtaining the actual dynamic properties of a structure. These dynamic properties or modal parameters consist of natural frequencies, mode shapes and damping ratios. The natural frequencies of a structure are directly related to the stiffness and mass of the structure while the mode shapes are related to deflected shape. Modal analysis can be done experimentally either by exciting the structure with mechanical means such as shakers or by use of ambient forces such as wind.

Dams are large civil engineering structures difficult to excite mechanically and even when it is possible, the costs involved are high. Ambient vibration testing provides an effective and economic means of identification of modal parameters of dams. This is because it has the advantages of being relatively inexpensive and testing the structure in its operating conditions.

The main challenge in operational modal analysis has been extracting modal parameters from ambient test data of dams. Different researchers have developed techniques which are being used in modal parameter identification. There are three main categories of output-only modal identification methods namely, non-parametric methods developed in frequency domain, parametric methods in time domain and wavelet transform in time-frequency domain. In ambient vibration testing of dams, literature suggests that frequency domain techniques have been mostly used in ambient tests of concrete dams in determining the dynamic properties of dams such as

Claewern dam in the United Kingdom (Danielle and Taylor, 1999), the arch dam of Mauvoisin in Switzerland (Darbre and Proulx, 2002), Hitotsuse arch dam in Japan (Okuma et al., 2008), Cabril dam in Portugal (Mendes and Oliviera, 2009) and Kouga dam in South Africa (Moyo and Oosthuizen, 2010). Modal parameter identification techniques such as stochastic subspace identification, frequency domain decomposition, enhanced frequency domain decomposition, curve fitting frequency domain decomposition, rational fraction polynomial and complex exponential have been developed over the last decade for the extraction of modal parameters in ambient vibration testing of civil engineering structures. These techniques, however, have been conventionally used in the extraction of modal parameters from ambient vibration tests of flexible structures such as bridges (Peeters and Ventura, 2003, Siringoringo and Fujino, 2008 and Brownjohn et al. 2010) and buildings (Giraldo et al., 2009, Ren and Zong 2004, Brownjohn 2003). Therefore, there is a need to study the performance of these techniques for the identification of the dynamic properties of concrete dams since dams are stiff structures and behave differently from bridges and buildings.

1.3 Objective

The purpose of this research described herein is to study the performance of seven different estimation techniques using operational data obtained from an ambient vibration test of Roode Elsberg and Kouga dams in the Western Cape Province, South Africa.

1.4 Scope

The scope of this work is as follows:

i). Conduct a critical literature review to determine the state of the art of ambient vibration testing of concrete dams and operational modal analysis techniques used to extra modal parameters.

ii). Obtain modal parameters using the following techniques, namely; stochastic subspace identification, frequency domain decomposition, enhanced frequency domain decomposition, curve fitting frequency domain decomposition, rational fraction polynomial and complex exponential.

iii). Carry out an analysis of variance on the natural frequencies obtained from the different modal parameter techniques to find out if there is a significant difference between them.

iv). Provide a recommendation as to which method or combination of methods is suitable for testing concrete arch dams.

1.5 Thesis structure

Chapter 1

The chapter introduces the concept of modal analysis and the different types of modal analysis namely experimental modal analysis and operational modal analysis. It concentrates more on operational modal analysis giving its advantages as compared to experimental modal analysis and a brief overview of the modal parameter estimation techniques is also presented. Research needs in operational modal analysis in concrete dams are discussed; problem statement and objectives are defined. Scope of the proposed study is also form part of this chapter.

Chapter 2

This chapter reviews ambient vibration testing of concrete dams, reasons for carrying out these tests on the reviewed case studies are presented and the modal parameter estimation techniques that were used to analyze the response data obtained from the tests are also reported.

Chapter 3

This chapter describes modal parameter estimation techniques in operational modal analysis which are used in the analysis of data obtained from ambient vibration tests. Different modal parameter identification algorithms are presented while addressing their advantages, disadvantages and applications.

Chapter 4

Practical issues in operational modal analysis are discussed in this chapter. These issues include instrumentation, i.e. the kind of equipment to be used while conducting ambient vibration tests and how they affect the overall results if not used properly. Data preprocessing also known as

signal processing before extraction of modal parameters and harmonics are the other issues that are thoroughly discussed in this chapter.

Chapter 5

The methodology of this thesis is reported in chapter 5. This details the experimental work to be done which included ambient vibration testing of Roode Elsberg and Kouga dams and describes of the equipment used in the field tests. The procedures of extraction of modal parameters from raw data using ARTeMIS Extractor Pro 2010 and ME' Scope ves 5.1 are described in detail. Analysis of variance analysis process for comparing natural frequencies across all the methods is described. Modal assurance criterion used for comparing mode shapes is also presented. Lastly, the validation process of the estimation methods is done by comparing results from FEM model of Roode Elsberg dam and experimental results.

Chapter 6

The findings of this research are reported in this chapter. Discussion and analysis of experimental results is done.

Chapter 7

This concludes which methods perform best in extracting modal parameters from ambient data of dams. Recommendations for future work are presented.

2 REVIEW OF AMBIENT VIBRATION TESTS IN CONCRETE DAMS

2.1 Introduction

Concrete dams play a big role in a country's economy by providing essential services such as domestic water, irrigation water, hydro-electricity generation and flood control. When these dams fail, there is an economical loss and loss of life. Therefore to evaluate the safety of these structures, there has always been a need to understand their dynamic behavior under different environmental conditions through vibration testing.

Literature indicates that research into vibration testing and analysis of concrete dams started in the early 1960's in Japan (Takahashi, 1964). Forced vibration tests have been reported on gravity and arch dams for example Wimbleball buttress dam in the United Kingdom (Severn et al, 1980), Emosson arch dam in Switzerland (Deinum et al, 1982) Morrow point dam in United States of America (Duron et al., 1988) and Norsjo dam in Switzerland (Cantieni,2001). In the early 1990's, ambient vibration testing started becoming popular in the vibration testing of concrete dams and since then it has been used worldwide.

In order to understand the art of ambient vibration testing of concrete dams, a review of past case studies is presented in the next section. This review will highlight reasons why ambient vibrations were carried out on dams, the type of instrumentation used and modal parameter estimation techniques used.

2.2 Case studies

A summary of related ambient vibration testing and analysis of concrete dams is given in this section. Many of these dams are arch dams but gravity dams are also presented. These case studies are included in this thesis because they are beneficial in gaining a proper historical perspective of the development of ambient vibration testing of dams, how the data obtained was analyzed and identifying the missing links in the ambient vibration testing and analysis of ambient data from dams.

Ambient vibration tests were been first reported on 220 m high arch dam known as Contra dam located in Ticino, Switzerland (Brownjohn et al., 1986). Weak and non stationary vibrations

observed, made it possible for investigation of eight upstream-downstream modes in the range 0-50 Hz. The frequencies were determined by peaking peaks on the auto-spectrum while the mode shapes where obtained from the transfer functions between the travelling and reference accelerometers (Schavitz servo-type). Test results showed that frequencies of the measured modes increased with a decline in the reservoir level and that the excitation process was directly related to hydro-electricity generating activity. The report concluded that: "*The ambient vibration testing of stiff structures can be expected to provide a limited amount of information about dynamic responses, unless both sensitive, low noise accelerometers and a reasonable level of excitations are available"*.

Brownjohn, (1990) carried out ambient tests on Hermitage dam (Figure 2.1) a concrete gravity dam located on the Wag River, Kingston, Jamaica. The major objective of the study was to investigate the safety and stability of the dam and validate a mathematical model. Schaevitz LSOC14 inclinometers and Sundstrand QA700 accelerometers were used in the acquisition of signals during testing. Sundstrand accelerometer was placed at one position and used as a reference while two other accelerometers (Schaevitz and Sundstrand) were used as "travelers". However, the signals from the Schaevitz type accelerometer was so noisy that it was not used and the measurements taken before were repeated. This implies that only Sundstrand type accelerometers were used for the rest of the measurements.

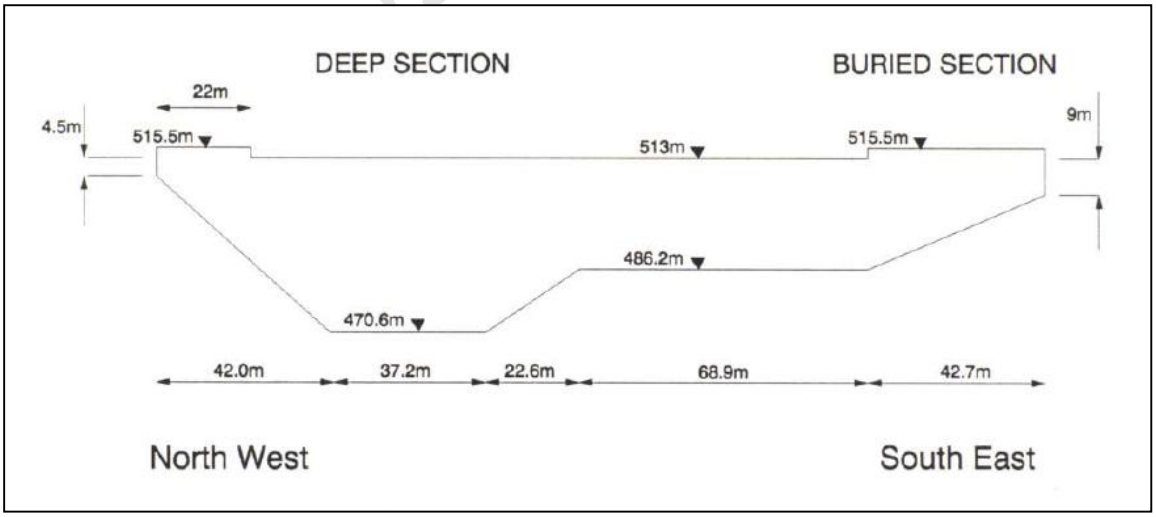

Figure 2.1: Front elevation of Hermitage dam crest (Brownjohn, 1990)

Natural modes in the range 7-30 Hz picked from the auto spectra were identified and were compared with a finite element model of the dam. The report concluded that although there were some discrepancies between the predictions of the mathematical model and the experimental results, the agreement was good enough to justify the usage of the mathematical model. At the end of the tests, it was observed that even for stiff structures with low levels of ambient excitation, it is possible to make sensible estimates of modal parameters derived by sensitive instruments.

Loh and Wu, (1996) tested on a 122.5 m high and 510 m long Fei-Tsui concrete arch dam located in Taiwan. The purpose of the study was to obtain the dynamic characteristics of the dam using the seismic response data and ambient vibration data. To determine the modal parameters, only radial upstream-down direction of motion on the dam was measured. The measuring stations along the crest of the dam were 20 m apart with three sensors deployed for each layout measurement. Four different modal parameter estimation methods were employed to identify the dynamic properties of the dam using ambient vibration data. These included: random decrement method, auto regressive model with least-squares method, two-stage least-squares method and extension of auto regressive model with least-squares method to estimate the mode shapes. Two modes were identified with the first and second having average frequencies of 2.49 Hz and 3.33 Hz respectively. The conclusion of the tests was that the dynamic characteristic obtained from ambient vibration data was consistent with the seismic response data.

Kemp (1996) conducted ambient vibration tests on Ruskin dam a 58 m high concrete gravity dam located in British Columbia. The purpose of these tests was to determine the suitability of ambient vibration testing and analysis as part of seismic evaluation studies of concrete gravity dams, the dynamic properties obtained were used to calibrate a numerical model of the dam. The natural frequencies in the range of 6.5 – 14 Hz for the high reservoir and 8.5- 14.5 Hz for low reservoirs were obtained from the peaks of average normalized power spectral densities (ANPSDs), mode shapes were constructed from the magnitude and phase factors of the relative transfer functions. Following these tests, it was concluded that dynamic properties of Ruskin dam identified using ambient vibration testing and analyses were useful in calibration of the finite element model of the dam.

The arch dam of Mauvoisin was subjected to a number of investigations as an attempt to identify low-amplitude resonance frequencies at the various reservoir levels (Darbre et al., 2000). Mauvoisin dam is a double curvature arch dam located dam in the Swiss Alps with a height of 250.5 m. Seven ambient vibration tests at different water levels were carried out between 1995 and 1996. Resonant frequencies were obtained by inspection of the aggregation of normalized power spectral densities of individual acceleration. Results showed that the resonance frequencies initially increased with rising water level and then decrease with further rise (Figure. 2.2).

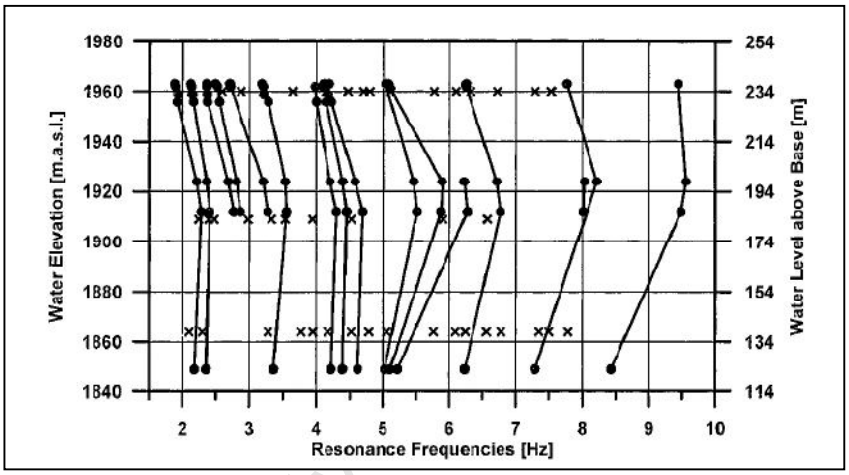

Figure 2.2: Resonance frequencies as a function of water level (Darbre et al., 2000)

This is attributed to the two competing features of increasing entrained mass of water (reduction of the resonance frequencies) and of the dam stiffening due to closing of the vertical construction joints.

Danielle and Taylor (1999) presented results of ambient vibration tests conducted on a 56 m high gravity dam called Claewern dam (Figure.2.3). The tests were to measure the dam's modal properties for validating a finite element model for the dam-reservoir foundation system. Six lateral modes were identified from modal analysis in the frequency range of 6.1 Hz – 11.8 Hz.

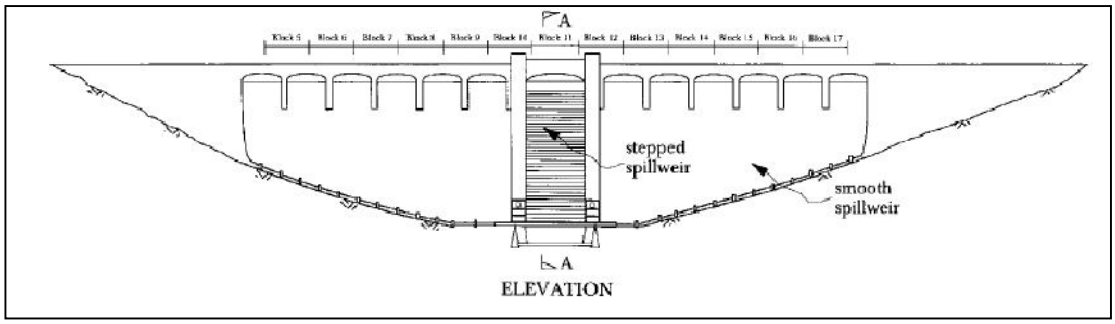

Figure 2.3: Cross section of Claewern dam (Danielle and Taylor, 1999)

The finite element model was analyzed using EACD-3D program. The computed mode shapes and natural frequencies compared well with the experimental results. The study demonstrated that ambient vibration testing can offer a viable alternative to forced vibration testing when only the modal properties of a dam are required.

Mivehchi et al (2003) carried out ambient vibration tests on Shahid-Rajaee and Saveh dams, two concrete arch dams located in Iran. The purpose of the tests was to verify the results obtained from mathematical model used regularly in the Iranian dam design practice by comparing with the behavior of the actual as-built structures. The ambient tests were conducted during winter of 1999 to autumn of 2000. At this time the water level in the reservoir of Shahid-Rajaee dam was at 18 m below the crest while that of Saveh dam was at 47.5 m below the crest. Facilities from the International Institute of Earthquake Engineering and Seismology (IIEES) where used in the measurement and recording of the vibrations of the two dams. Because of limited number of sensors and in order to determine different mode shapes, the tests were performed in several stages of equipment arrangements. Figure 2.4 below shows general layout of field tests on Shahid-Rajaee dam. Each set of three sensors closely spaced are named as *A*, *B*, *C*, and *R* (as the reference set) so that for instance stations are called as *A*1, *A*2, and *A*3, or *R*1, *R*2, and *R*3.
To recognize the hidden modes in ambient vibration tests, artificial exciting was also generated by partial and rapid opening and closing of the bottom outlet gates of the dam body as the fifth loading. Modal parameters from both dams were extracted using the peak picking method. Natural frequency range of Shahid-Rajaee and Saveh dams were reported as 1.46 – 3.58 Hz and 3.91 -7.91 Hz respectively. The damping ratio of both dams was 0.9 – 1.74 %.

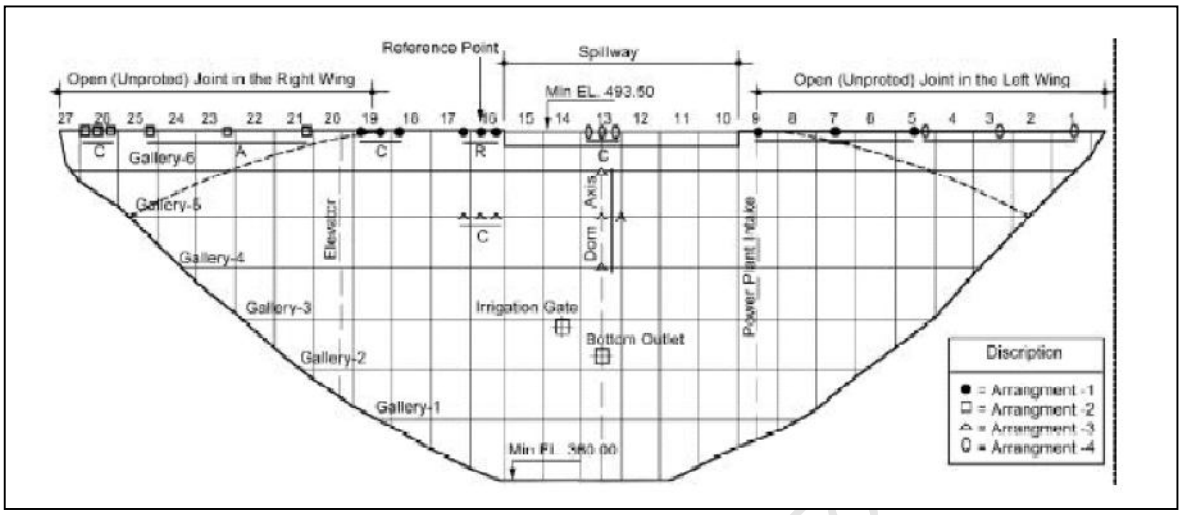

Figure 2.4: General layout of ambient tests on Shahid-Rajaee dam (Mivehchi et al., 2003)

Mendes and Oliviera, (2009) reported ambient vibration tests which were conducted on Cabril arch dam. Cabril arch dam (Figure. 2.5) is double curvature dam with a height of 130 m. The dam was constructed for hydropower electricity generation. The objective of these tests was to evaluate the source of the resonance, from some reservoir water levels which may be of use in exploitation during the operation of the power groups at the dam. The ambient vibration tests were performed with 12 Kinemetrics ES-U force balance accelerometers, signal conditioning equipment developed at LNEC and data acquisition hardware and software from National instruments. The ambient vibration data was acquired using a sampling frequency of 200 Hz, during more than 30 minutes in each test.

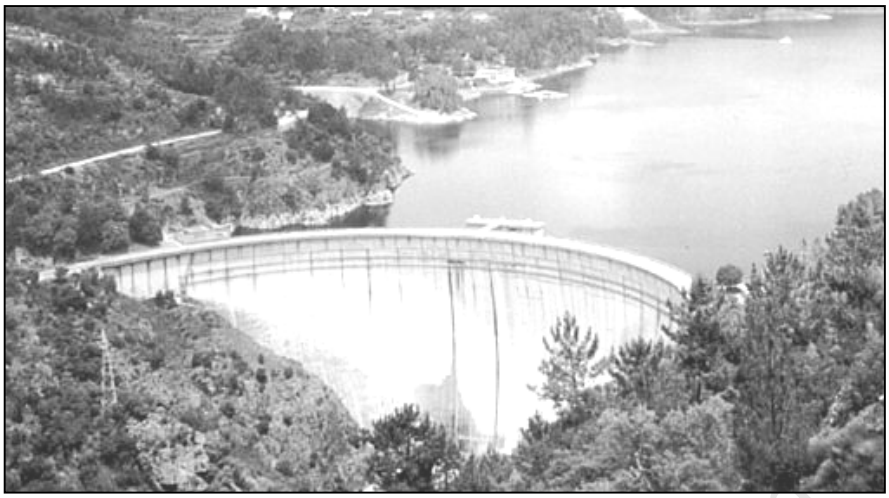

Figure 2.5: Cabril dam (Mendes and Oliviera, 2009)

A 3D finite element model for the intake tower structure of Cabril dam was developed using EACD 3D. This was to study the dynamic behavior of the intake tower structure of the dam and its effect on the behavior of the dam. Natural frequencies of the dam were extracted from the ambient test data using frequency domain decomposition. A resonant frequency of 3.57 Hz was obtained from the tests which corresponded to the frequency of the operation of the power groups. From the numerical results, it was possible to guarantee the existence of two natural frequencies around 1 Hz which agreed with the experimental results from ambient vibration tests. The paper concluded that: "*the use of experimental and numerical results is a fundamental in analyzing and understanding the correct dynamic behavior of civil engineering structures and the influence of auxiliary structures such as intake towers on the analysis of results from modal identification of data collected on dam's body.*"

Okuma et al., (2008) performed long-term and short term ambient vibration measurement test on Hitotsuse dam. Hitotsuse dam (Figure. 2.6) is a concrete arch dam, 130 m high and consists of 5 by 27 blocks which was built for hydropower electricity generation. The ambient vibration tests were conducted to evaluate seismic safety of the concrete arch dams as well as to collect the fundamental data for developing structural damage detection based on ambient vibration testing.

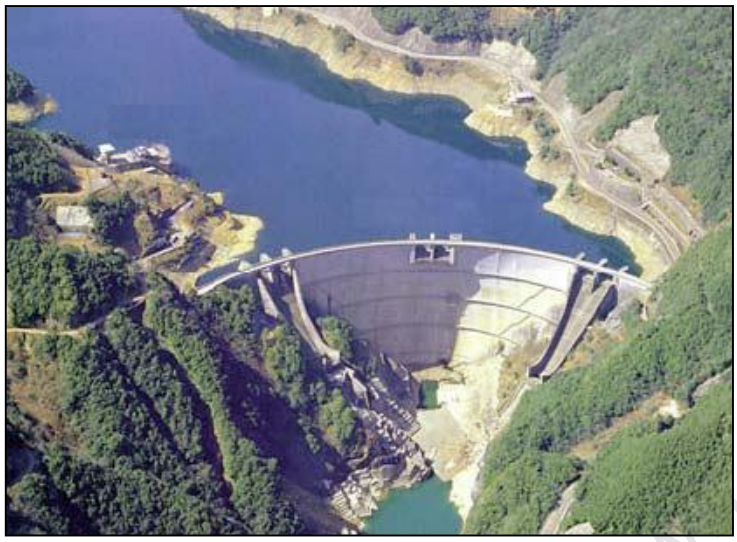

Figure 2.6: Hitotsuse dam (Okuma et al., 2008)

Natural frequencies were identified from the cross spectrum of autoregressive moving average models. From the two tests and modal analysis, the identified natural frequencies were in good agreement with the earthquake observation records, and the identified natural frequencies of three modes strongly correlated with the water level of the dam.

Moyo and Oosthuizen (2010) did ambient vibration survey trials on two arch dams namely Roode Elsberg and Kouga dams found in South Africa. The major aim of the tests was to obtain dynamic characteristics of these dams to be used as baseline measurements for long term dam safety monitoring. Four sets of ambient vibration measurements were taken on Roode Elsberg dam between a period of December 2008 and April 2010 while only one measurement test in September 2009 was carried out on Kouga dam. Roving force balance accelerometers acted as travelling accelerometer whereas seismic piezoelectric accelerometers were used as references.
Using frequency domain based method modal parameters of both dams were extracted. Natural frequencies of Roode Elsberg dam and Kouga dam were in the range of 3 and 7.70 Hz and 3.72 and 8.30 Hz respectively. It was concluded that ambient vibration tests add value safety surveillance of dams.

2.3 Chapter Summary

Literature has shown that ambient vibration testing and analysis of concrete dams has been going for the last two decades. From the literature on dams presented in the previous section, the ratio of arch dams to gravity dams is 9:2. This shows that concrete arch dams have been subjected to ambient vibration tests more than gravity dams which give us an idea of how arch dams behave. The major aim of all the tests was to determine the dynamic characteristics of dams and calibrating mathematical models. Other aims included: - studying the effect of water reservoir levels to the resonant frequency, structural health monitoring and for seismic evaluation studies. This has contributed to better understanding of the behavior of such structures.

In the extraction of modal parameters from the ambient data from the dams, frequency domain procedure (peak picking) was widely used. However, peak picking is not the only method used in extracting modal parameters from ambient test data. There are other techniques divided into frequency domain (non-parametric), time domain (parametric) and wavelet transform (time-frequency domain). The modal parameter estimation techniques under the mentioned categories are described in detail in Chapter 3.

3 MODAL PARAMETER ESTIMATION IN OPERATIONAL MODAL ANALYSIS

3.1 Introduction

Modal parameter extraction algorithms in operational modal analysis can be divided into time domain, frequency domain and time-frequency domain. A brief summary of the available operational modal analysis identification techniques is given below.

Time domain based methods are divided into three namely: (1) Natural Excitation Technique (NExT) type procedures which are used for modal identification from natural excitations. Examples of algorithms under the NExT type procedures include least square complex exponential (LSCE), eigensystem realization algorithm (ERA) and extended Ibrahim time domain (EITD). (2) Autoregressive moving average (ARMA)-type procedures: These are can also be used for output-only measurements for multiple natural excitations. Examples of common algorithms include prediction error method-autoregressive moving average (PEM-ARMAV) and recently linear multi-stage (LMS) ARMAV which is effective in operational modal analysis for cases where there is noise (Fassois, 2001). (3) Stochastic subspace-based procedures which offer numerically reliable and effective state-space model for a large system from ambient response measured data (Overshee and de Moor, 1996). Stochastic subspace identification (SSI) technique is an example of stochastic subspace-based procedure developed for stochastic excitation (Brincker and Andersen, 2006).

Frequency domain based methods are categorized into two procedures:- (1) Frequency domain decomposition (FDD)-type procedures: The FDD methods are extensions of peak-picking technique and uses the fact that modes can be estimated from spectral densities in the condition of a white noise input and a lightly damped structure (Gade et al.,2005). Examples of algorithms under FDD include frequency domain decomposition (Brincker et al., 2000), enhanced frequency domain decomposition (Brincker et al., 2001) and curve-fitting frequency domain decomposition (Jacobsen, 2008). (2) Least square complex frequency (LSCF)-type procedures:- these are based on parametric function model represented by rational fractional polynomial (Richardson, 1982). Examples of algorithms under this method include rational fractional polynomial commercially

known as alias free polynomial (Vold, 2007), polyreference least square complex frequency also known as operational polymax (Peeters et al., 2004).

Time-frequency domain method is the third category of modal parameter identification techniques in operational modal analysis. It uses the wavelet transform which decouples automatically the modal components in analyzing a multi degree freedom system (Lardies and Gouttebroze, 2002)

In this thesis, non parametric (frequency domain) methods such as frequency domain decomposition, enhanced frequency domain decomposition, curve-fitting domain decomposition, rational fractional polynomial and polyreference least square complex frequency also known as operational polymax are described in details. Parametric (time domain) methods such as complex exponential and stochastic subspace identification, eigensystem realization algorithm and autoregressive moving average are presented. Wavelet transform which is a time-frequency based technique is reported.

3.2 Frequency domain, frequency domain decomposition-type methods

Frequency domain decomposition (FDD) type techniques are based on the formula of input and output power spectrum density (PSD) relationship (equation 3.1) for stochastic process (Bendat and Piersol, 1986).

$$G_{yy}(j\omega) = \overline{H}(j\omega)G_{xx}(j\omega)H(j\omega)^{P} \tag{3.1}$$

Where $G_{xx}(j\omega)$ is the input PSD, $G_{yy}(j\omega)$ is the output PSD, $H(j\omega)$ is the FRF which is expressed as partial fractions (equation 3.2) form via poles λ_k and residues R_k containing information about mode shapes (Zhang et al., 2005).

$$H(j\omega) = \sum_{k=1}^{n} \frac{R_k}{j\omega - \lambda_k} + \frac{\overline{R}_k}{j\omega - \overline{\lambda}_k} \tag{3.2}$$

Where

$$R_k = \phi_k \gamma_k^T \tag{3.3}$$

ϕ_k and γ_k^T are the mode shape vector and the modal participation vector respectively.

When all output measurements are taken as references, then the FRF becomes a square matrix and $\gamma_k = \phi_k$. If the input is assumed to be white noise, i.e. its PSD is a constant matrix ($G_{xx}(j\omega) = C$, then equation 3.1 becomes (Brincker et al.,2000):

$$G_{yy}(j\omega) = \sum_{k=1}^{n}\sum_{s=1}^{n}\left[\frac{R_k}{j\omega - \lambda_k} + \frac{\overline{R}_k}{j\omega - \overline{\lambda}_k}\right] \times C\left[\frac{R_s}{j\omega - \lambda_s} + \frac{\overline{R}_s}{j\omega - \overline{\lambda}_s}\right]^p \tag{3.4}$$

Using Heaviside partial fraction theorem, multiplying the two partial fractions, the output PSD can be reduced to a pole/ residue form as shown below:

$$G_{yy}(j\omega) = \sum_{k=1}^{n}\frac{A_k}{j\omega - \lambda_k} + \frac{\overline{A}_k}{j\omega - \overline{\lambda}_k} + \frac{B_k}{-j\omega - \lambda_k} + \frac{\overline{B}_k}{-j\omega - \overline{\lambda}_k} \tag{3.5}$$

where A_k is the kth residue (m x m) matrix of the output PSD also known as the Hermitian matrix (Brincker et al.,2000) given by:

$$A_k = R_k C\left(\sum_{s=1}^{n}\frac{R_s^p}{-\lambda_k - \overline{\lambda}_s} + \frac{\overline{R}_s^p}{-\lambda_k - \overline{\lambda}_s}\right) \tag{3.6}$$

The contribution to the residue from the *kth* mode is given by

$$A_k = \frac{R_k C \overline{R}_k^p}{2\alpha_k} \tag{3.7}$$

where α_k is the negative of the real part of the pole $\lambda_k = -\alpha_k + j\omega_k$. It appears this term becomes dominating when the damping is light, and, thus, for case of light damping, the residue becomes proportional to the mode shape vector (Brincker et al., 2000):

$$A_k \alpha R_k C R_k = \phi_k \gamma_k^p C \gamma_k \phi_k^p = d_k \phi_k \phi_k^p \tag{3.8}$$

Where $d_k = \gamma_k^p G_{xx} \gamma_k$, is a real scalar for white noise excitation. In the vicinity of a natural frequency, PSD can be approximated by modal decomposition (Zhang et al., 2005):

$$G_{yy_{\omega\to\omega_k}}(j\omega) \approx \phi_k \frac{2d_k}{j\omega - \lambda_k}\phi_k^p = \alpha_k \phi_k \phi_k^p \tag{3.9}$$

The classical frequency domain technique which is based on the fact that resonance frequencies are directly obtained from the PSD plot at the peak is known as peak picking (PP) method (Felber, 1993). Mode shapes in the peak picking method are obtained as a column of PSD at the corresponding damped natural frequency while damping ratio is obtained by half power method.

The PP method gives reasonable estimates of modal parameters if the mode shapes are well separated (Ventura et al., 1997). It has advantages of being fast, easy to use. However, for complex structure, the PSD peak picking method is inaccurate, i.e. the accuracy of natural frequencies is limited to the frequency resolution of the PSD spectrum (Zhang et al., 2005). The other disadvantage of the PP method is that it cannot be used in structures with closely spaced modes yet real complex structures have close modes.

Brincker et al., (2000) proposed a method which has the same advantages as PP method but eliminates its disadvantages. This method is known as frequency domain decomposition (FDD).

3.2.1 Frequency Domain Decomposition

The FDD method is the backbone of the frequency domain decomposition-type methods. It uses the output PSD as the PP method but it carries out singular value decomposition (SVD) of the output PSD, estimated at discrete frequencies $\omega = \omega_i$ (Brincker et al., 2000) This decomposition is performed to identify single degree of freedom models of the system (Batel, 2002)

The singular value decomposition of an m x n complex matrix A is the following factorization:

$$A = U\Sigma V^H \tag{3.10}$$

Where U and V are unitary and Σ is a diagonal matrix that contains the real singular values.

$$\begin{aligned} \Sigma &= diag(s_1, ..., s_r) \\ r &= \min(m, n) \end{aligned} \tag{3.11}$$

The superscript *H* on the matrix *V* denotes a Hermitian transformation (transpose and complex conjugate). In the case of real valued matrices, the *V* matrix is only transposed. The s_i elements in the matrix S are called the singular values and their following singular vectors are contained in the matrices *U* and *V*.

This singular value decomposition is performed for each of the matrices at each frequency and for each measurement taken. The spectral density matrix is then approximated to the following expression after SVD decomposition:

$$[G_{yy}(j\omega)] = [\Phi][\Sigma][\Phi]^H \tag{3.12}$$

with $$[\Phi]^H[\Phi] = [I]$$

$[\Sigma]$ being the singular value matrix and $s_1, \ldots, s_r$ the singular vectors unitary matrix:

$$[\Sigma] = diag(s_1, \ldots s_r) = \begin{bmatrix} s_1 & 0 & 0 & . & . & 0 \\ 0 & s_2 & 0 & . & . & . \\ 0 & . & s_3 & . & . & . \\ . & . & . & . & . & 0 \\ . & . & . & & s_r & 0 \\ 0 & . & . & 0 & 0 & 0 \end{bmatrix} \tag{3.13a}$$

$$[\Phi] = [\{\varphi_1\}\{\varphi_2\}\{\varphi_3\}\ldots\{\varphi_r\}] \tag{3.13b}$$

The number of nonzero elements in the diagonal of the singular matrix corresponds to the rank of each spectral density matrix. The singular vectors correspond to an estimation of the mode shapes and the corresponding singular values are the spectral densities of the SDOF system expressed in equation (3.9).

In the repeated mode case, the rank of the PSD matrix will be equal to the number of multiplicity of the modes. Therefore, the SV function can be utilized as a modal indication function (MIF). Modal frequencies can be located by peaks of the SV plots. From the corresponding singular vectors, mode shapes can be obtained. Since SVD has the ability of separating signal space from

noise space, the modes can be indicated from SV plots, and closely spaced modes or even repeated modes can easily be detected (Zhang et al., 2005)

The FDD has the advantages of calculating closely spaced modes, being user friendly but it cannot give modal damping ratios. Therefore a second generation of FDD-type method called Enhanced Frequency Domain Decomposition (EFDD) was proposed. This estimates not only modal frequencies and mode shapes but also damping ratios (Brinker et al., 2001).

3.2.2 Enhanced Frequency Domain Decomposition

Enhanced frequency domain decomposition (EFDD) is an extension of FDD technique. From equation 3.12, the first singular vector is an estimate of the mode shape and the corresponding singular value is the auto power spectral density function of the corresponding single degree of freedom system. EFDD allows the natural frequency and damping of a particular mode to be extracted by computing auto-and cross-correlation functions (Batel, 2002). The natural frequency and damping ratios are obtained from the fully or partially identified SDOF auto spectral density function. The modal parameters are obtained by taking the spectral density function back to time domain by inverse FFT.

From the free decay domain function, which is also the auto correlation function of the SDOF, the natural frequency and damping ratio is found by estimating crossing times and logarithmic decrement. First all the extremes p_k both peaks and valleys on the correlation function are found. The logarithmic decrement δ is given by

$$\delta = \frac{2}{k} In\left(\frac{p_0}{|p_k|}\right) \tag{3.14}$$

where p_0 is the initial value of the correlation function and p_k is the k^{th} extreme. Then the logarithmic decrement and the initial value of the correlation function can be found by linear regression on $k\delta$ and $2ln(|p_k|)$, and the damping ration is given by

$$\zeta = \frac{\delta}{\sqrt{\delta^2 + 4\pi^2}} \tag{3.15}$$

The frequency is calculated by making a linear regression on the crossing times and the times corresponding to the extremes and using the damped natural frequency f_d and the undamped natural frequency f is related

$$f = \frac{f_d}{\sqrt{1-\zeta^2}} \tag{3.16}$$

The extreme values and corresponding times are found by quadratic interpolation, whereas the crossing times are found by linear interpolation.

3.2.2.1 Estimation of mode shapes using EFDD method

Mode shapes are estimated by using a weighted sum of the singular vectors ϕ_i and singular values s_i where by random noise is efficiently averaged out.

$$\phi_{weight} = \sum_i \phi_i s_i \tag{3.17}$$

The improved version of estimating mode shapes is from the *SDOF* Bell functions. The SDOF bell function is estimated using the mode determined by the previous FDD peak-picking operation. The latter is used as a reference vector in a correlation analysis based on the Modal Assurance Criteria (MAC). A MAC value is computed between the reference FDD vector and a singular vector for a particular frequency region. The MAC value describes the degree of correlation between 2 modes X and Y and it takes a value between 0 and 1 (Allemang, 2002)

$$MAC(\{X\},\{Y\}) = \frac{\left\|\{X\}^*\{Y\}\right\|^2}{\|X\|\|Y\|} \tag{3.18}$$

If the largest MAC value of this vector is above a user-specified *MAC Rejection Level*, the corresponding singular value is included in the description of the SDOF Spectral Bell function. The lower this MAC Rejection Level the larger the number of singular values included in the identification of the SDOF Bell function. A good compromise value for this rejection criterion is 0.9. An average value of the singular vector (weighted by the singular values) is then obtained.

Most of the potential uses of the modal assurance criterion are well known but a few may be more subtle. Partial lists of the most typical uses that have been reported in the literature are as follows (Allemang, 2002):

a) Validation of experimental modal models
b) Correlation with analytical modal models (mode pairing)
c) Mapping matrix between analytical and experimental modal models
d) Modal vector error analysis
e) Modal vector averaging
f) Experimental modal vector completion and/or expansion
g) Weighting for model updating algorithms
h) Modal vector consistency/stability in modal parameter estimation algorithms
i) Repeated and pseudo-repeated root detection

3.2.3 Curve-Fitting Frequency Domain Decomposition

The curve fitting frequency domain decomposition (CFDD) technique is an enhanced alternative approach of FDD utilizing curve fitting of the SDOF spectrum *S*(*f*) directly in the frequency domain. The main advantage of CFDD is that it has a more accurate estimation of the natural frequencies and damping ratios both in case of pure stochastic excitation and in the presence of deterministic excitation (Jacobsen et al, 2008). From equation 3.1 the spectral density is defined in terms in terms of the FRF. The FRF for an SDOF can be presented in a polynomial form as (Ljung, 1999). From the roots of the denominator polynomial the natural frequency and damping ratio can be extracted directly.

$$H(f) = \frac{B_0 + B_1 e^{2\pi fT} + B_2 e^{2\pi fT}}{1 + A_1 e^{2\pi fT} + A_2 e^{2\pi fT}} \tag{3.19}$$

where T is the sampling interval.

Assuming that unknown excitation $G_{xx}(j\omega)$ in equation 3.1 is broad-banded and can be approximated by white noise having a constant spectrum $G_{xx}(j\omega) = G_{xx}$ (Jacobsen et al., 2008). Consequently the SDOF spectrum becomes proportional to the product $H(f)H^p(f)$ indicating that the polynomial order of SDOF spectrum is twice the order of $H(f)$. In order to avoid having

to fit the product $(f)H^p(f)$, SDOF spectrum is manipulated. This is helpful because curve fitting is done directly on $H(j\omega)$. This can be achieved by transforming the full power spectrum to a positive half power spectrum which is obtained from by calculating the respective correlation function obtained by inverse Fourier transformation (Jacobsen et al., 2008). Following this step, the negative lags part of the correlation functions is set to zero and is obtained by Fourier transformation of the result back to frequency domain.

3.2.3.1 Curve fitting algorithm

The key step of the curve-fitting algorithm is to calculate the positive half-power spectrum *P*(*f*). Using equation 3.19 the following relationship can be obtained:

$$(1 + A_1 e^{2\pi fT} + A_2 e^{2\pi fT})P(f) = B_0 + B_1 e^{2\pi fT} + B_2 e^{2\pi fT} \tag{3.20}$$

This can be rearranged so the unknown polynomial parameters are isolated:

$$P(f) = \begin{bmatrix} -P(f)e^{2\pi fT} & -P(f)e^{4\pi fT} & 1 & e^{2\pi fT} & e^{4\pi fT} \end{bmatrix} \begin{bmatrix} A_1 \\ A_2 \\ B_0 \\ B_1 \\ B_2 \end{bmatrix} \tag{3.21}$$

Given the spectral estimates $P(f_i)$ for all discrete frequencies f_i = i = 0 to v, where v is the index of the Nyqusit frequency. Equation 3.21 makes it possible to formulate the following regression problem:

$$A_c\theta = B_c \tag{3.22}$$

where

$$A_c = \begin{bmatrix} -P(f_0)e^{2\pi f_0 T} & -P(f_0)e^{4\pi f_0 T} & 1 & e^{4\pi f_0 T} & e^{4\pi f_0 T} \\ -P(f_1)e^{2\pi f_1 T} & -P(f_1)e^{4\pi f_1 T} & 1 & e^{4\pi f_0 T} & e^{4\pi f_0 T} \\ -P(f_2)e^{2\pi f_2 T} & -P(f_2)e^{4\pi f_2 T} & 1 & e^{4\pi f_0 T} & e^{4\pi f_0 T} \\ -P(f_3)e^{2\pi f_3 T} & -P(f_3)e^{4\pi f_3 T} & 1 & e^{4\pi f_0 T} & e^{4\pi f_0 T} \\ -P(f_v)e^{2\pi f_v T} & -P(f_v)e^{4\pi f_v T} & 1 & e^{4\pi f_0 T} & e^{4\pi f_0 T} \end{bmatrix}, B_c = \begin{bmatrix} P(f_0) \\ P(f_1) \\ . \\ . \\ P(f_v) \end{bmatrix}, \theta = \begin{bmatrix} A_1 \\ A_2 \\ B_0 \\ B_1 \\ B_2 \end{bmatrix} \quad (3.23)$$

In order to ensure that the parameters of θ will be estimated as real valued parameters as they are defined, the complex notation in equation 3.22 is reformulated to a regression problem of double size:

$$\begin{bmatrix} \mathrm{Re}(A_c) \\ \mathrm{Im}(A_c) \end{bmatrix} \theta = \begin{bmatrix} \mathrm{Re}(A_c) \\ \mathrm{Im}(A_c) \end{bmatrix} \quad (3.24)$$

and a solution is found as:

$$\hat{\theta} = \begin{bmatrix} \mathrm{Re}(A_c) \\ \mathrm{Im}(A_c) \end{bmatrix}^{-1} \begin{bmatrix} \mathrm{Re}(B_c) \\ \mathrm{Im}(B_c) \end{bmatrix} \quad (3.25)$$

The main benefit of CFDD method is that it is a more accurate estimation of the natural frequencies and damping ratios both in case of pure stochastic excitation and in the presence of deterministic excitation. The CFFD technique is advantageous both in the case of pure stochastic excitation and when harmonic components are present.

In summary, the frequency domain decomposition procedures are based on decomposing the power spectral density function using singular value decomposition.SVD decomposes the spectral response into a set of single degree of freedom system each corresponding to a single mode. There are three algorithms including frequency domain decomposition which only estimates modal frequencies and mode shapes. The second method is the enhanced frequency domain decomposition method which adds estimation of damping as well and the estimates of frequency and mode shape are improved by fitting a SDOF model to the singular values in a user-defined frequency band around the peak. The third method that falls under this category is

the curve fitting frequency domain decomposition which utilizes the SDOF spectrum directly in the frequency domain, it estimates the modal parameters both in stochastic and deterministic excitations.

3.3 Frequency domain, least squares complex frequency- type methods.

The least square complex frequency (LSCF)-type procedures in operational modal analysis are divided into two namely: - rational fraction polynomial (RFP) commercially known as AF-Poly and the polyreference version of least square complex frequency also known as operational polymax.

3.3.1 Rational fraction polynomial method

The idea of the rational fraction polynomial (RFP) method is to express an FRF in terms of rational fraction polynomials, and through numerical manipulations, the coefficients of these polynomials can be identified (He and Fu, 2001). The RFP method is a MDOF that curve fits the analytical expression (equation 3.26) in a least square sense to an FRF measurement, and in the process, the coefficients a_k and b_k of the numerator and denominator respectively are determined. This method initially identifies the denominator or the characteristic polynomial, whose roots are related to the natural frequencies and damping ratios of all the available data.

The analytical expression or rational fraction form shown in equation (3.26) below is a ratio of two polynomials whose the orders in general are independent of one another (Richardson and Formenti, 1982).

$$H(j\omega) = \left. \frac{\sum_{k=0}^{m} a_k s^k}{\sum_{k=0}^{n} b_k s^k} \right|_{s=j\omega} \tag{3.26}$$

Upon determining the coefficients of the both the numerator and denominator polynomials, then the modal properties of the FRF can be obtained.

3.3.1.1 RFP algorithm

In the formulation of the rational fraction polynomial algorithm, coefficients a_k and b_k are to be determined. This is done in such a way that the error between the FRF measurements and analytical expression (equation 3.26) is minimized over a chosen frequency range (Richardson and Formenti, 1982). To find a solution on how to obtain the coefficients, there is a need to define an error criterion.

Let the error e_i at a specific frequency be the difference between the analytical value and the measurement value given by:

e_i = Analytical FRF- Measurement FRF at ω_i or

$$e_i = \sum_{k=0}^{m} a_k (j\omega_i)^k - h_i \left[\sum_{k=0}^{n} b_k (j\omega_i)^k + (j\omega_i)^n \right] \tag{3.27a}$$

where: h_i=FRF measurement data at ω_i

This can also be presented in a squared error criterion as:

$$J = \sum_{i=1}^{L} e_i^* e_i = \{E^*\}^t \{E\} \tag{3.27b}$$

$$\text{Error vector} = \{E\} = \begin{Bmatrix} e_i \\ e_2 \\ : \\ e_n \end{Bmatrix} \tag{3.28}$$

*- denotes complex conjugate

t- denotes transpose

The total error can also be presented in a vector form as:

$$\{E\} = [P]\{A\} - [T]\{B\} - \{W\} \tag{3.29}$$

where:

$$[P]=\begin{bmatrix}1 & j\omega_1 & (j\omega_1)^2 & .. & (j\omega_1)^m\\ 1 & j\omega_2 & (j\omega_2)^2 & .. & (j\omega_2)^m\\ : & : & : & & :\\ 1 & j\omega_L & (j\omega_L)^2 & .. & (j\omega_L)^m\end{bmatrix} \tag{3.30}$$

$$[T]=\begin{bmatrix}h_1 & h_1(j\omega_1) & h_1(j\omega_1)^2 & .. & h_1(j\omega_1)^{n-1}\\ h_2 & h_2(j\omega_2) & h_2(j\omega_2)^2 & .. & h_2(j\omega_2)^{n-1}\\ : & : & : & & :\\ h_L & h_L(j\omega_L) & h_L(j\omega_L)^2 & .. & h_L(j\omega_L)^{n-1}\end{bmatrix} \tag{3.31}$$

$$\{A\}=\begin{Bmatrix}a_0\\ a_1\\ :\\ a_m\end{Bmatrix},\ \{B\}=\begin{Bmatrix}b_0\\ b_1\\ :\\ b_m\end{Bmatrix},\ \{W\}=\begin{Bmatrix}h_1(j\omega_1)^n\\ h_2(j\omega_2)^n\\ :\\ h_L(j\omega_L)^n\end{Bmatrix} \tag{3.32}$$

To determine the coefficient vectors {A} and {B} that will minimize the total deviation, the following partial derivatives should be equated to zeros:

$$\frac{\partial J}{\partial\{A\}}=\frac{\partial J}{\partial\{B\}}=0 \tag{3.33}$$

This leads to the following equation for estimation of coefficient vectors

$$\begin{aligned}\frac{\partial J}{\partial A}&=2\left[P^*\right]^t[P]\{A\}-2\,\mathrm{Re}([P^*][T]\{B\})-2\,\mathrm{Re}([P^*]^t\{W\})=\{0\}\\ \frac{\partial J}{\partial B}&=2\left[T^*\right]^t[T]\{B\}-2\,\mathrm{Re}([T^*][P]\{A\})-2\,\mathrm{Re}([T^*]^t\{W\})=\{0\}\end{aligned} \tag{3.34}$$

Re( )- denotes the real part of a complex number ( ).

The coefficients {A} and {B} are related to the modal data of the FRF. The solution equation of equation (3.34) is given by:

$$\begin{bmatrix} Y & : & X \\ .. & : & .. \\ X^t & : & Z \end{bmatrix} \begin{Bmatrix} A \\ .. \\ B \end{Bmatrix} = \begin{Bmatrix} G \\ .. \\ F \end{Bmatrix} \tag{3.35}$$

where:

$$[X] = -\mathrm{Re}([P^*]^t[T])$$

$$[Y] = [P^*]^t[P]$$

$$[X] = [T^*]^t[T]$$

$$\{G\} = \mathrm{Re}([P^*]^t\{W\})$$

$$\{F\} = \mathrm{Re}([T^*]^t\{W\}) \tag{3.36}$$

According to Kelly (1967), the solution equations were ill conditioned and could not be solved by a mini-computer even for simple cases. To solve this problem, the ordinary polynomials had to be reformulated in terms of orthogonal polynomials or Forsythe orthogonal polynomials (Friswell and Penny, 1993). The solution equations using orthogonal polynomials were numerically stable, exhibiting a dramatic improvement and the problem of size was cut in half which uncoupled the solution equations for the denominator polynomial coefficients from those for the numerator coefficients (Formenti and Richardson, 2002)

3.3.1.2 FRF in terms of orthogonal polynomials

The FRF in terms of two sets of orthogonal polynomials is shown in equation 3.37 below. The unknown coefficients in this expression are c_k and d_k and it is these values which are sought as solutions during the curve fitting process. Once these values are known, the coefficients of the ordinary polynomials, i.e. the a's and b's in equation.3.26, can be easily recovered.

The denominator polynomials differ from the numerator polynomials in that they must satisfy a different orthogonality condition which contains a weighting function. This function is the

square of the FRF magnitude, measurement data, and it will become apparent from the solution equation formulation which follows, that this orthogonality condition greatly reduces the complexity of this equation (Richardson and Formenti, 1982)

$$H(\omega_i) = \frac{\sum_{k=0}^{m} c_k \phi_{i.k}}{\sum_{k=0}^{n} d_k \theta_{i.k}} \quad i,\ldots\ldots L \tag{3.37}$$

Orthogonality:

$$\sum_{i=1}^{L} \left(\phi_{i,k}{}^{+}\right)^{*} \phi_{i,j}{}^{+} = \begin{cases} 0, k \neq j \\ .5, k = j \end{cases} \tag{3.38}$$

$$\sum_{i=1}^{L} \left(\phi_{i,k}{}^{+}\right)^{*} |h_i|^2 \phi_{i,j}{}^{+} = \begin{cases} 0, k \neq j \\ .5, k = j \end{cases} \tag{3.39}$$

Using the same procedure as problem formulation for ordinary polynomials, a new set of solution equations can also be derived in terms of orthogonal polynomials. First, the error vector can be re-written in terms of orthogonal polynomials as shown below. Again, it is assumed that the highest order denominator coefficient is unity*;* (d_n=1). Then following the same steps as before; namely, formulation of an error criterion, and taking derivatives of the criterion with respect to the unknown polynomial coefficients, a new set of solution equations results. These equations are expressed as equations (3.44), (3.45a) and (3.45b).

3.3.1.3 The error vector in terms of orthogonal polynomials

$$\{E\} = [P]\{C\} - [T]\{D\} - \{W\} \tag{3.40}$$

where:

$$[P] = \begin{bmatrix} \phi_{1,0}^{+} & \phi_{1,1}^{+} & .. & \phi_{1,m}^{+} \\ \phi_{2,0}^{+} & \phi_{2,1}^{+} & & \phi_{2,m}^{+} \\ : & : & & : \\ \phi_{L,0}^{+} & \phi_{L,1}^{+} & .. & \phi_{L,m}^{+} \end{bmatrix} \tag{3.41}$$

$$[T] = \begin{bmatrix} h_1\phi_{1,0}^{+} & h_1\phi_{1,1}^{+} & h_1\phi_{1,n-1}^{+} \\ h_2\phi_{2,0}^{+} & h_2\phi_{2,1}^{+} & h_2\phi_{2,n-1}^{+} \\ & & \\ h_L\phi_{L,0}^{+} & h_L\phi_{L,1}^{+} & h_L\phi_{L,n-1}^{+} \end{bmatrix} \tag{3.42}$$

$$\{C\} = \begin{Bmatrix} c_0 \\ c_1 \\ : \\ c_m \end{Bmatrix}, \{D\} = \begin{Bmatrix} d_0 \\ d_1 \\ : \\ d_{n-1} \end{Bmatrix}, \{W\} = \begin{Bmatrix} h_1\phi_{1,n}^{+} \\ h_2\phi_{2,n}^{+} \\ : \\ h_L\phi_{L,n}^{+} \end{Bmatrix} \tag{3.43}$$

The solution equations in terms of orthogonal polynomials are given by:

$$\begin{bmatrix} I_1 & : & X \\ .. & : & .. \\ X^t & : & I_2 \end{bmatrix} \begin{Bmatrix} C \\ .. \\ D \end{Bmatrix} = \begin{Bmatrix} H \\ .. \\ 0 \end{Bmatrix} \tag{3.44}$$

where:

$$[X] = -\mathrm{Re}\left(\left[P^*\right]^t [T]\right) \tag{3.45a}$$

$$\{H\} = \mathrm{Re}\left(\left[P^*\right]^t [W]\right) \tag{3.45b}$$

$[I_1]$ and $[I_2]$ are Identity matrices and $\{0\}$ = Zero vector.

$$\left[I - [X]^t [X]\right]\{D\} = -[X]^t \{H\} \tag{3.46}$$

$$\{C\} = \{H\} - [X]\{D\} \tag{3.47}$$

Having uncoupled the solution equations through the use of orthogonal polynomials, it is clear that a two-step global curve fitting approach could be implemented (Formenti and Richardson, 2002)

3.3.1.4 Global curve fitting

Modal parameter estimation methods which curve fit each measurement individually can result into significant errors especially if an MDoF curve fitter is used to estimate parameters of many modes. Accurate damping and residue estimates are, in general more difficult to obtain than accurate frequency estimates. Many times the accuracy of the modal parameters is scarified during the curve fitting process to yield a re-synthesized curve fit function which means that the values of the estimated parameters can trade off errors. Damping is the most difficult parameter to estimate accurately from FRF measurements, and the residue is often tightly coupled to damping (Richardson and Formenti, 1985). Hence, if damping is in a large error, the residue estimate will be in large error even though the curve fitting function closely the measurement data.

An approach that can reduce errors is to divide the curve fitting process into two procedures namely; (1) estimate the frequency and damping and (2) the residue or mode shape parameters. The process of estimating frequencies and damping first and then mode shapes is known as global curve fitting.

The use of orthogonal polynomials uncouples the solution equations of RFP method so that the denominator (characteristic) polynomial coefficients can be obtained independently of the numerator polynomial coefficients. Taking advantage of the fact that the characteristic polynomial is the same structure, the solution equations for the characteristic polynomial can be written for as many measurements as desired. This is shown in equation (3.48) below:

$$\begin{bmatrix} U_1 \\ .. \\ U_2 \\ .. \\ : \\ .. \\ U_p \end{bmatrix} \{B\} = \begin{Bmatrix} V_1 \\ .. \\ V_2 \\ .. \\ : \\ .. \\ V_p \end{Bmatrix} \tag{3.48}$$

Where

$$\begin{aligned} [U_k] &= \left[I - [X_k]^t [X_k]\right][BM_k]^{-1} \\ \{V_k\} &= [X_k]^t \{H_k\} \\ [X_k] &= -\mathrm{Re}\left(2[P_k^*]^t [T_k]\right) \\ \{H_k\} &= \mathrm{Re}\left(2[P_k^*]^t [W_k]\right) \end{aligned} \tag{3.49}$$

$[P_k]$ = numerator polynomial $[T_k]$ = denominator polynomial $[W_k]$ = denominator polynomials and data

$[BM_k]$ = orthogonal to ordinary transform

The least square solution of equation (3.49) is given by:

$$\sum_{k=1}^{p} [U_k]^2 \{B\} = \sum_{k=1}^{p} [U_k]\{V_k\} \tag{3.50}$$

{B} = characteristic polynomial coefficients

If there are (n) unknown polynomial coefficients in the vector (B), then there are (n by p) equations in the expression of equation (3.48) This is an over specified set of equations since only (n) equations are needed to solve for the unknowns. Because of this, the least square error set of equations is instead solved. These equations can use data from any desired number of FRF measurements.

The Global RFP frequency and damping algorithms consists setting up and solving equation (3.51) to set up the process, the operator must specify the total number of modes, the frequency

band of FRF measurement data to be used, and the number of extra numerator polynomial terms, if desired. When equation (3.51) is solved and the polynomial coefficients determined, they are passed into a polynomial root solver which finds the global frequency and damping estimates.

FRF in terms of polynomial coefficients, c_k

$$h_i = \sum_{k=0}^{m} z_{i,k} c_k \quad i=1,\ldots L \tag{3.51}$$

where

$$z_{i,k} = \frac{\phi_{i,k}}{\sum_{k=1}^{msdes} (\omega_k^2 - \omega_i^2 + j2\sigma_k\omega_i)}$$

$$= \frac{\phi_{i,k}}{g_i} \tag{3.52}$$

$$\sum_{i=1}^{L} \frac{\phi_{i,k}\phi_{i,j}}{|g_i|^2} = \begin{cases} .5 & k = j \\ 0 & k \neq j \end{cases} \tag{3.53}$$

In the matrix form

$$\begin{Bmatrix} h_1 \\ h_2 \\ : \\ h_n \end{Bmatrix} = \begin{bmatrix} z_{1,0} & z_{1,2} & .. & z_{1,m} \\ z_{2,0} & z_{2,2} & .. & z_{1,0} \\ : & : & & : \\ z_{L,0} & z_{L,2} & .. & z_{L,m} \end{bmatrix} \begin{Bmatrix} c_0 \\ c_1 \\ : \\ c_m \end{Bmatrix} \tag{3.54}$$

Least Squared Error Equation

$$\{C\} = \mathrm{Re}\left(\left[Z^*\right]^t \{Y\}\right) \tag{3.55}$$

{Y}= L- vector of measurement data

Once the modal frequencies and damping are known, the mode shape (eigenvectors) can be obtained by solving an eigenvalue set of equations. This type of an approach generally involves the manipulation of large matrices. The approach discussed here is “global” in the sense that global frequency and damping estimates are used, but is “local” in the sense that the FRF measurement are processed one at a time in order to obtain modal residue estimates. These residue estimates are then assembled from all the various measurements to obtain the mode shapes.

The RFP is a non-iterative method which works directly with FRF data in frequency domain. It has advantages of handling noisy measurements and using additional numerator polynomial terms as a means of compensating for the residual effects of out-of-band modes in the curve fitting frequency band. This permits the accurate estimation of modal parameters.

3.3.2 Operational PolyMax

Peeters et al. (2004) presented the PolyMax algorithm which is a polyreference version of the LSCF method. It forms part of the LMS test lab software and uses the right half spectrum model in the estimation of the modal parameters. The motivation of the development of the PolyMax algorithm was due to the fact that while converting the common denominator model in the least square complex frequency to modal model (Peeters et al., 2005) by (1) reducing the residues to a rank one matrix using SVD, the quality of the fit decreased (2) stabilization diagrams were only constructed using eigenfrequencies and damping ratios with participation factors and mode shapes unavailable. Because of this, closely spaced modes erroneously showed up as a single pole (Guillanaume et al., 2003). The PolyMax algorithm overcomes the problems associated with the original LSCF method because of its polyreference version, the use of the right hand matrix fraction model, avoiding of the SVD step in the decomposition of residues and separation of the closely spaced modes. Its advantages include:

a) It estimates the so called denominator transfer function model (Guillanaume et al., 1996). The initial values yielded already very accurate modal parameter with a very small computational effort.
b) Gives a very clear stabilization diagram with participation factors available

c) Singular value decomposition step which decomposes the residues is avoided and that closely spaced poles separated.
d) Non physical poles are estimated with negative damping ratios so that they are not included in the plotting.
e) Has no problems in correctly estimating modes having low damping ratios
f) Does not suffer numerical problems as it is formulated in the Z-domain while the existing frequency domain methods use Laplace domain formulation.

3.3.2.1 PolyMax algorithm

This method uses measured FRF as primary data. The right-matrix fraction model is assumed to represent the measured FRFs (Peeters et al., 2004)

$$[H(\omega)] = \frac{\sum_{r=0}^{p} z^r [\beta_r]}{\sum_{r=0}^{p} z^r [\alpha_r]} \tag{3.56}$$

Where:

$[\beta_r]$ is the numerator matrix polynomial coefficients

$[\alpha_r]$ is the denominator matrix polynomial coefficients

p is the model order.

Using the Z-domain model used in equation 3.56 above with $Z = e^{-j\omega\Delta t}$, Δt is the sampling rate.

Equation 3.56 above can be written for all values of ω of the frequency axis of the FRF data. Basically the unknown model coefficients α_r and β_r are found as the least square solution of this equation after linearization

3.3.2.2 Poles and modal participation

Once α_r is determined, the poles and modal participation factors are retrieved as eigen values and eigen vectors of their companion matrix.

$$\begin{pmatrix} 0 & I & \dots & 0 & 0 \\ 0 & 0 & \dots & 0 & 0 \\ \dots & \dots & \dots & \dots & \dots \\ 0 & 0 & \dots & 0 & I \\ -\left[\alpha_o^T\right] & -\left[\alpha_1^T\right] & \dots & -\left[\alpha_{P-2}^T\right] & -\left[\alpha_{p-1}^T\right] \end{pmatrix} .V = V\Lambda \tag{3.57}$$

The modal participation factors are the last *m* rows of the V matrix, the matrix Λ contains the discrete time poles $e^{-\lambda_i \Delta t}$ on its diagonal. They are related to the eigen frequencies ω_i and damping ratios ζ_i

$$\lambda_i, \lambda_i^* = -\zeta_i \omega_i \pm j\sqrt{1-\zeta_i^2}\omega_i \tag{3.58}$$

This method is similar to what happens in the time domain LSCE method and allows constructing a stabilization diagram for increasing model orders p and using stability criteria for eigen frequencies, damping ratios and modal participation factors.

$$\left[H(\omega)\right] = \sum_{i=1}^{n} \frac{\{v_i\} < l_i^T >}{j\omega - \lambda_i} + \frac{\{v_i^*\} < l_i^H >}{j\omega - \lambda_{_I}^*} + \frac{\left[LR\right]}{\omega^2} + \left[UR\right] \tag{3.59}$$

n = number of modes

$\{v_i\}$ = mode shapes

$< l_i^T >$ = modal participation factor

λ_i = poles

$\left[LR\right]$ and $\left[UR\right]$ lower and upper residuals modeling the influence of the out-of –band modes in the considered band.

In summary, frequency domain, least square complex frequency based procedures namely; the rational fractional polynomial and operational polymax have been presented. The rational fractional polynomial estimates modal parameters using the Laplace domain while operational

polymax uses the Z-domain. Under the RFP, global curve fitting method which curve fits FRF data directly in frequency domain estimates global frequency and damping ratio are estimated in the first step and these estimates are used to estimate residues (mode shapes) in the second step. Operational polymax which uses the z-domain has advantages of giving clear stabilization diagrams and has less computation time.

Frequency domain based methods reviewed have been divided into FDD based methods and LSCF based methods. The methods which follow under these two categories have been discussed. The advantages and disadvantages of each of the methods have been presented. However, as already mentioned in section 3.1, there are different modal parameter methods in OMA divided into frequency, time and time-frequency methods. Only frequency domain methods have been discussed, section 3.4 discusses the time domain based methods.

3.4 Time domain based procedures

3.4.1 Complex Exponential

Complex Exponential (CE) algorithm is one of the first time domain methods to be proposed in 1974 based on Prony's method which can be classified as the first important single input single output parametric method (Zhang et al.,2005). CE algorithm has then been extended into SIMO version based on Least Squares (LS) estimation, and named as Least-squares complex exponential method (Brown et al., 1979).

Least squares complex exponential method exploits the relationship between the impulse response function (IRF) of an MDOF system and its complex poles and residues through a complex exponential. By establishing the analytical links between the two, we can construct an AR model. The solution of this model leads to the establishment of a polynomial whose roots are the complex roots of the system. Having estimated the roots (thus natural frequencies and damping ratios), the residues can be derived from the AR model for the mode shapes. The IRF can be derived from the inverse Fourier transform of an FRF or from random decrement process.

This method begins with the transfer function of an N- MDOF system and is given by:

This method begins with the transfer function of an N- MDOF system is given by:

$$H_{ij}(s) = \sum_{r=1}^{N} \left(\frac{{}_r A_{ij}}{s - s_r} + \frac{{}_r A_{ij}^*}{s - s_r^*} \right) \tag{3.60a}$$

$$\text{or} \quad H_{ij}(s) = \sum_{r=1}^{2N} \left(\frac{rA_{ij}}{s - s_r} \right) \text{for } r > N : {}_r A_{ij} = {}_r A_{ij}^*; s_r = s_r^* \tag{3.60b}$$

The inverse Laplace transform for this transfer function is the IRF given as:

$$h_{ij}(t) = \sum_{r=1}^{2N} {}_r A_{ij} e^{s_r t} \tag{3.60c}$$

For simplicity, the subscript of the transfer function $H_{ij}(s)$ is omitted from the following analysis. If this IRF is sampled at a series of equally spaced time intervals $k\Delta$ (k=0,1,…,2N), then we will have a series of sampled IRF data:

$$h(k\Delta) = \sum_{r=1}^{2N} {}_r A_{ij} e^{s_r tk\Delta} (k = 0,1,....,2N) \tag{3.61a}$$

$$\text{or } h_k = \sum_{r=1}^{2N} {}_r A_{ij} z_r^k \quad (k = 0,1,...,2N) \text{ for } z_r^k = e^{s_r k\Delta} \tag{3.61b}$$

At this point a fitting method called Prony's method will be used for the discrete impulse response data. This method extracts valuable information from a uniformly sampled signal and builds a series of damped complex exponentials or sinusoids. This allows for the estimation of frequency, amplitude, phase and damping components of a signal. By using this method the poles of the system can be found.

All these samples are real-valued data, although the residues ${}_r A_{ij}$ and the roots s_r are complex quantities. It is easy to show all imaginary parts will cancel each other because of the complex conjugates for both ${}_r A_{ij}$ and s_r. the next step is to estimate the roots and residues from the sampled data. This solution is aided by the conjugacy of the roots s_r, therefore z_r. Mathematically, this means that z_r are roots of a polynomial with only real coefficients:

$$\beta_0 + \beta_1 z_r + \beta_2 z_r^2 + ... + \beta_{2N-1} z_r^{2N-1} + \beta_{2N} z_r^{2N} = 0 \tag{3.62}$$

This equation is known as the Prony equation (He and Fu, 2001) the coefficients can be estimated from the samples of the IRF data. Since there are *2N+1* equalities is equation (3.60b), we can simply multiply each equality with a corresponding coefficient β and add all the equalities together to form the following equation:

$$\sum_{k=0}^{2N} \beta_k h_k = \sum_{r=1}^{2N}{}_r A_{ij} \sum_{k=0}^{2N} \beta_k z_r^k \tag{3.63}$$

From equation (3.62) we know that the right-hand side of equation (3.63) becomes zero when Z_r is a root polynomial in equation (3.62). This will lead us to a simple relationship between the coefficients β and the IRF samples, namely:

$$\sum_{k=0}^{2N} \beta_k h_k = 0 \tag{3.64}$$

Equation (3.64) offers a numerical way of estimating the β coefficients. In equation (3.62) we can assign β_{2N} to be one. Taking a set of 2N samples of IRF, one linear equation is formed in equation (3.64). Taking 2N sets of 2N samples of IRF, we have 2N linear equations. The coefficients can be estimated from the linear simultaneous equations:

$$\begin{bmatrix} h_0 & h_1 & h_2 & \cdots & h_{2N-1} \\ h_1 & h_2 & h_3 & \cdots & h_{2N} \\ \vdots & \vdots & \vdots & \vdots & \vdots \\ h_{2N-1} & h_{2N} & h_{2N+1} & \cdots & h_{4N-2} \end{bmatrix} \begin{pmatrix} \beta_0 \\ \beta_1 \\ \vdots \\ \beta_{2N-1} \end{pmatrix} = \begin{pmatrix} h_{2N} \\ h_{2N+1} \\ \vdots \\ h_{4N-1} \end{pmatrix} \tag{3.65}$$

The selection of IRF data samples can vary provided that the h elements in each row are evenly spaced in sampling and sequentially arranged. No two rows have identical h elements. The number of rows in equation (3.65) can exceed the number of β coefficients for the least-square solutions.

With known β coefficients, equation (3.62) can be solved to yield the z_r root. These roots are related to the system complex natural frequencies s_r, as given in equation (3.59b). Since the

complex natural frequencies s_r are determined by the undamped natural frequencies ω_r and damping ratios ζ_r as shown below:

$$s_r, s_r^* = -\zeta_r \omega_r \pm j\sqrt{1-\zeta_r^2}\omega_r \tag{3.66}$$

We can derive the natural frequency and damping ratio of the *rth* mode as:

$$\begin{aligned} \omega_r &= \frac{1}{\Delta}\sqrt{\ln z_r \ln z_r^*} \\ \zeta_r &= \frac{-\ln(z_r z_r^*)}{2\omega_r \Delta} \end{aligned} \tag{3.67}$$

To determine the mode shapes of the system from the IRF data, we can simply rewrite equation (3.60b) in a new form as:

$$\begin{bmatrix} 1 & 1 & \cdots & 1 \\ z_1 & z_2 & \cdots & z_{2N} \\ \vdots & \vdots & \vdots & \vdots \\ z_1^{2N-1} & z_2^{2N-1} & \cdots & z_{2N}^{2N-1} \end{bmatrix} \begin{Bmatrix} {}_1A_{ij} \\ {}_2A_{ij} \\ \vdots \\ {}_{2N}A_{ij} \end{Bmatrix} = \begin{Bmatrix} h_0 \\ h_1 \\ \vdots \\ h_{2N-1} \end{Bmatrix} \tag{3.68}$$

The solution to the above set of linear equations yields the residues. The LSCE method can be summarized as follows: use either random decrement methods or inverse Fourier transform a set of FRFs to form IRFs, and then form linear equations for coefficients β. By the use of Prony equations, natural frequencies and damping ratios can be calculated, while the linear equations of the residues form mode shapes.

3.4.2 Stochastic Subspace Identification

The stochastic subspace identification method is one of the most powerful time domain methods for estimating modal parameters from ambient data. Overschee et al (1996) published a book on the algorithms of SSI triggering the break-through of this method among system control engineers with respect to practical acceptance and application.

Overschee et al (1996) provided a framework which covers both deterministic as well as stochastic estimation algorithms. This framework is not well understood by all engineers for example mechanical engineers have not been trained to address problems with unknown loads enabling them to get used to concepts of stochastic theory, while many civil engineers have been trained to do so to be able to deal with natural loads like wind, waves and traffic, but on the other hand, civil engineers are not used to deterministic thinking (Brincker and Andersen, 2006).

While there exist subspace methods dealing either with deterministic input signals only, with stochastic input only and combined methods, the algorithm presented in this section is only limited to stochastic inputs as it is the case within the application of this method to operational modal analysis. Just like in frequency domain decomposition, the input is not measured and it is assumed to consist of white noise. The properties of Gaussian white noise are (Maybeck, P. 1979):

1) White noise has equal power at all frequencies, i.e. the PSD is constant for all frequencies. This property was also stated in the formulation of frequency domain decomposition.
2) White means that the signal is uncorrelated in time. In other words, if you know the value of the noise signal at specific time there is no way of using this knowledge for a prediction of the value at any other time. The flatness of the PSD is a direct effect of this property.
3) Gaussian reflects the fact that at any given point in time the value of the signal follows a probability density function (PDF) with the shape of the normal distribution also known as Gaussian distribution.

3.4.2.1 Formulation of the algorithm

The system can be considered in classical formulation as a multi degree of freedom structural system (Andersen, 2010)

$$M\ddot{y}(t) + C\dot{y}(t) + Ky(t) = F(t) \tag{3.69}$$

Where M is the mass matrix, C is damping matrix, K is the stiffness matrix and F(t) is the force vector.

The stochastic response from a system can be expressed as a function of time

$$y(t) = \begin{Bmatrix} y_1(t) \\ y_2(t) \\ . \\ . \\ y_m(t) \end{Bmatrix} \tag{3.70}$$

Introduction of the state space formulation takes the classical continuous time formulation to the discrete time domain as follows:

$$x(t) = \begin{Bmatrix} y(t) \\ \dot{y}(t) \end{Bmatrix} \tag{3.71}$$

Let the second order system equation given by equation (3.69) be simplified to a first order equation by introducing the state space formulation:

$$\dot{x}(t) = A_c x(t) + B_c f(t) \tag{3.72a}$$

$$y(t) = Cx(t) \tag{3.72b}$$

Where the system matrix A_c in continuous time and load matrix B_c is given by

$$A_c = \begin{bmatrix} 0 & I \\ -M^{-1}K & -M^{-1}C \end{bmatrix} \tag{3.73a}$$

$$B_c = \begin{bmatrix} 0 \\ M^{-1} \end{bmatrix} \tag{3.73b}$$

Kailath (1980) showed that this formulation has an advantage in that the general solution is directly available for example

$$x(t) = \exp(A_c t)x(0) + \int_0^t \exp(A_c(t-\tau))Bf(\tau)d\tau \tag{3.74}$$

Where the first term is the solution to the homogeneous equation and the last term is the particular solution. To take this solution to discrete time, all variables are sampled like

$y_k = y(k\Delta t)$ and thus the solution to the homogenous equation becomes (Brincker and Andersen, 2006)

$$\begin{aligned} x_k &= \exp(A_c k\Delta t)x_0 = A_d^k x_0 \\ A_d &= \exp(A_c \Delta t) \\ y_k &= CA_d^k x_0 \end{aligned} \tag{3.75}$$

This construction is simply defined by its power series, and in practice is calculated by performing an eigen-value decomposition of the involved matrix and then taking the exponential function of the eigen values. Note that the system matrix in continuous time and in discrete is time is not the same.

3.4.2.2 The Block Hankel matrix

In discrete time, the system response is normally represented by the data matrix

$$Y = \begin{bmatrix} y_1 & y_2 & \dots & y_N \end{bmatrix} \tag{3.76}$$

Where N is the number of data points.

Consider a more simple case where we perform the product between two matrices that are modifications of the data matrix given by equation (3.75). Let $Y_{(1:N-k)}$ be the data matrix where we have removed the last *k* data points, and similarly, let $Y_{(k:N)}$ be the data matrix where we have removed the first data points, then

$$R_k = \frac{1}{N-k} Y_{(1:N-k)} Y_{(k:N)}^T \tag{3.77}$$

Is an unbiased estimate of the correlation matrix at time lag *k*. This follows directly from the definition of the correlation estimate, see for instance Bendat et al., (1986) The Block Hankel matrix defined in SSI is simply a gathering of a family of matrices that are created by shifting the data matrix

$$Y_h = \begin{bmatrix} Y_{(1:N-2s)} \\ Y_{(2:N-2s+1)} \\ : \\ Y_{(2s:N)} \end{bmatrix} = \begin{bmatrix} Y_{hp} \\ Y_{hf} \end{bmatrix} \tag{3.78}$$

The upper half part of this matrix is called “the past” and denoted Y_{hp} and the lower half part of the matrix is called “the future” and is denoted Y_{hf} . The total data shift is 2*s* and is denoted “the number of block rows” (of the upper or lower part of the Block Hankel matrix).

3.4.2.3 The Projection

Operational modal analysis deals with stochastic responses where projection can be defined as a conditional mean (Overschee and De Moor, 1996). It is useful in combining the future into the past defined by the matrix

$$O = E(Y_{hf} \,|\, Y_{hp}) \tag{3.79}$$

Melsa and Sage (1973) suggested that such a conditional mean can for Gaussian processes be totally described by its covariance. Since the shifted data matrices also defines covariances, it is not so strange that the projection can be calculated directly as also defined by van Overschee and De Moor (1996).

$$O = Y_{hf} Y_{hp}^T (Y_{hp} Y_{hp}^T)^{-1} Y_{hp} \tag{3.80}$$

The last matrix in this product defines the conditions, the first four matrices in the product introduces the covariances between channels at different time lags. A conditional mean like given by equation (3.78) simply consist of free decays of the system given by different initial conditions specified by Y_{hp} (Brincker and Andersen. 2006). The matrix is *sM x sM* and any column in the matrix O is a stacked free decay of the system to a (so far unknown) set of initial conditions. Using equation (3.75) any column in O can be expressed by

$$O_{col} = \Gamma_s x_0$$
$$\Gamma_s = \begin{bmatrix} C \\ CA_d \\ CA_d^2 \\ : \\ CA_d^{s-1} \end{bmatrix} \tag{3.81}$$

Now, if we knew the so-called observability Γ_s matrix, then we could simply find the initial conditions directly from equation. (3.81) (it is a useful exercise to simulate a system response from the known system matrices, use the SSI standard procedure to find the matrix **O** and then try to estimate the initial conditions directly from equation. (3.81).

3.4.2.4 The Kalman States

The so-called Kalman states are simply the initial conditions for all the columns in the matrix O, thus

$$\mathbf{O} = \Gamma_s X_0 \tag{3.82}$$

Where the matrix X_0 contains the so defined Kalman states at time lag zero. Again, if we knew the matrix Γ_s, then we could simply find all the Kalman states directly from equation (3.79), however, since we don't know the matrix Γ_s , we cannot do so, and thus we have to estimate the states in a different way. The trick is to use the SVD on the O matrix

$$O = USV^T \tag{3.83}$$

And then define the estimate of the matrix Γ_s and the Kalman state matrix X_0 states by

$$\hat{\Gamma} = US^{1/2}$$
$$\hat{\mathbf{X}}_0 = S^{1/2}V^T \tag{3.84}$$

The so defined procedure for estimating the matrices $\hat{\Gamma}$ and $\hat{\mathbf{X}}_0$ is not unique. A certain arbitrary similarity transformation can be shown to influence the individual matrices, but can also be shown not to influence the estimation of the system matrices.

The Kalman state matrix $\hat{\mathbf{X}}_0$ is the Kalman state matrix for time lag zero. If we remove one block row of O from the top, and then one block row of $\hat{\Gamma}$ from the bottom, then similarly we can estimate the Kalman state matrix $\hat{\mathbf{X}}_1$ at time lag one. Thus by subsequently removing block rows from O all the Kalman states can be defined. Using the Kalman states a more general formulation for estimating also the noise part of the stochastic response modeling can be established. However, in this paper we focus on explaining how the system matrices can be found, and in this context, there is no further need for Kalman states.

The system matrix A_d can be found from the estimate of the matrix Γ by removing one block from the top and one block from the bottom yielding

$$\hat{\Gamma}_{(2:s)}\hat{A}_d = \hat{\Gamma}_{(1:s-1)} \tag{3.85}$$

And thus, the system matrix $\hat{A}_d$ can be found by regression. The observation matrix C can be found simply by taking the first block of the observability matrix

$$\hat{C} = \hat{\Gamma}_{(1:1)} \tag{3.86}$$

3.4.2.5 Determination of modal parameters

First step of finding the modal parameters is to perform an eigenvalue decomposition of the system matrix $\hat{A}_d$

$$\hat{A}_d = \Psi[\mu_i]\Psi^{-1} \tag{3.87}$$

The continuous time poles λ_i are found from the discrete time poles μ_i by

$$\mu_i = \exp(\lambda_i) \tag{3.88}$$

where

$$\lambda_i = \frac{In(\mu_i)}{\Delta T}$$
$$\omega_i = |\lambda_i|$$
$$\varsigma_i = \frac{\mathrm{Re}(\lambda_i)}{|\lambda_i|} \tag{3.89}$$

The mode shape matrix is found from

$$\Phi = C\Psi \tag{3.90}$$

Andersen and Brinker (2010) presented all the three SSI algorithms namely Unweighted Principal Component (UPC), Principal Component (PC) and Canonical Variate Analysis (CVA). These can be described with the use of two weight matrices W_1 and W_2 applied to O_i. Still, O_i is common to all three algorithms. Thus, it is also called the common SSI input matrix.

$$\begin{aligned} W_1 O_i W_2 &= W_1 \Gamma_i \hat{X}_i W_2 \\ &= \begin{bmatrix} U_1 & U_2 \end{bmatrix} \begin{bmatrix} S_1 & 0 \\ 0 & 0 \end{bmatrix} \begin{bmatrix} v_1^T \\ v_2^T \end{bmatrix} \\ &= U_1 S_1 V_1^T \end{aligned} \tag{3.91}$$

(1)The Unweighted Principal Component

This algorithm provides the easiest way to incorporate into the stochastic subspace frame work. As the name says it is an unweighted approach which means that both weight matrices equals the unity matrix, see Overschee et al.(1996)

$$W_1 = I$$
$$W_2 = I \tag{3.92}$$

(2) The Principal Component (PC) method

The Principal Component algorithm determines the system matrices from the singular values and the left singular vectors of the matrix $L_{i.}$ This means that the singular values and left singular vectors of $W_1 0_i W_2$ must equal the singular values and left singular vectors L_i. To accomplish this, the weight matrices are chosen as:

(3) The Canonical Variant Analysis (CVA) method.

The Canonical Variate Analysis algorithm, computes the principal angles and directions between the row spaces of the matrix of past outputs Y_p and the matrix of future outputs Y_f. The matrix of past outputs Y_p is defined in equation (3.80), and the matrix $\boldsymbol{Y_f}$ is defined in a similar manner

$$W_1 = L_i^{-1/2}$$
$$W_2 = I \tag{3.93}$$

Since the weight matrices are the only effective differences, the results of the algorithms should be very similar. The advantage of the CVA algorithm is the ability to estimate modes with a larger difference in energy level. This comes from the fact that CVA evaluates the principal directions of the row spaces rather than the length of the row vectors. On the other hand, according to (Andersen et al.,2010), the algorithm demands a larger state space dimension in order to distinguish weakly excited modes when they are close to well-excited ones.
The advantages of SSI are:

a) No leakage - The SSI algorithms work in time domain and are data-driven methods. Since the model estimation is not relying on any Fourier transformations to frequency domain no leakage is introduced. Leakage is always introduced when applying the Fourier transformation and assuming periodicity. Leakage always results in an unpredictable overestimation of the damping.
b) No problems with deterministic signals (harmonics) - Since the modal parameters are extracted directly by fitting parameters to the raw measured time histories, the presence of deterministic signals, such as harmonics introduced by rotating machinery, does not create problems. Harmonics are just estimated as very lightly damped modes. Methods

relying on the estimation of half power spectral densities all assume that the excitation is broad-banded (white noise) and the presence of deterministic signals introduce bias in the modal parameter estimation.

c) Less random errors- The SSI techniques are born as linear least-squares fitting techniques fitting state space systems with correct noise modeling. The benefit is that low-order model estimators can be used. High-order model estimators are, however, often used to approximate a non-linear least squares fitting problem with a linear least-squares fitting problem. This is an often seen approximation when fitting e.g. polynomial matrix fractions, where a high polynomial order is required. As a result more parameters have to be estimated compared to using a low-order technique and with the same amount of data available, less independent information per estimated parameter is obtained. Consequently the uncertainties of the high-order parameter estimates become significantly larger.
d) All modal parameters are fitted in one operation. All parameters fitted are taking advantage of the noise cancellation techniques of the orthogonal projection of SSI. Other commercially available methods often fit the poles (frequency and damping) first, and then use the noisy spectral data and the estimated poles to fit the mode shapes resulting in poor mode shape estimates.
e)

3.4.3 Eigen value realization algorithm

The eigen value realization algorithm (ERA) is a time domain system identification based on the evolution of the Ho-Kalman method, which introduces the concept of minimum realization (Juang et al., 1985). The minimum realization method identifies a system model with the smallest state dimension that holds an equivalent relationship of input-output as in the real system. The principle of ERA involves identification of system matrix A from free-vibration responses. Suppose an equation of motion of a discrete structural system under acting vector force $f(t)$ be expressed in the first-order form of the state-space equation:

$$\dot{z}(t) = Az(t) + Bf(t) \tag{3.94}$$

Where the matrices are defined as:

$$A = \begin{bmatrix} -M^{-1}K & -M^{-1}C \\ I & 0 \end{bmatrix}$$
$$z(t) = \begin{bmatrix} \dot{x}(t) \\ x(t) \end{bmatrix}$$
$$B = \begin{bmatrix} M^{-1} \\ 0 \end{bmatrix} \tag{3.95}$$

The frequency(ω) and damping ratio(ζ) of the mass M, damping C and stiffness K system appear as conjugate pairs of the eigenvalues of matrix A:

$$\lambda_A = -\zeta\omega \pm \sqrt{1-\zeta^2} \tag{3.96}$$

In the case of free vibrations, the eigenvectors of A become the eigenvectors of the equation of motion. Therefore, once the matrix A can be realized from the measurement, modal parameters of the system can be extracted.

ERA identifies a candidate of matrix A from IRFs of a multi-mode system. The IRF can be shown to be equivalent and contain the same information, and accordingly can be derived using following methods.

a) Measurement of free-decay in time domain directly.
b) Inverse Fast-Fourier Transform (FFT) of the frequency response functions
c) Cross-correlation functions of random response
d) Inverse FFT of the cross-spectral densities of the random responses.

Information from IRF at the discrete k^{th} time sample, defined as, is stacked to form a matrix known as the Hankel matrix 'at time 0':

$$H(0) = \begin{bmatrix} Y_0 & Y_1 & \cdots & Y_r \\ Y_1 & Y_2 & \cdots & Y_{r+1} \\ \vdots & \vdots & \ddots & \vdots \\ Y_s & Y_{s+1} & \cdots & Y_{r+s+2} \end{bmatrix} \tag{3.97}$$

This discrete time sample Y_k is known as the Markov parameter. It contains information from the IRFs, which represent vibration characteristics of a structure, the modal parameters can therefore be identified from the Hankel matrix. The scalar r and s in $\mathsf{H}(0)$ are the parameters that define the number of samples used, and they require a certain balance to cover the long frequency components of IRFs. As more rows and columns added to H(0), the rank increases until it covers all vibration modes that contribute to the responses.

Then, the minimum rank of H(0) is computed and a state matrix A is realized from it. To select the system order, SVD of the Hankel matrix is performed:

$$PDQ^T = SVD[H(0)] \tag{3.98}$$

The rank of the Hankel matrix is selected by retaining the N largest singular values associated with the real modes come first in order, while the smaller singular values associated with computational modes come last in order (Siringoringo et al., 2007). Examining the nonzero floor of the singular values and truncating the matrices P and Q by keeping only their first 2n columns (Zhou and Chelidze, 2007).

Construct $nr \times n$ E_n and $ls \times l$ E_l matrices

$$\begin{aligned} E_n^T &= [I_n \quad 0 \quad \cdots \quad 0] \\ E_l^T &= [I_l \quad 0 \quad \cdots \quad 0] \end{aligned} \tag{3.99}$$

where I_n and I_l are identity matrices.

If we estimate the realization matrices as:

$$\begin{aligned} A &= D_N^{-1/2} P_N^T H(1) Q_N D_N^{-1/2} \\ B &= D^{1/2} Q^T E_l \\ C &= E_n^T P D^{1/2} \end{aligned} \tag{3.100}$$

Then all modal parameters can be estimated using system matrices A and C

The eigenvalues that contain natural frequencies and damping ratios are identified by solving the eigenvalue problem of matrix A. This also means that the eigenvectors of A become the eigenvectors of the system obtained using this transformation:

$$[\phi] = C[\varphi] = E_n^T PD^{1/2}\varphi \tag{3.101}$$

3.4.4 Autoregressive moving average (ARMA) method

The ARMA time series method is used for modal analysis of a structure from measured random responses. The basic idea behind this method is to identify a system and predict its present and future response from the information of its past inputs and outputs. The ARMA model suggests that samples can be related by a finite difference equation as:

$$x_t - \sum_{r=1}^{n} \phi_r x_{t-r} = a_t - \sum_{s=1}^{m} \theta_s a_{t-s} \quad n>m \tag{3.102}$$

Here (s = 1, 2,….., m) is the random input series. n is the order of autoregressive model and m is the order of the moving average. Are auto-regressive coefficients and are moving average coefficients. The terms $\emptyset_r x_{t-r}$ and $\theta_s a_{t-s}$ signify the weighed contribution of the historical samples x_{t-r} and a_{t-s} respectively to the present response x_t

Let $\alpha_{ij}(s)$ be the transfer function defined by $\alpha_{ij}(s) = \frac{x_j(s)}{a_j(s)}$, applying the z-transform to the transfer function will reveal the z-function:

$$\left(1 + \phi_1 z^{-1} + ... + \phi_{2N} z^{-2N}\right)x(z) = (\theta_0 + \theta_1 z^{-1} + \theta_{2N-1} z^{-2N+1})a(z) \tag{3.103}$$

Using the inverse z-transform, equation (3.103) can be converted to the time domain:

$$x_t + \phi_1 x_{t-1} + ... + \phi_{2N} x_{t-2N} = a_t + \theta_1 a_{t-1} + ... + \theta_{2N-1} a_{t-2N+1} \tag{3.104}$$

Taking the first n+1 terms from the left-hand side and m+1 terms from the right-hand side, and embedding negative signs into coefficients ϕ_r $(r = 1,2,\dots,n)$ and θ_r $(r = 1,2,\dots,m)$, equation

(3.104) becomes identical to equation for the ARMA model. However, for an N Dof system, the ARMA model should be written as:

$$x_t - \phi_1 x_{t-1} - .... - \phi_{2N} x_{t-2N} = a_t - \theta_1 a_{t-1} - ... - \theta_{2N-1} a_{t-2N+1} \tag{3.105}$$

For an N Dof system subject to random inputs of zero means ($a_1 = 0$), the response at time t from ARMA model is given as:

$$x_t = \left\{ -x_{t-1} ... - x_{t-2N} a_{t-1} ... a_{t-2N+1} \right\} \begin{Bmatrix} \phi_1 \\ \vdots \\ \phi_{2N} \\ \theta_1 \\ \vdots \\ \theta_{2N-1} \end{Bmatrix} \tag{3.106}$$

If we sample the response $x(t)$ and input a(t) from t = 2N + 1 sequentially to t = 2N + L for a large number L, then equation can be used to construct a set of linear equations from where auto-regressive coefficients and moving average coefficients can be estimated. Knowing the moving average coefficients, the residues of the transfer function can be identified.

The characteristic equation of the system is given as:

$$1 + \phi_1 z^{-1} + \phi_{2N} z^{-2N} = 0 \tag{3.107}$$

With estimated auto-regressive coefficients, equation 3.107 can be used to identify roots z which comes in complex conjugate pairs. These roots are related to natural frequencies and damping ratios of the system. Using the relationship between Laplace transform and z-transform we have:

$$z_r = e^{s_r t} \tag{3.108}$$

where t is the sampling period.

The rth eigenvalue is written as follows:

$$\lambda_r = -\zeta_r \omega_r + j\omega_r \sqrt{1 - \omega_r} \tag{3.109}$$

where ω_r is the natural frequency and ξ_r is the damping ratio.

If $\lambda_r = a_r + jb_r$ then

$$\omega_r = \sqrt{a_r^2 + b_r^2}$$
$$\zeta_r = \frac{-a_r}{\omega_r} \tag{3.110}$$

In summary Modal analysis using ARMA model involves the following steps: (1) identifying the auto-regressive coefficients, (2) identifying complex roots of a characteristic equation and (3) identifying modal parameters from the roots.

3.4.5 Summary of time domain methods

In summary, four time domain based method namely;- complex exponential (CE), eigenvalue realization algorithm (ERA), autoregressive moving average (ARMA) and stochastic subspace identification (SSI) algorithm have been reviewed. CE algorithm is a time domain based method which is based on Prony's theory. It utilizes free impulse responses then formulates a Hankel matrix to form a generalized eigenvalue problem. This problem is a crucial part in the extraction of modal parameters. ERA utilizes free responses and formulates a generalized Hankel matrix, which contains the Markov parameters. Then the realization matrices, which can reproduce system's input-output relationship, are derived. Modal parameters are extracted from the realized system matrices. ARMA incorporates model order selection, model validation and structural mode distinction and extraction. This method allows not only the extraction of modal parameters from a given measured output but also the estimation if their uncertainties on the basis if the covariances matrix of the ARMA model parameters. Modal parameters are extracted by solving a standard eigen decomposition problem of the companion matrix containing AR coefficients.

SSI is the other time domain based method that has been reviewed. It is capable of detecting closely distributed modes and yielding modal parameters for all of them. Since it works in time domain, leakage is not an issue. The main disadvantage of the stochastic method is the less straight forward validation process. Also, due to the time domain nature of SSI, it is not capable of eliminating the negative influence of harmonic excitation components.

All the above time domain methods require data measured from all measurement points on a structure simultaneously. This avoids unnecessary phase difference among responses and ensures that all responses come from the same initial forcing conditions.

Following a review of time domain based methods, section 3.5 reviews the wavelet transform which is a time-frequency domain method.

3.5 Time-frequency domain method

3.5.1 Wavelet transform technique

Wavelet transform is a new identification procedure in operational modal analysis in structural characterization. This technique works in the time-frequency domain and is used to identify the dynamic characteristics of the structural system in terms of natural frequencies, damping coefficients and mode shapes using ambient vibration records. The wavelet transform decouples automatically the modal components hence in analysis of a multidegree of freedom system; the wavelet transform does not need any band-pass filtering procedure (Lardies and Gouttebroze, 2002).

3.5.1.1 The wavelet transform

The wavelet transforms a non stationary signal by transforming its input time domain into a time- scale domain (Staszewski, 1997). Mathematically, wavelet transforms are inner products of the signal and a family of wavelets (Meyer 1993). Let be ψ (t) the analyzing wavelet called the mother wavelet of the analysis. The corresponding family of wavelets consists of a series of son wavelets, which are generated by dilation and translation from the mother wavelet ψ (t) as shown below:

$$\psi_{a,b}(t) = \frac{1}{\sqrt{a}}\psi\left(\frac{t-b}{a}\right), \mathbf{a > 0}, \; b \in R, \tag{3.111}$$

where a is the dilation or scale parameter defining the support width of the son wavelet and b is the translation parameter localizing the son wavelet function in time domain. The function $1/\sqrt{a}$ is used to ensure energy preservation in the wavelet transform. The difference between these wavelets is mainly due to the different lengths of filters that define the wavelength and scaling functions. Wavelets must be oscillatory, must decay quickly to zero and must integrate to zero (Chui, 1992).

Lets decompose a signal $x(t)$ into wavelet coefficients $W_\psi(a, b)$ using the basis of son wavelets $\psi_{a,b}(t)$. Under the hypothesis that $x(t)$ satisfy the condition:

$$\int_{-\infty}^{+\infty} |x(t)|^2 \, dt < \infty \tag{3.112}$$

which implies that $x(t)$ decays to zero as $t \to \pm\infty$, the wavelet transform of $x(t)$ is expressed by the following inner product in the Hilbert space:

$$W_\psi(a,b) = \langle x(t), \psi_{a,b}(t) \rangle = \int_{-\infty}^{+\infty} x(t) \psi^*_{a,b}(t) dt \tag{3.113}$$

where the asterisk stand for a complex conjugate. This shows that the wavelet transform is a linear scalar product normalized by the factor $1/\sqrt{a}$ which measures the fluctuation of the signal $x(t)$ around point b at the scale a. The scaling operation performs stretching and compressing on the son wavelet, which in turn can be used to obtain the different frequency information of the signal to be analyzed. The compressed version is used to satisfy the high-frequency needs, and the dilated version is used to meet low-frequency requirements. The translated version is used to obtain the time information of the signal to be analyzed. As a result, a family of scaled and translated wavelets is created and serves as the base, the base for representing the signal to be analyzed. This means, the wavelet transform $W_\psi(a, b)$ can be considered as functions of translations b with each fixed scale a. It is also important to note that the wavelet transform represents the convolution between the signal $x(t)$ and the wavelet function. This implies that a wavelet can be used for feature discovery if the wavelet used is similar to the feature components (eigenfrequencies and damping coefficients) hidden in the analyzed signal. For the function $\psi(t)$ to qualify as an analyzing wavelet, it must satisfy the admissibility condition (Chui, 1992):

$$0 < c_\psi = \int_{-\infty}^{+\infty} \frac{|\psi(\omega)|^2}{\omega} \, d\omega < \infty \tag{3.114}$$

Where is the Fourier transform of $\psi(\omega)$. Then the wavelet transform can be inverted and the signal $x(t)$ recovered:

$$x(t) = \frac{1}{c_\psi} \int_{-\infty}^{+\infty} \int_{-\infty}^{+\infty} W_\psi(a,b) \psi_{a,b}(t) \frac{dadb}{a^2} \tag{3.115}$$

Note that since $|\psi(\omega)|$ tends to zero when tends to $\pm\infty$, the Fourier transform of the wavelet can be considered as a band-pass filter.

For practical purposes, the possibility of time-frequency localization arises if the wavelet $g(t)$ is a window function, which means $\psi(t)$ that decays to zero as $t \to \pm\infty$:

$$\int_{-\infty}^{+\infty} |\psi(t)| dt < \infty \tag{3.116}$$

and the wavelet transform analyses a signal $x(t)$ only at windows defined by the wavelet function $\psi(t)$. If one assumes a fast decay of $\psi(t)$: the values of $\psi(t)$ are negligible outside a given time domain interval, the transform becomes local in time domain, in this interval.

The frequency localization can be estimated when the wavelet transform is expressed in terms of the Fourier transform. Note $X(\omega)$ the Fourier transform of the signal $x(t)$ and $a\psi^*(a\omega)e^{jwb}$ the Fourier transform of the son wavelet $\psi^*(t-b)/a$. Using the Parsveal's theorem (Meyer, 1993), we obtain

$$W_\psi(a,b) = \frac{\sqrt{a}}{2\pi} \int_{-\infty}^{+\infty} X(\omega) \psi^*(a\omega) e^{j\omega b} d\omega \tag{3.117}$$

and the frequency localization depends on the scale parameter a. Note that this operation is equivalent to a particular filter band analysis in which the relative frequency band width $\Delta\omega/\omega$ are constant and related to the parameters a ,b and to the frequency properties of the wavelet. The local resolution of the wavelet transform in time and frequency is determined by the duration and bandwidth of the analyzing functions given by $\Delta t = a\Delta t_\psi$ and $\Delta f = a\Delta f_\psi$ where Δt_ψ and Δf_ψ are the duration and bandwidth of the wavelet function. The resolution of the analysis is therefore good for high dilation in the frequency domain and for low dilation in the time domain. For Morlet analyzing wavelet function, the relationship between the dilatation parameter a and the frequency f at which the analyzing wavelet function is focused is given by

$a = f_0 f_s / f_w$ where f_0 is the frequency of the wavelet, f_s and f_w are the sampling frequencies of the signal and wavelet respectively.

3.5.1.2 Estimation of modal parameters

Consider a free response of a viscously damped single degree of freedom described by:

$$x(t) = Be^{-\xi\omega_n t}\cos(\omega_n t + \psi_0) \tag{3.118}$$

with ω_n the undamped natural frequency, $\omega_d = \omega_n\sqrt{1-\xi^2}$ the damped natural frequency and ξ the damping ratio. If the system is undamped, that is damping ratio less than 1, the signal $x(t)$ can be considered asymptotic, and therefore the results obtained previously can be used considering:

$$A(t) = Be^{-\xi\omega_n t},$$
$$\varphi(t) = \omega_d t + \psi_0 \Rightarrow \varphi'(t) = \omega_d \tag{3.119}$$

The wavelet transform of the damped sinusoid is

$$W_\psi(a,b) = \frac{\sqrt{a}}{2} Be^{-\xi\omega_n b}\psi^*(a\omega_d)e^{j(\omega_d b+\psi_0)} \tag{3.120}$$

Let $a = a_0 = \omega_0/\omega_d$, where a_0 is the dilatation parameter which maximizes the amplitude of the wavelet transform, corresponding and is related to the analyzed modal frequency of the system. For a fixed value of the dilatation parameter $(a = a_0)$, the wavelet transform modulus is

$$\left|W_\psi(a_0,b)\right| = \frac{\sqrt{a_0}}{2} Be^{-\xi\omega_n b}\left|\psi^*(a_0\omega_d)\right| \tag{3.121}$$

and applying the logarithm to this function we obtain

$$In\left|W_\psi(a_0,b)\right| = -\zeta\omega_n b + In\left(\frac{\sqrt{a_0}}{2} B\left|\psi^*(a_0\omega_d)\right|\right) \tag{3.122}$$

Thus the damping ratio ξ of the system can be estimated from the slope of the straight line of the logarithm of the wavelet transform modulus, assuming that the natural frequency ω_n has been previously estimated say by FFT plot of the signal $x(t)$.

3.6 Chapter Summary

This chapter has presented nine modal parameter estimation techniques in operational modal analysis in details. These have been categorized into frequency domain, time domain and time-frequency domain methods. Below is a summary of each of the methods described. Table 3-1 synthesizes the main features of each of the method.

Frequency domain decomposition based procedures (FDD, EFDD, and CFDD) are based on singular value decomposition in the estimation of modal parameters. They share the same advantages of being simple to use, and can be used also as indicators of harmonics (Brincker et al., 2000). However, they also share disadvantages of the estimates relying on heavily the observation of the analyst to detect modes and have problems with estimating modes with high damping.

Least square complex frequency based procedures (RFP and Operational polymax) which are based on least square solution. The RFP method is based on a common denominator model in the estimation of modal parameters has advantages of handling noisy measurements and allows the use of additional numerator polynomial terms as a means of compensating for the effects of out-of-band mode. It has disadvantages of mode shapes and modal participation factor are difficult to obtain via reduction of the residues to a rank-one matrix using SVD (2) closely spaced modes show up as a single pole. Operational polymax on the other hand is based on modal decomposition of half PSD, computed from FFT of the COR with positive time lags. It has advantages of (1) yielding extremely clear stabilization diagrams (2) suitable for systems with high modal density and both high and low damping (3)does not suffer from numerical problems as it is formulated in the Z- domain.

The time domain based methods (CE, ARMA, SSI, and ERA) share advantages of being fully parametric implying that they do not rely heavily on the observation of the analyst to detect modes and that stabilization diagrams can be constructed by identifying parametric models of increasing order. These diagrams are very valuable in separating the true system poles from the spurious numerical poles. The disadvantage of these methods is that with heavily damped systems, modal parameters tend to suffer and the computation time is high.

The wavelet transform is a time-frequency method which has an advantage of allowing for the adoption of both traditional time and frequency domain system identification approaches to examine non-linear and non-stationary data. This method has not been fully exploited in civil engineering.

In conclusion, the methods that have been reviewed have been applied to different civil engineering structures say bridges, buildings. This calls for further exploitation of the performance of these methods when applied to dams. These modal parameter estimation methods will not give accurate results unless some important practical issues for example instrumentation, data preprocessing and harmonics are dealt with. Chapter four discusses these issues.

Table 3-1: Summary of OMA methods and their features

Method		**Features**
Parametric	LSCE	• Fast to use • Problems with out-band modes
	SSI	• Relatively fast • Data reduction step • Detects harmonics • Successful applications
	ARMA	• Not be practical in some OMA cases • No convincing cases in literature
	ERA	• Successful applications • Limited number of samples
Non-parametric	FDD	• Still picking peaking • Detects closely spaced modes • SDOF extension highly interactive and tedious
	PolyMax	• Uses FRFs • Clear stabilization diagram • Highly automatic
	RFP	• Compensates for out-band mode effects • Handles noisy measurements

4 PRACTICAL ISSUES IN OPERATIONAL MODAL ANALYSIS

4.1 Introduction

Operational modal analysis is has grown over the last two decades. However, there are still some issues that have not been addressed in this discipline. Issues such as instrumentation, data pre-processing and harmonics are of great importance in determining the correct modal parameters of structures in question. If they are not dealt with properly, erroneous results can be obtained. This chapter discusses problems in signal acquisition and the solutions, then issues with signal processing and finally consequences of harmonics and how to deal with them.

4.2 Instrumentation

Dynamic characterization of large structures such as dams requires high performance, large scale, data acquisition and analysis systems. These are so important in that if not properly chosen, interference of external electromagnetic noise will be excessive. Data acquisition involves gathering signals from measurement sources and digitizing signals to storage, analysis and presentation on a computer.

4.2.1 Components of a basic acquisition system

4.2.1.1 Accelerometers

Accelerometers are based on the principle that in a single-DOF spring, mass, damper system, excited via the base, the displacement of the spring is proportional to the acceleration at the base up to a certain frequency. When the damping is low, as in most accelerometers used in vibration testing, this frequency is often taken as 20% of the natural frequency, since the error is then limited to about 0.5 dB, or about 6%. Thus the natural frequency is the most important parameter in defining the upper limit of the useful frequency response, and this is independent of the type of accelerometer. Accelerometers used in vibration work are usually of two types: piezoelectric and piezoresistive. In the piezoelectric types, which are the more common, the inertia force produced by a small mass, when acted upon by acceleration, is applied to a piezoelectric element, which both acts as a spring and generates an electric charge proportional to the acceleration. A piezoelectric accelerometer must be used with a suitable pre-amplifier, which can

be a charge amplifier or a voltage amplifier. The former type is generally preferred, since the sensitivity of the combined system is largely unaffected by the length of the connecting coaxial cable, a problem with voltage amplifiers. The frequency response of piezoelectric accelerometers cannot extend down to 'DC', or constant acceleration. Charge amplifiers are better than voltage amplifiers in this respect, and can be used down to a fraction of 1 Hz.

Piezoresistive accelerometers work on a different principle, in that the inertia force of the mass acts upon an actual spring element, of which the displacement is measured, essentially by strain gages made of semiconductor material, and require a low voltage DC supply. The main advantage of piezoresistive accelerometers over the piezoelectric type is that they can be used when response down to DC is required.

A fairly recent development in accelerometer design is to incorporate some of the amplifier electronic components into the same casing as the accelerometer itself. A point to watch when ordering accelerometers of this type is that sometimes the sensitivity is fixed in the design, and can only be changed by replacing the whole unit.

4.2.1.2 Data acquisition hardware

This acts as the interface between the computer and the outside world. It acts as a device that digitizes incoming analog signals so that the computer can interpret them.

A/D Converter: The A/D converter, a key element in any data acquisition system, is used to convert dc voltages acquired from the transducers into digital data. The measured voltages may correspond to a specific temperature, pressure, flow, or speed. While there are several types of A/D conversion techniques, they can generally be divided into two types: integrating and non-integrating. The integrating techniques measure the average input value over a defined time interval, thereby rejecting many noise sources.

The non-integrating techniques sample the instantaneous value of the input (plus noise) during a very short time interval.

Digital Input: Some data acquisition systems contain a digital input card that senses a digital bit pattern to determine whether an external device is on or off. Digital input cards typically contain 8, 16, or 32 channels that can be used to monitor a number of external devices. For example, a

digital input card can be connected to an operator panel to determine the position of various switches on the panel.

The number of bits used to represent an analog signal determines the *resolution* of the ADC. You can compare the resolution on a DAQ device to the marks on a ruler. The more marks you have, the more precise your measurements. Similarly, the higher the resolution, the higher the number of divisions into which your system can break down the ADC range, and therefore, the smaller the detectable change. A 3-bit ADC divides the range into 23 or 8 divisions. A binary or digital code between 000 and 111 represents each division. The ADC translates each measurement of the analog signal to one of the digital divisions.

4.2.1.3 Signal condition

Sometimes transducers generate signals too difficult or too dangerous to measure directly with a data acquisition system. This can be cases when dealing with noisy environments, high or low signals or simultaneous. Signal condition is essential for an effective data acquisition system. It maximizes the accuracy of a system, allows sensors to operate properly and guarantees safety. Hence, it is important to choose the right system with a signal condition device.

Signal conditioning is used to amplify, attenuate, shape, or isolate signals from transducers before they are sent to the measurement hardware. Signal conditioning converts the signal to a form that is better measured by the system, or in some cases, makes it possible to measure the signal at all. Examples of signal conditioning include:

i). Amplification of small signals
ii). Attenuation of large signals
iii). Thermocouple compensation for temperature measurements
iv). Current sourcing for 2-wire and 4-wire resistance measurements
v). Filtering to remove system noise
vi). Shunt resistors for current measurements

4.2.2 Characteristics of a good data acquisition system

i). A good system should be able to record data that is significantly larger than what is expected. The solution is to take advantage of the dynamic range of available instrumentation and data acquisition systems.

ii). It should monitor test data and display and react to the results. Two facets:-Data viewing for sanity: usually takes the form of multi-channel, graphic displays in time of spectral-domain format. Challenge is to present huge amounts of data in a format that the test engineer can understand and react if there are unexpected results.

iii). The system must acquire data for the duration of the experiment. In addition, it is often desirable to monitor the test throughout the whole period that the system is energized. The product of the number of channels, the sample rate and the duration defines the quantity of data that must be stored and reduces.

iv). The system (exclusive of the transducer) should be accurate to within 1% over the measurement frequency range. This requires a very stable system and analytical, post-test data correction (Smith and Hollowell, 1991)

v). It should provide a high dynamic range (signal-to-noise ratio) that allows conservative selection of gain gauges.

vi). Detection of saturation/overload at the system in-put (before any filtering is performed). Anomalies should be displayed and logged, and the acquired data should be tagged.

4.2.3 Problems in signal acquisition

i). Aliasing is an error that cannot be removed after measurement is made and often cannot be recognized. Properly implemented sigma-delta acquisition systems attenuate these errors to values below the system measurement resolution. Error signals will look exactly like the response from vibration transducer and cannot be rejected once the data are collected.

ii). Systems that do not have adequate alias-signal rejection will produce corrupt data sets. Worse the fact that the results are corrupt usually cannot be detected

iii). Noise and signal corruption due to external magnetic and electric fields must be minimized. Proper amplifier, wiring and grounding techniques are required to take advantage of the concepts.

4.3 Data Pre-processing

4.3.1 Introduction

Before applying system identification algorithms, some pre-processing techniques must be applied to experimental measurements. By using these techniques, noise in measurements can be reduced, and then the IRF or FRF data of the system can be found clearly. Windowing, averaging, filtering are the main pre-processing techniques (Fig.4.1).

4.3.2 Sampling time domain records

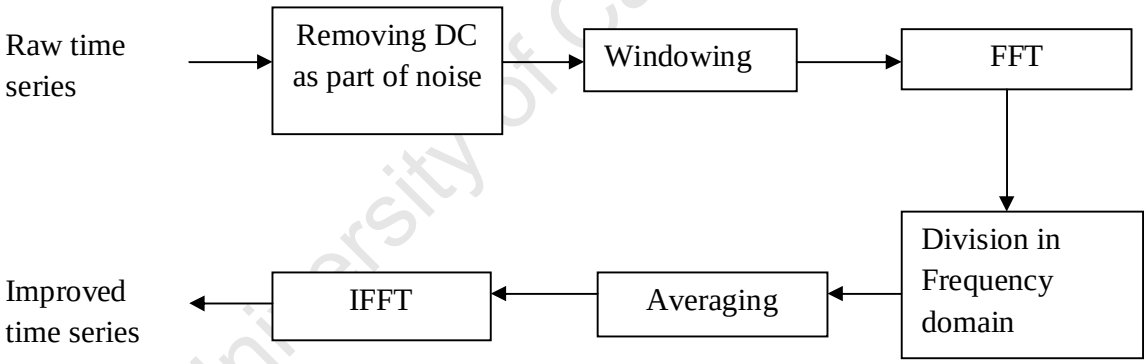

Figure 4.1: Data Processing procedure

The first signal processing task to perform on the measured data is usually decimation which reduces the frequency range to the frequency range of interest. For instance, if a signal has been sampled at 200 Hz, i.e. 200 samples per second, then the Nyquist frequency is 100 Hz and the Spectral Density Estimates will be defined in the interval from 0 - 100 Hz. If only one is interested in the modal properties lower than 10 Hz you should decimate the signal 10 times.

If one wants to work in the frequency domain it is desirable to decimate to zoom to the range of interest. If one is working with parametric models in the time domain, you should decimate in order to introduce poles only in the frequency range of interest.

The decimation is basically a process where some samples are discarded. However, in order to prevent aliasing the signal is first low-pass filtered and then the excessive samples are discarded. If the signal is decimated 2 times then every 2nd sample is kept and the rest is discarded. If the signal is decimated 3 times every 3rd sample is kept the rest is discarded, etc.

Now, since the anti-aliasing filter is active into the frequency range of the decimated signal, you should only use the modal results in the frequency range from 0 to 80 % of the new Nyquist frequency.

Note: Decimation is an irreversible process which will change the data of the project permanently. After the decimation has been applied to the data the decimation of this configuration is reset and if the project contains any estimated modes they will all be deleted.

4.3.3 Filtering

Filtering is used to attenuate unwanted the signal components in the frequency domain. A typical reason for filtering could for example be to high-pass filter the signal to get rid of a slowly varying zero-offset of the signal, or to band-pass filter the signal to reduce the necessary parametric model order for cases with high modal density (Andersen P., 2010)

There is a possibility to apply one of the following types of filters: low-pass, high-pass, band-pass and band-stop. In each case the filter is of the Butterworth type and filter orders between 1 and 50 can be selected. The Butterworth filter is a good all-round filter that is simple to use. At the specified cut-off frequencies it attenuates 3 dB.

Filtering reduces the effect of aliasing (an effect that causes different signals to become indistinguishable), a low pass filter can be used during sampling, to artificially cut out frequencies higher than the highest frequency of interest, which may alias themselves with lower frequencies due to sampling and degree of freedom calculation process

A major source of error in DFTs is the appearance of aliased frequencies. The resulting DFT would indicate a spike at the frequency of the signal, although the original signals contain two very distinct frequencies (one higher and aliased with the lower).

4.3.4 Windowing

Windowing is simply defined as multiplying the signal by a typical window function. This process is used to minimize edge effects that results in spectral leakage in the FFT spectrum. Leakage is a problem which is a direct consequence of the need to take only a finite length of time history coupled with the assumption of periodicity. Figure 4.2 shows an example of two DFTs calculated from the different sample lengths of the same signal. In the second case, due to non-periodicity of the sample length recorded, the DFT is incorrect due to leakage of energy to adjacent frequencies.

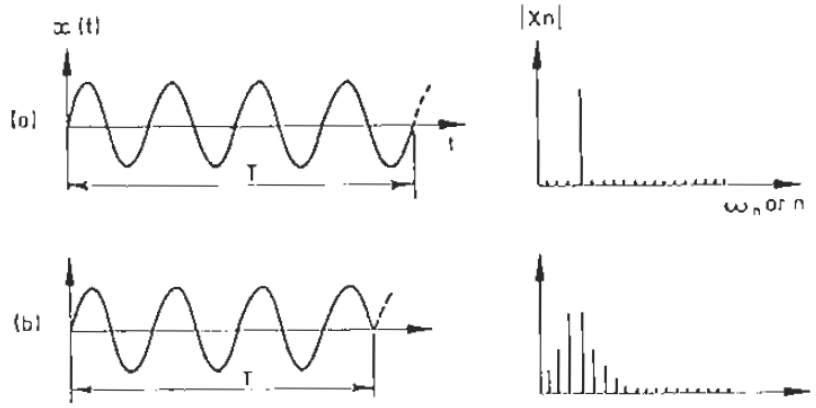

Figure 4.2: DFTs calculated at different sample lengths of a time signal (Kemp, 1994)

It is seen that leakage distorts the spectrum and makes it inaccurate. Leakage cannot be eliminated from its spectrum, but the amount can be reduced. This is done by applying a special weighting function to the time domain data. These are called windows and must be applied to the time domain traces before FFT is applied to them. The effect of these windows is shown in figures 4.3, 4.4 and 4.5. The available windows include:

a) Hanning window: This is for wide band signals and it is effective in reducing leakage in the spectrum of a broad band signal such as a random signal. In particular, this window reduces the spread of the spectrum surrounding resonant peaks which is important for modal parameter estimation.

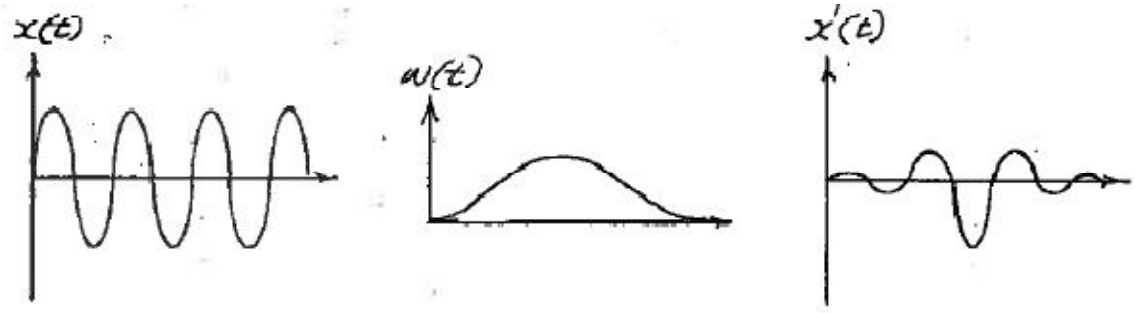

Figure 4.3: Hanning Window (Ewins, 1984)

b) Flat Top windows: This is good for narrow band signals such as sinusoidal signals. This window makes peak values of a sinusoidal signal more accurate, but also makes the peak wider.

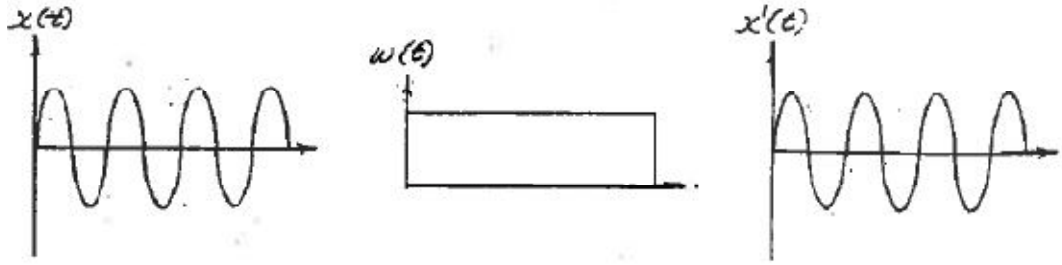

Figure 4.4: Flat Top Window (Ewins, 1984)

c) Exponential widow: This should be applied to transient or impulse response signals that do not completely decay in the sampling window. This window artificially damps the signal towards zero before the end of the window.

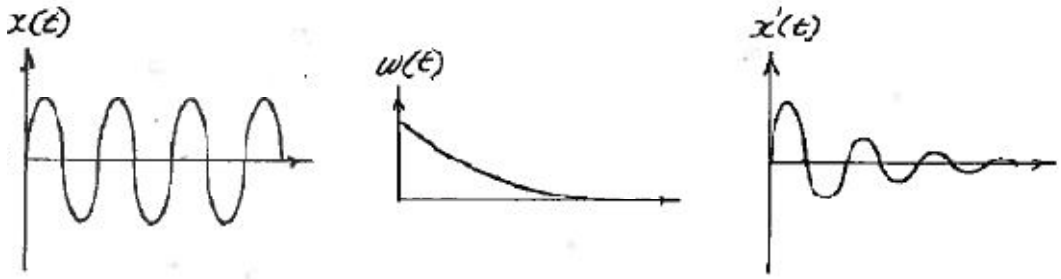

Figure 4.5: Exponential Window (Ewins, 1984)

4.3.5 Steps in data preprocessing

Data preprocessing of the signals is performed before any modal parameter estimation can be done. The preprocessing tasks include:

a) Detrend: The best straight line fit is removed from the data. This removes the DC-component that can badly influence the identification results.
b) High pass filtering: to remove any unwanted components that may obscure any curve fitting process in the analysis
c) Decimation: specifying the order of decimation (fraction of the original sampling frequency, and the number of spectral lines of the Fourier analysis)
d) Spectral estimation: This is performed using the periodgram method (Welch technique) with an overlap specified by the user and a weighing window. This ensures that all data are equally weighted in the overlapping process and minimizes leakage and picket fence effects. The Welch method performs a splitting of time series, and then an overlap of the windowed segments, before averaging them altogether. This technique minimizes the spectral noise and artifacts effects.

4.4 Harmonics in operational modal analysis

Testing civil engineering structures as compared to testing mechanical structures is advantageous in that ambient excitations are nearly always broad banded and multiple input. This makes response measurements obtained from such structures extremely suitable for all popular

estimation algorithms in operational modal analysis. They all rely on the assumptions that the input forces are derived from Gaussian white noise and are exciting in multiple points.

However, even with good measurements system it is impossible to prevent the harmonics from sinusoidal excitations to appear in the acquired data, which means that also the modal estimation algorithms must be able to handle the presence of harmonics. Presence of harmonics is not only limited to mechanical applications, but also in civil engineering applications for example gravity dams have rotating parts in terms of turbines.

In the presence of harmonic excitation, standard OMA procedures can still be applied and the harmonic response components are then identified as pseudo-modes of the system with theoretically zero damping (Mohanty and Rixen, 2005). In practice, however, the identified damping of the pseudo modes (the harmonic response) will not be exactly zero and the analyst cannot always distinguish between harmonic response and true eigen response.

In many practical cases, the harmonic frequencies are known for a given system, say in case for dams where there are turbines generating electricity. If the harmonic frequencies are unknown, they can be evaluated by assuming the harmonic frequency signal is much stronger than the response signal of the system. So, in the auto-spectrum or cross-spectrum of the response signal, peaks due to harmonic frequencies would be distinct and can be accurately known.

4.4.1 Consequences of harmonic components

The consequences of having harmonic components present in the response depend on both the nature of the harmonic component (number, frequency and level) and the modal parameter extraction method used. Jacobsen (2006) points out that the presence of harmonic components in the response is not always a problem. However, it is very important to be able to identify potential modes as being either harmonic components or true structural modes and to know the consequences and the pros and cons of the different identification techniques. It should however be noted that harmonic components cannot be removed by simple filtering as this would in most practical cases significantly change the poles of the structural modes and thereby the estimated values of natural frequency and modal damping. The other problem is that harmonic components can be potentially mistaken as being structural modes.

4.4.2 Identification of harmonics in OMA

Harmonics can be identified using either frequency domain methods or stochastic subspace identification methods. Jacobsen et al (2006) presented an overview of various methods for identifying harmonic components and structural modes. These methods include Short Time Fourier Transform (STFT), Singular Value Decomposition (SVD), Visual Mode Shape Comparison, Modal Assurance Criterion (MAC), Stabilization diagrams and Probability Density Functions (PDFs).

4.4.2.1 Short time Fourier transform

In OMA, data acquisition is done by recording time histories. A pre-requisite for extracting the modal parameters is that all frequencies of interest are sufficiently excited. How long excitation time is needed depends on various factors such as the spectral shape and duration of the excitation signal, the complexity of the test object and the quality of the data acquisition. However, as a rule of thumb, the time histories should be around 500 times longer than the period of the lowest mode of interest:

$$T_{\min} \geq 500 / f_{\min} \tag{4.1}$$

To optimize the settings of the frequency range, frequency resolution and the length of the time histories, the first step in an OMA test should be to make one or more broadband trial measurements. These measurements will also disclose information of the structural behavior of the test object and the nature of the excitation. The Short Time Fourier Transform (STFT) is an easy-to-use tool for this purpose. By dividing the time history for each measurement channel into smaller time records, calculating the FFT of each time record and displaying the FFT auto spectra in a 3D plot as a function of time. The STFT is a powerful first indicator of structural modes and harmonic components. When responses are shown in a contour plot, structural modes are shown as thick vertical lines. Harmonic components are shown as thin vertical lines for stable conditions (Figure. 4.6 say at 500 Hz).

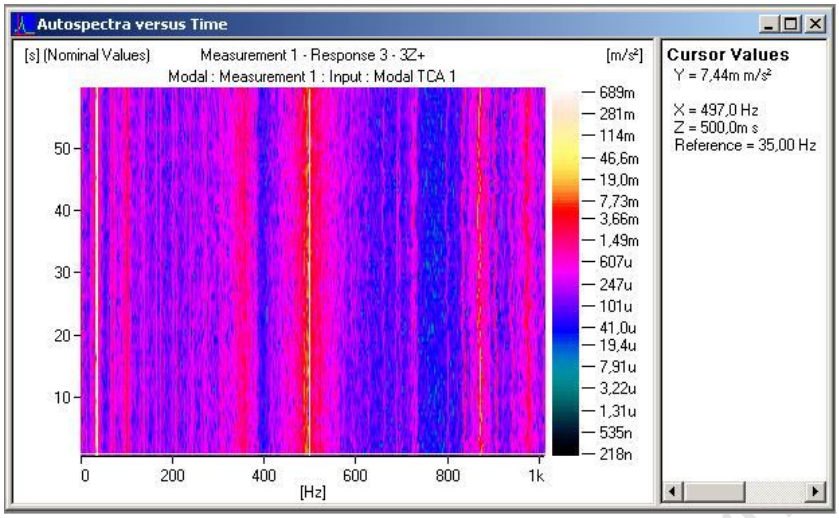

Figure 4.6: Short time Fourier transform showing harmonic presence (Jacobsen, 2006)

4.4.2.2 Singular value decomposition

Another harmonic indicator is the Singular Value Decomposition (SVD) tool. Using the SVD algorithm on the spectral density response matrix for each frequency, the response matrix [R] is transformed into matrices containing singular values [S] and singular vectors [U] and [V]:

$$[R] = [U][S][V]^H = \sum_{i=1}^{n} u_i s_i v_i^H \tag{4.2}$$

where n is the number of responses and the superscript H denotes the Hermitian operator i.e. complex conjugation and transposing.

For a shaped broadband white noise signal exciting the structure, the rank of [S] will be 1 at frequencies, where only one mode is dominating and higher, if closely-coupled modes or repeated roots are present. In the case of harmonic components, a high rank will be seen at these frequencies as all modes will be excited (Jacobsen et al., 2008). The rank will correspond to the number of responses assuming the dynamic range in the measurement is sufficiently high.

The SVD plot is also useful for validating if sufficient data has been measured. If a high rank is obtained, but no clear peaks are seen, it indicates that an insufficient number of cycles have been measured to identify especially heavily damped modes. This lack of data will result in loss of mode separation.

4.4.2.3 Visual Mode Shape Comparison

Visual validation of the mode shapes should always be done as it in many cases clearly reveals whether a calculated "mode shape" is from a true structural mode, a computational mode or an Operating Deflection Shape (ODS). This is especially true, if the structure is relatively simple and the boundary conditions well defined.

When a harmonic component is far away from a structural resonance, the deflection pattern will be a combination of several excited modes and the loading forces acting on the structure. However, when a harmonic component is close to an isolated structural resonance, the deflection pattern will resemble the mode shape and thus can be mistaken for being a mode shape.

4.4.2.4 Modal Assurance Criterion

It expresses how similar the shapes are by calculating the coherence between them. Where the visual mode shapes comparison gives visual feedback through animations, the MAC returns a value between 0 and 1 for each pair of shapes.
As a harmonic component will excite all modes, the MAC value between a true structural mode shape and an ODS will show high correlation, if the frequency of the ODS is close to the frequency of the mode shape. On the other hand, the MAC value between two closely spaced structural modes will, in general, show low correlation. The MAC value between two ODS will depend on the modes being excited.

4.4.2.5 Stabilization diagrams

In modal analysis, a stabilization diagram or chart is an important tool that is often used to assist the user in separating physical poles from computational ones. It is obtained by repeating the analysis for increasing model order n. For each model order, the poles are calculated for the estimated denominator coefficients. The stable poles are then graphically presented in ascending model order in a so called stabilization chart. Estimated poles corresponding to physically relevant system, modes tend to appear for each estimation order at nearly identical locations, while the computational poles tend to jump around. These computational poles are mainly due to presence of noise and harmonics.

Using SSI techniques, a stabilization diagram showing stable, unstable and noise modes is used to select the optimal state space dimension. For modes to be classified as stable, they must fulfill certain mode indicator requirements for which one is a valid range of damping ratios. By adjusting this range, both harmonic components and non physical modes can be filtered out thereby only indicating the true structural modes as stable modes. Goursat et al., 2010 has introduced an improved version of SSI method also commonly referred to as Crystal clear SSI method is automatically deals with with harmonics in OMA

4.4.2.6 Kurtosis

The idea is that probability density function (PDF) for a structural mode excited by stochastic excitation differs significantly from the PDF for deterministic excitation such as sinusoidal excitation.

The kurtosis of a stochastic variable x provides a way of expressing how peaked or flat the PDF of x is. The kurtosis is defined as the fourth central moment of the PDF normalized with respect to the standard deviation as follows:

$$\gamma = \frac{E\left[(x-\mu)^4\right]}{\sigma^4} \tag{4.3}$$

where μ is the mean value of x and E is the denoting the expectation value..

often the number 3 is subtracted from equation above as this givesa kurtosis of zero, when x follows as normal distribution:

$$\gamma = \frac{E\left[(x-\mu)^4\right]}{\sigma^4} - 3 \tag{4.4}$$

Using equation above, a PDF with a positive kurtosis is said to be leptokurtic, if negative it is said to be platykurtic. A PDF with a zero kurtosis is said to be mesokurtic. Leptokurtosis is associated with PDFs that are simultaneously peaked and have flat tails. Platykurtosis is associated with PDFs that are simultaneously less peaked and have thinner tails. For a pure structural mode, the PDF will be normally distributed and hence the kurtosis will be zero while the PDF of a harmonic component is associated with leptokurtosis (Jacobsen et al., 2006).

The significant difference in the statistical properties of a harmonic component and a narrowband stochastic response of a structural mode can be used as a harmonic indicator. By separating each potential mode by band-pass filtering and subsequently calculating the Probability Density Function (PDF) on the result, the shape of the PDF will be quite different in the two cases. For a pure structural mode, the PDF will be normally distributed as shown in the left plot of Figure 4.7. The PDF is given by:

$$y = f\left(x|\mu,\sigma\right) = \frac{1}{\sigma\sqrt{2\pi}} e^{\frac{-(x-\mu)^2}{2\sigma^2}} \tag{4.5}$$

where y is the probability density of the stochastic variable x given the mean value μ and the standard deviation σ.

In the case of a pure harmonic component, the PDF will have two distinct peaks (Figure. 4.8) approaching infinity at ±a, where *a* is the amplitude of the harmonic component. The PDF is given by:

$$y = f\left(x|a\right) = \left(\pi \cos\left(\arcsin(x/a)\right)\right)^{-1} \tag{4.6}$$

In many practical measurements, where closely-coupled modes and harmonic components are present, the resulting PDF will be a combination of the two unique PDF shapes. Still it is often possible to identify the potential modes by using the PDF.

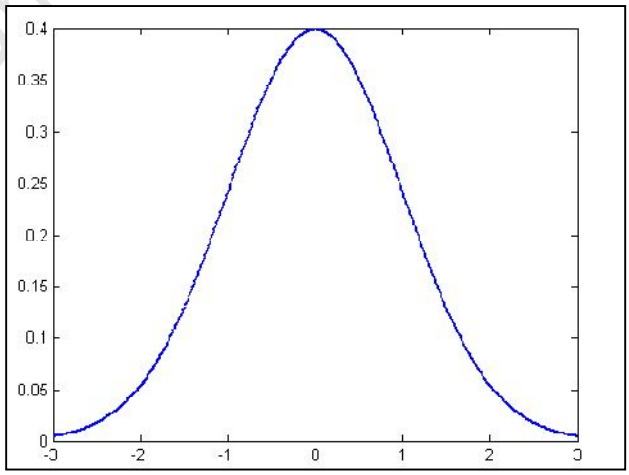

Figure 4.7: Probability density function of stochastic excitation (Jacobsen, 2006)

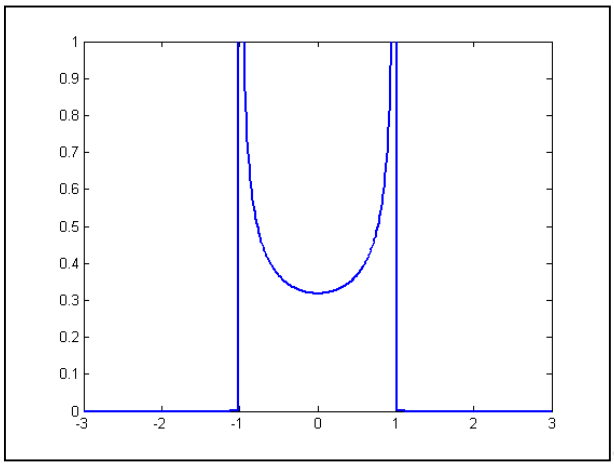

Figure 4.8: Probability density function under sinusoidal excitation (Jacobsen, 2006)

4.4.2.7 Fast Kurtosis checking

When detecting harmonics, calculating the kurtosis for every frequency line for every channel can be very time consuming. Since there is much redundant information in a full-sized PSD-matrix G_{yy}, including all measurement channels of a large test setup, it might not be necessary to include all measurement data into the calculation of harmonic detection. The use of projection channels reduces the amount of data by eliminating redundant information.

For a system with q measurement channels, the spectral density matrix $G_{yy}(f)$ of the meaasured responses typically consist of much more rows/columns than there are structural modes. Many of the rows/columns ae linear dependent resulting in a rank deficiency of the spectral matrix $G_{yy}(f)$. For such a system there is consquently a substantial amount of redudancy, indicating that it might not be necessary to include all of the measurement channels in the algorithm for the harmonic indicator. The subset of measurement channels to be used is called projection channels (m)

Selection of the projection channels is based on a simple correlation analysis calculating the correlation coefficients between measurement channels,

$$C_{ij}^2 = \frac{E\left[\left(y_i(t)y_j(t)\right)^2\right]}{E\left[\left(y_i(t)y_i(t)\right)\right]E\left[\left(y_j(t)y_j(t)\right)\right]} \tag{4.7}$$

where E is the expectation operator

The number of projection channels can be determined using the procedure below:

a) In a multiple test set up, a good intial choice is to use the reference channels as projection channels. This is because reference channels correlate most with the other channels, since they are present in all data sets

b) If the test is performed in a single data set, find the channel i that correlates most with other channels. This channel most likely contains maximum physical information. The channel i is found, where the function W_i is at maximum.

$$W_i = \sum_{j=1}^{n} \left| C_{ij} \right| \qquad j \neq i, i = 1,....q \tag{4.8}$$

where n is the number of measurement channels.

c) Discard channels that have insignificant correlation with any other channel. It might be bad due to a faulty sensor.

d) Subsequently, select the channel with the lowest correlation to the previously selected projection channels. It should introduce the most new information.

The number of projection channels required can be found by applying the Singular Value Decomposition (SVD) to the spectral densities matrices

$$USV^H = G_{yp}(f) \tag{4.9}$$

Where index y indicate the measurement vector y(t) and p the subset of channels selected as the projection channels. The matrices $G_{yp}(f)$ and S both have dimension $n_y \times n_p$ S is a diagonal matrix consisting of m singular values.

By plotting the singular values for all frequencies for every projection channel, all modes will be revealed. The lower singular value curve should approximate a horizontal line over the frequency range of interest, and the other singular value curves should show good mode separation. In that case, the choice of projection channels is optimal as more projection channels will just create new horizontal singular value curves with no additional information. Otherwise more or less projection channels should be used.

4.5 Chapter Summary

The chapter described in details issues which are of concern in operational modal analysis. These included: instrumentation, data preprocessing and harmonics. Problems associated with signal acquisition, characteristics of good data acquisition systems and the solutions to the problems are discussed under this section. Filtering, decimation, windowing and the effects of different windows in reducing leakage form part of the data preprocessing process that has been reviewed. Various powerful and yet very easy-to-use techniques to deal with the issue of harmonics were reported. These include: Short Time Fourier Transform, Singular Value Decomposition, Visual Mode Shapes Comparison, Modal Assurance Criterion, Stabilization Diagram and Probability Density Function.

Concrete dams are stiff structures hence their behavior differs from that of bridges and buildings. They exhibit low natural frequencies and have close modes; therefore while carrying out OMA on such structures the practical issues discussed above have to be considered. The instrumentation should be so sensitive that all the existing modes are detected. Sometimes, there are harmonics on dams, for example the presence of a generator and the opening and closing of sluice gates. Therefore several procedures of detecting these harmonics need to be implemented such that they are not mistaken for structural modes.

Following a thorough literature review in chapters:- 2, 3 and 4, chapter 5 concentrates on the methodology of this thesis. The chapter describes how experimental work was done, how the methods reviewed in chapter 3 were implemented and how the special issues in OMA were addressed.

5 METHODOLOGY

5.1 Introduction

Ambient vibration testing (AVT) of dams has been going on for the last 20 years. This is so because AVT advantages over FVT of being cheap to conduct and is carried out while the structure is under operational conditions. In chapter 2, a literature review of the past experiences of ambient vibration testing on concrete dams was presented. These tests were carried out mainly to determine the dynamic characteristics of dams and calibration of finite element models.

In the extraction of modal parameters from ambient tests of dams reported, peak picking method which is a parametric method was used by most of the researchers. However, there are several modal parameter estimation techniques in time domain, frequency and time-frequency domain which have been developed and have not been tested on dams. This research fills that gap by studying the performance of these methods on dams.

Following the reviews in chapters 2, 3 and 4, chapter 5 concentrates on how ambient vibration testing was carried on two arch dams in South Africa. The performance of several modal parameter estimation techniques is studied and it is discussed how the practical issues are addressed.

Experimental work involved ambient vibration testing of two arch dams namely Roode Elsberg and Kouga dams. Modal parameters from both dams were extracted from tests using commercial software, i.e. ME'Scope Ves and ARTeMIS Extractor Pro 2010 software.

Using analysis of variance, natural frequencies from the different techniques were compared to see if there were any significant differences between the results from the methods. Mode shapes from the different techniques were compared using modal assurance criteria (MAC).

Validation of the natural frequencies from Roode Elsberg dam was done by comparing the experimental results with the Finite Element Model (FEM) results. This was done to identify which method or set of methods perform best on dams.

5.2 Extraction of Modal Parameters

Modal parameter estimation methods described in chapter three were implemented in two commercial software i.e. ARTeMIS Extractor Pro and ME 'Scope Ves 5.0. Below is a description on how modal parameters were obtained using the various techniques available.

5.2.1 ARTeMIS Extractor Pro 2010

In order to be import measured data into ARTeMIS Extractor, the geometrical information of the instrumentation needs to be specified in a format that is suitable as input for the software. This geometrical information includes the positions of the accelerometers on the tested structure as well as their direction of measurement. This was done by creating a SVS Configuration File (see appendix A) is an ASCII file in Notepad editor. The SVS Configuration File is the file that specifies the title of the project, the sampling interval, the geometry of the structure, DOF information (measurement locations and directions), and the data file names and the organization of the data in different test setups.

Once the SVS configuration file was created, then it was possible to import the measured data into the software. Signal processing was the next step carried out such that the data could be cleaned before the actual extraction of the mode parameters. The signal processing procedure is described in section 4.3.5.

Extraction of modal parameter procedures in ARTeMIS followed in this piece work are given below in detail:

a) Frequency domain decomposition

   The software estimates spectral density matrices from raw time series data and performs singular value decomposition density matrices automatically when data is processed. Then peaks of the average singular values (Figure. 5.1) were picked representing the frequency of the picked mode. Using the animation tab, the inspection of the estimated made shape was made.

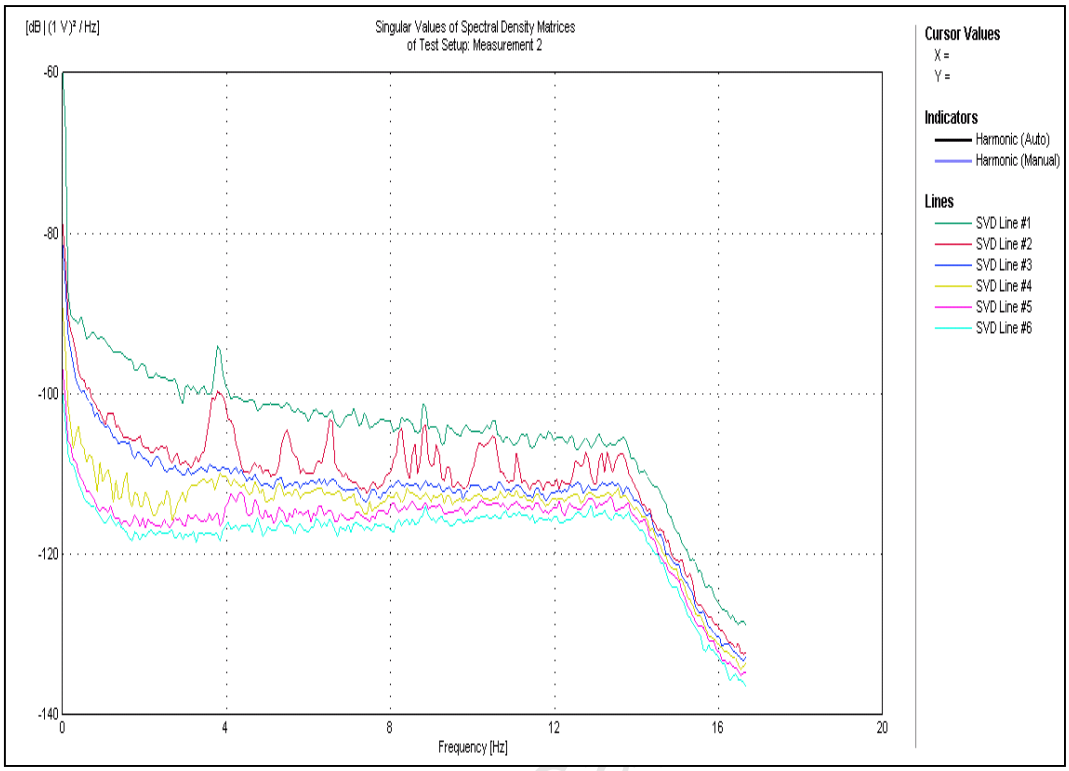

Figure 5.1: Singular value decomposition values for FDD

b) Enhanced frequency domain decomposition

The same procedure for determining the frequency was followed as in FDD but the difference between FDD and EFDD is not only to obtain a reference frequency but also a mode shape to be used in EFDD modal estimation. A reference mode was picked and the frequency estimated. To validate the estimated mode shape (natural frequency and damping ratio) by animation, all set ups were shifted to one of the tests set up (measurement 1). MAC rejection level of 0.8 was used to verify the identified SDOF spectral bell. (Figure.5.2). MAC rejection level controls how many singular values that are included in the identified SDOF displayed in the frequency domain window.

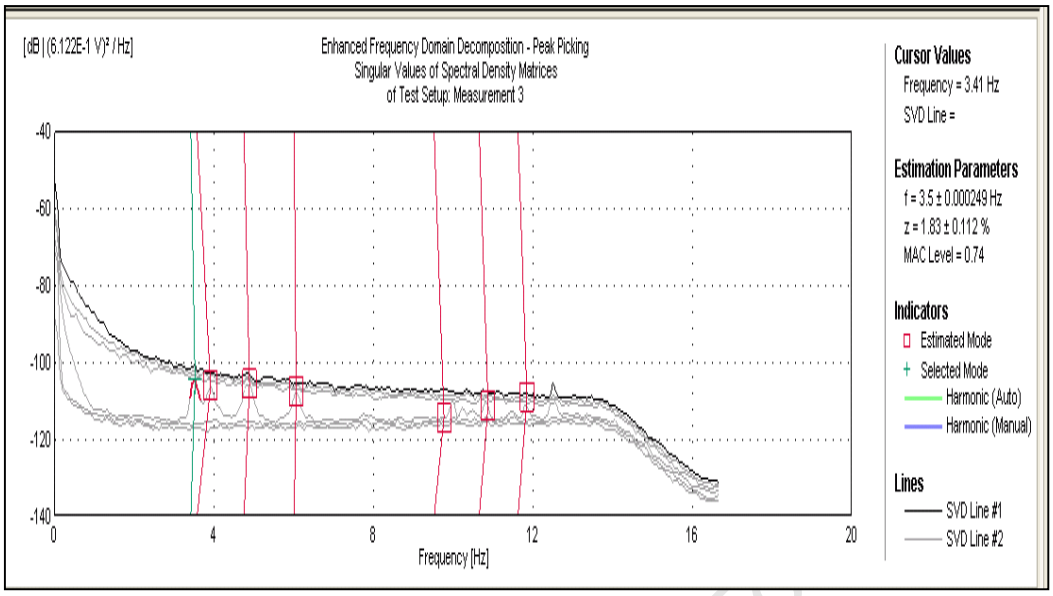

Figure 5.2: enhanced frequency domain decomposition

c) Curve frequency domain decomposition

Modal estimation in CFDD was divided into two steps: (1) perform the FDD peak picking and (2) use FDD identified mode shapes to identify the SDOF spectral bell function and from these bells natural frequency and damping ratio can be estimated using frequency domain curve fitting technique. The same procedure as EFDD was followed in choosing the MAC rejection level for verification of the SDOF spectra bell identified although this time a curve fit of the SDOF bell is also shown (Figure.5.3)

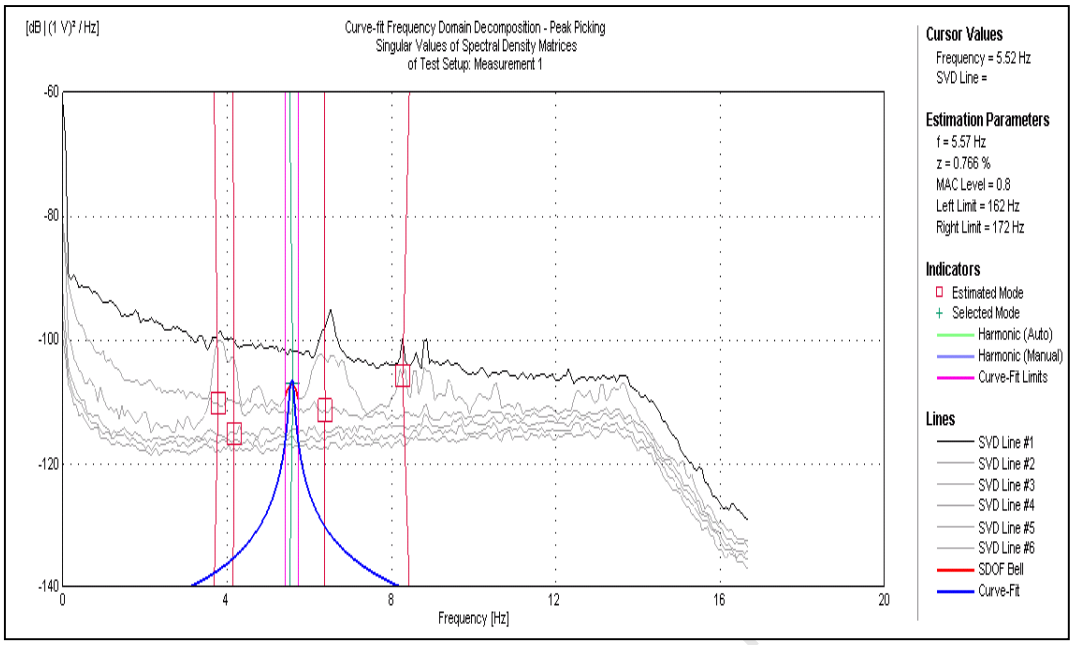

Figure 5.3: curve fitting frequency domain decomposition

d) Stochastic subspace identification

The SSI method involved estimating a range of state space modes which was initially chosen as a maximum of 90 in the signal processing control configuration editor. All the SSI methods i.e. CVA, PC and UPC followed the same procedure. Models with a state space dimension from 20 to 80 were estimated. A stabilization diagram (Figure.5.4) was clearly observed showing stable, unstable modes and noise. From the indicator tab the frequency resolution, maximum and minimum damping ratios, mode shape MAC and mode amplitude MAC were all varied until stable modes were obtained. Using the select and link tab mode shapes are estimated. This was applied to all test setups.

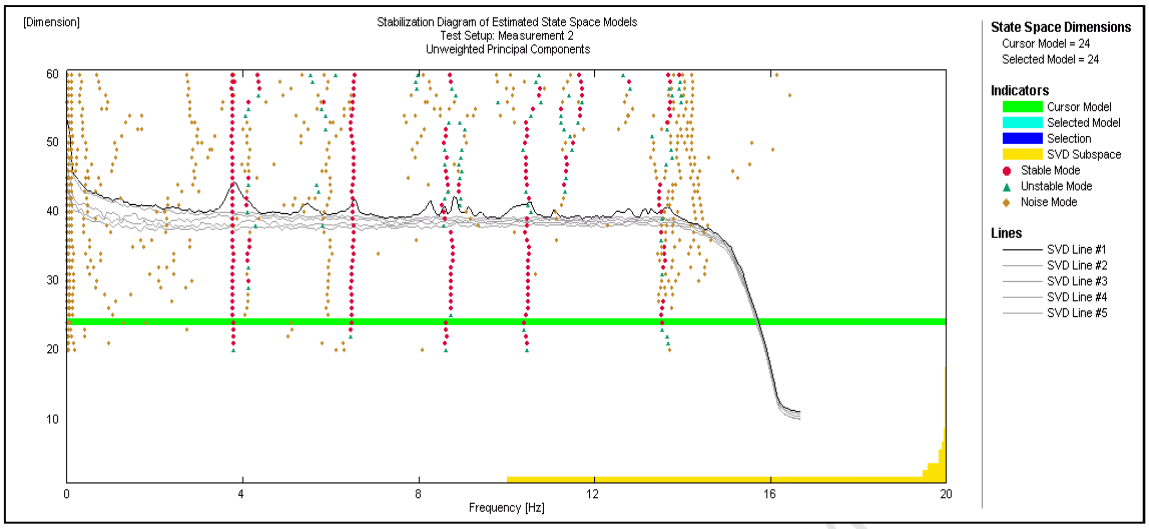

Figure 5.4: Stabilization chart showing stable and unstable modes and noise

5.2.2 ME 'Scope Ves 5.0

a) Rational Fractional Polynomial

Frequency response functions in particular direction either in the vertical, horizontal or radial direction were chosen and overlaid. Using the stabilization tab, AF polynomial (an extension of orthogonal polynomial) was chosen as a method of analysis. To obtain stable modes on the chart, suitable frequency resolution, minimum poles and damping tolerance were carefully chosen. Natural frequencies and damping ratios were obtained, while the mode shapes were determined from the residues and shapes saved.

b) Complex Exponential

Frequency response functions in particular direction either in the vertical, horizontal or radial direction were chosen and overlaid. Using the stabilization tab, AF polynomial (an extension of orthogonal polynomial) was chosen as a method of analysis. To obtain stable modes on the chart, suitable frequency resolution, minimum poles and damping tolerance were carefully chosen. Natural frequencies and damping ratios were obtained, while the mode shapes were determined from the residues and shapes saved.

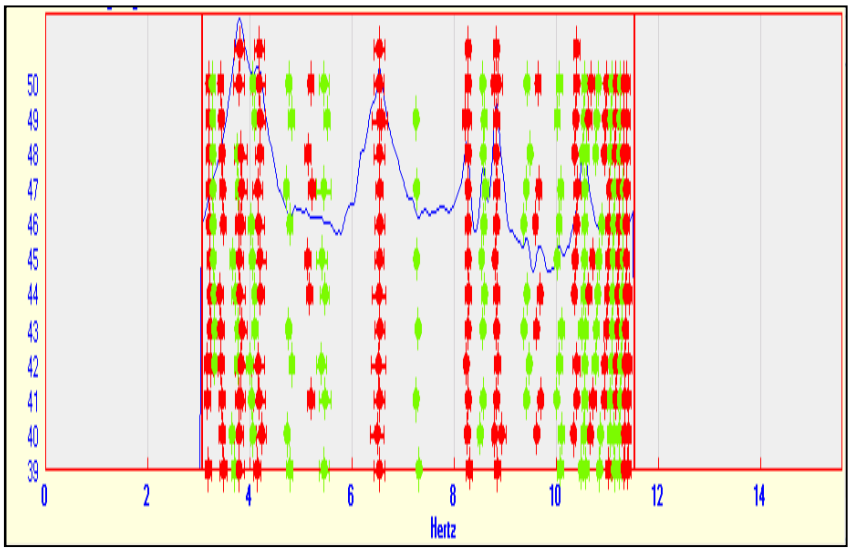

Figure 5.5: Stabilization chart for complex exponential

5.3 Comparison of modal parameters

The modal parameters to be compared included natural frequencies and mode shapes. Natural frequencies were compared using analysis of variance described in section 5.3.1.1 while the mode shapes were compared using modal assurance criteria presented in section 4.4.2.4.

5.3.1 Natural frequencies

5.3.1.1 Analysis of Variance

Analysis of variance (ANOVA) is a method for testing the hypothesis that there is no difference between three or more population means. This method is used to test the null hypothesis that the population mean of two or more means are the same. The t-test is used for testing the null hypothesis that the population mean of two means are the same. The t-test, which is based on the standard error of the difference between two means without increasing the Type I error rate, can only be used to test differences between two means. Conducting multiple t-tests can lead to severe inflation of the Type I error rate (false positives) and is NOT RECOMMENDED. It uses data from all groups to estimate standard errors, which can increase the power of the analysis.

ANOVA is often used for testing the hypothesis that there is no difference between a number of treatments.

One-way ANOVA considers one treatment factor with two or more treatment levels. The goal of the analysis is to test for differences among the means of the levels and to quantify these differences. If there are two treatment levels, this analysis is equivalent to a t test comparing two group means. This method is robust to moderate violations of its assumptions, meaning that the probability values (*P*-values) computed in ANOVA are sufficiently accurate even if the assumptions are violated.

The assumptions taken in analysis of variance are:

i). Each of the populations is Normally distributed with the same variance (homogeneity of variance)

ii). The observations are sampled independently; the groups under consideration are independent.

The objective of analysis of variance is to determine whether population means differs. The null and alternative hypotheses are stated:

$$H_0 : \mu_1 = \mu_2 = \mu_3 = ...\mu_n \qquad (5.1)$$

$$H_1 : \text{at least one population mean differs.}$$

where μ_i is the mean of population *i*.

i). If the null hypothesis is true then the between-groups variance and the within-groups variance are both estimates of the population variance

ii). If the null hypothesis is not true, the population means are not all equal, then will be greater than the population variance, it will be increased by the treatment differences.

To test the null hypothesis we compare the ratio of variances of two samples to 1 using an F-test

Thus, if the null hypothesis is true, each observation consists of overall mean μ plus a realization of the random error component ε_{ij}.

Let x_{ij} = observation *j* in group *i*

$\bar{x}$ = sample mean of group i

$\bar{\bar{X}}$ = mean of all observations

N = total sample size

The ANOVA partitions the total variability in the sample data into two component parts. Then, the test of the hypothesis in Equation 5.2 is based on a comparison of two independent estimates of the population variance. The total variability in the data is described by the **total sum of squares** (Montgomery et al., 2003)

$$SS_T = \sum_{i=1}^{a}\sum_{j=1}^{n}\left(x_{ij}..\bar{\bar{X}}\right)^2 \tag{5.2}$$

The partition of the total sum of squares is given by the following definition.

$$SS_T = SS_E + SS_{Treatment} \tag{5.3}$$

Equation 5.3 above implies that the total variability in the data can be divided into a sum of squares of differences between treatment means and the grand mean denoted $SS_{Treatment}$ and a sum of squares of differences of observations within a treatment from the treatment mean denoted SS_E

$$SS_{Treatment} = \sum_{i=1}^{a}\frac{x_i^2}{n} - \frac{X^2}{N} \tag{5.4}$$

The number of degrees of freedom can also be partitioned corresponding to the sum of squares as described in equation above…

If there are $an = N$ observations, thus SS_T has $an-1$ degrees of freedom. There are a levels of the factor, so $SS_{Treatment}$ has $a-1$ degrees of freedom. Also, within any treatment there are n replicates providing n-1 degrees of freedom with which to estimate the experimental error. Since there are a treatments, we have a(n-1) degrees for error. Therefore, the degrees of freedom partition is

$$an-1 = a-1+a(n-1) \tag{5.5}$$

There is a ratio called mean square of treatment which relates $SS_{Treatment}$ and its corresponding degree of freedom, i.e.

$$MS_{Treatments} = \frac{SS_{Treatments}}{(a-1)} \tag{5.6}$$

The corresponding ratio called error mean square relating SS_E and degrees of freedom such that;

$$MS_E = \frac{SS_E}{[a(n-1)]} \tag{5.7}$$

5.3.1.2 Testing null hypothesis (F-test)

If the null hypothesis is true, the F statistic has an F distribution with $(a-1)$ and $a(n-1)$ degrees of freedom in the numerator/denominator respectively. If the alternate hypothesis is true, then F tends to be large. We reject H_0 in favor of H_1 if the F statistic is sufficiently large. The factor F_0 is given by:

$$F_0 = \frac{MS_{Treatments}}{MS_E} \tag{5.8}$$

As with other hypothesis tests, we determine whether the F statistic is large by finding a corresponding P-value which indicates the probability of getting a mean difference between the groups as high as what is observed by chance. The lower the *p*-value, the more significant the difference between the groups

5.3.1.3 F distribution

The F distribution is the continuous distribution of the ratio of two estimates of variance. It has two parameters: degrees of freedom numerator (top) and degrees of freedom denominator

(bottom). The F-test is used to test the hypothesis that two variances are equal and its validity of is based on the requirement that the populations from which the variances were taken are Normal.

Table 5-5: Anova output table

Source of Variation	**Sum of Squares**	**Degrees of freedom**	**Mean Square**	**F_0**
Treatments	$SS_{Treatments}$	$a-1$	$MS_{Treatments}$	$\frac{MS_{Treatments}}{MS_E}$
Error	SS_E	$a(n-1)$	MS_E	
Total	SS_T	$an-1$		

The sum of squares of differences between treatment means and grand mean is given by $SS_{Treatments}$ while sum of squares of differences of observation within a treatment from the treatment mean is denoted by SS_E

5.3.2 Mode shapes

Comparison of mode shapes across all the employed methods was done using the modal assurance criterion as described in section 4.4.2.4. Mode shapes from rational fractional polynomial and Complex exponential methods were compared separately from Frequency domain decomposition based procedures and the stochastic substance identification based procedures since they are incorporated in ME' Scope ves 5.0 software and ARTeMIS Extractor Pro 2010 respectively.

5.4 Validation of results

For comparison, a numerical modal analysis with Finite Element Method (FEM) developed by Makha (2009) of Roode Elseberg dam was used. This model was developed using ABAQUS software with an objective of choosing the reliable dynamic elastic moduli of concrete and foundation for the dam such that the results from the model could match with the experimental results. The objective of FEM analysis is to validate the proper OMA algorithm to use while dealing with ambient data of dams. In order to find out which method had the greatest error,

absolute error method was used. This is defined as the difference between the analytically determined and experimentally determined natural frequencies. It is numerically as:

$$Error = \left| f_a - f_e \right| \tag{5.9}$$

where f_a and f_e are the analytical and experimental natural frequencies respectively.

5.5 Experimental work

As part of the experimental work of this thesis, a concrete arch dam was tested. The aim of the tests was to provide experimental data to be used in comparing modal parameter estimation techniques.

5.5.1 Roode Elsberg Dam

Roode Elsberg dam (Figure. 5.6) is a double curvature concrete arch dam with a centrally situated overspill section. It was built in 1968, situated on the Sanddrift River 30 km from Worcester, Western Cape Province, South Africa. The height above the lowest foundation is 72 m, the length of the crest is 274m and the gross capacity of the reservoir is 8.210 million m^3. The dam was constructed to provide supplementary water, so as to create a more assured supply of water for irrigation to the farms in the Hex River Valley. There is no machinery located close to the dam meaning that no disturbing dam vibrations generated by machinery occur.

Figure 5.6: Roode Elseberg dam

5.5.1.1 Field test equipment

The test program devised for this dam was largely determined by the restriction of testing to 1 day, number of accelerometers and the type of data acquisition system available. The vibration responses were measured with accelerometers and the time series data obtained were used to obtain the dynamic properties. These accelerometers were usually distributed on the crest of the dam and connected to the computer –controlled data acquisition system. The following section describes the test equipment used during the ambient vibration testing of Roode Elsberg dam.

Accelerometers

Q-Flex QA-700 accelerometers shown in Fig 5.7 below manufactured by Honeywell were used in measuring vibration responses from the dam. These accelerometers have the following characteristics: (1) Sensitivity of 6 V/g, (2) Intrinsic noise < 7 for a range of 0-10 Hz and (3) Resolution < 1μg

Figure 5.7: Forced balanced accelerometers

Data acquisition System

Specialized data acquisition hardware was needed to properly acquire the vibration signals from the dam. The system was used is manufactured by National Instruments with channels that can simultaneously acquire each channel with 24-bit high-resolution delta-sigma analog-to-digital converters (ADCs). The system has anti-aliasing filters to prevent aliasing and noise from affecting the measurement quality.

Measurements were taken by a data acquisition system (DAQ) built from hardware by National Instruments and using National Instruments' Lab VIEW software. The accelerometers were connected to NI PXI-4472B device cards mounted into a NI PXI 1045 chassis which was connected via fiber cable to a PCI card of an ordinary PC workstation running Windows 2003 (Figure. 5.8). Programs in Lab VIEW are called "virtual instruments" (VI). Such a virtual instrument has been programmed in order to configure the hardware, trigger data acquisition, process read data samples and export them into ASCII files in Universal File Format (UFF).

Figure 5.8: Computer used as part of the data acquisition system

5.5.1.2 Experimental procedure

Full scale ambient response tests at the dam were performed on 19th April, 2010 with the reservoir level being 25.9 m. Three forced balanced accelerometers mounted orthogonally to each other on a supporting steel plate leveled using a bubble level on the surface with three adjustable screws were used to measure the vibrations. The traveling accelerometer method was used in this field work. In this method, one set of accelerometers (Piezometeric type) was kept at a fixed location as a reference (block 1), and the other set (Q-A forced balanced type) was roved along different locations on the structure. The selection of the reference point is very important to the results obtained. Each data set is then composed of the reference accelerometers signal and the other set measuring the response at the specified point (channels).

To measure vibration responses of blocks 1-8, (see measurement gird, Figure.5.9) a long cable through the gallery of the dam was connected to the data acquisition system set up near block 1. This cable was then connected to the roving accelerometers. This was useful as there was no need to shift equipment in order to obtain data from blocks far away from the set up area. Measurement point grid (Figure 5.9 below) consisted of seventeen 3-D measurement points distributed over the dam crest.

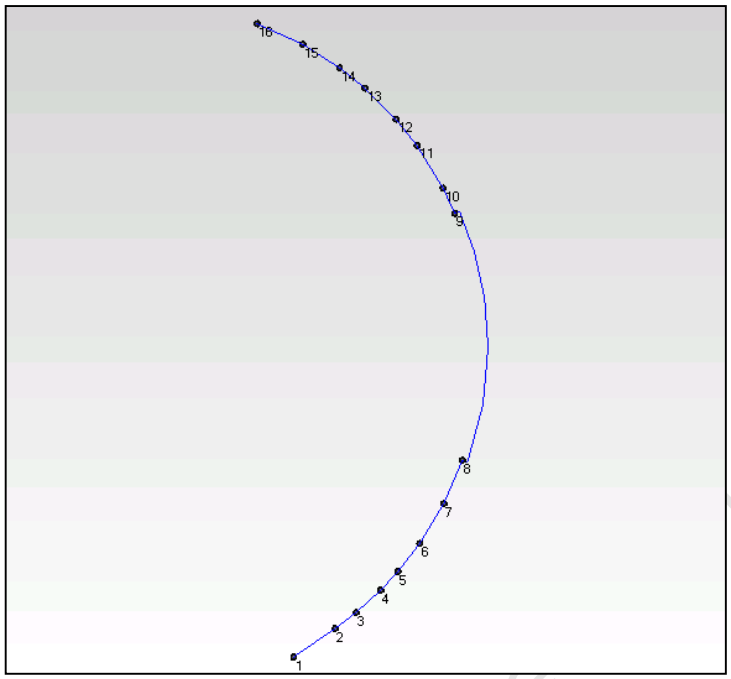

Figure 5.9: Measurement point grid of the dam

5.5.2 Kouga Dam

Kouga dam (Figure. 5.10) is a double curvature arch dam 82 m high with a storage capacity of 128.7 million m^3. Provision was made in the design to allow for a future rising of the water level by 15.2 m. The construction of the wall marked the beginning of an era of double curvature arch dams in South Africa. Besides the normal central overspill section, Kouga dam has flood-control sluice gates with chute and has a catchment area of 388700 ha.

Kouga Dam supplies irrigations water to the Kouga and Gamtoos valleys as well as drinking water to the Port Elizabeth metropolitan area via the Lourie, South Africa balancing dam. The Kouga Dam was also built to serve as a flood-control dam for floods originating from the catchment area of the Kouga River and to decrease the effects of these floods in the lower Gamtoos area.

Figure 5.10: Kouga dam

5.5.2.1 Test procedure

Ambient vibration measurements were taken along the upper gallery of the dam wall. The total number of test locations being 23 (Figure. 5.11). Measurements were taken at each of the blocks in three directions namely, vertical, horizontal and radial to the dam wall. The travelling accelerometer method was used.

Three roving force balance accelerometers were used in the testing of Kouga dam and three piezoelectric accelerometers with a sensitivity of 1V/g were used as fixed accelerometers. The accelerometers were mounted on a geodetic survey bracket mounted on the dam wall inside the gallery (Figure. 5.12.)

Data acquisition was done via the National Instruments 8 channel dynamic signal analyzer (NI PCI 4472B). All the six inputs were simultaneously sampled with a 24 bit resolution at 1000Hz.

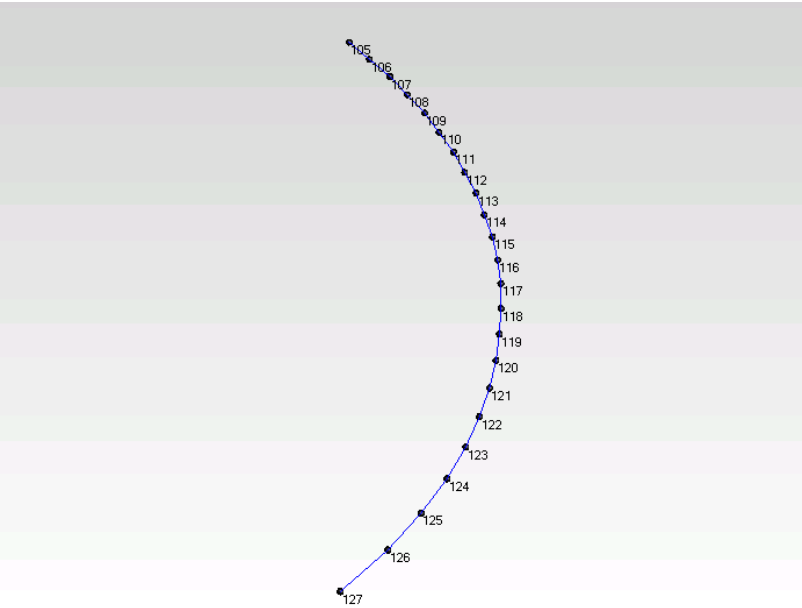

Figure 5.11: Measurement grid of Kouga dam

Figure 5.12: Arrangement of accelerometers mounted on a geodetic survey bracket

5.6 Chapter Summary

Dams are large civil engineering structures difficult to excite mechanically and even when it is possible, the costs involved are high. Ambient vibration testing provides an effective and economic means of identification of modal parameters of dams. This is because it has the advantages of being inexpensive and testing the structure in its operating conditions.

The main challenge in operational modal analysis has been extracting modal parameters from ambient test data of dams. Different researchers have developed techniques which are being used in modal parameter identification. There are three main groups of output-only modal identification methods namely, non-parametric methods developed in frequency domain, parametric methods in time domain, and wavelet transform in time-frequency domain. This chapter dealt with the experimental work and how modal parameters were estimated using the methods described in chapter 3. Ambient vibration tests of Roode Elsberg and Kouga dams have been described, i.e. instrumentation used and the actual testing carried out. Also described in this chapter are the commercial software (ARTeMIS Extractor Pro 2010 and ME'Scope ves 5.0) which were used to analyze the ambient data received from both dams. Under these commercial software, the different modal parameter estimation techniques have been described for example how they estimate the modal parameters. Methods which were used in the comparison of modal parameters have been described. These methods include: analysis of variance for comparing natural frequencies and modal assurance criterion for comparing mode shapes. Validation of results with finite element method for Roode Elsberg dam using error difference method has also been presented. Chapter six discusses results of the experimental investigations.

6 DISCUSSION AND ANALYSIS OF RESULTS

6.1 Results

6.1.1 Natural frequencies and damping ratios

The modal properties of both Kouga and Roode Elsberg dams were determined using the procedures described in chapter 3 using ARTeMIS Extractor Pro 2010 and ME' scope Ves 5.0 version. Table 6.1 shows the natural frequencies of first six modes of Kouga dam. Table 6.2 shows the radial natural frequencies of the first seven modes of Roode Elsberg dam. Tables 6.3 and 6.4 show the corresponding damping ratios (percentages) of Kouga and Roode Elsberg dams respectively. Please note that frequency domain decomposition (FDD) method does not determine damping ratios hence they are not presented in the results.

Figure 6.1 shows the radial frequency response functions (FRFs) of Kouga dam. The first dominant natural frequency is around 3.8 Hz.

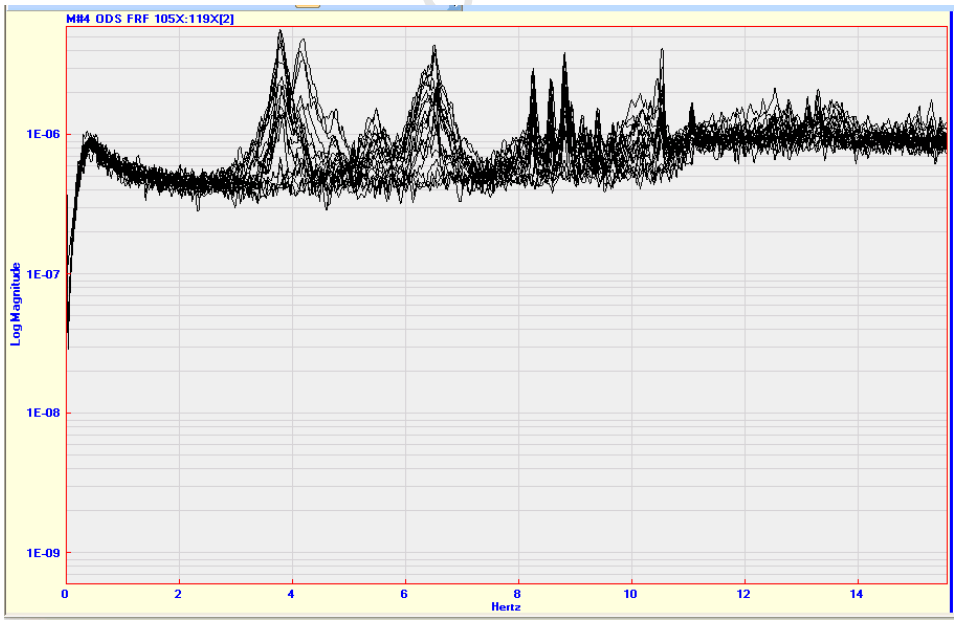

Figure 6.1: Radial FRFs of Kouga dam

Table 6-1: Natural Frequencies of Kouga dam

Mode/Method	RFP	CE	FDD	EFDD	CFDD	SSI-UPC	SSI-PC	SSI-CVA
1	3.78	3.8	3.776	3.729	3.739	3.777	3.795	3.785
2	4.09	4.18	4.232	4.102	4.183	4.166	4.162	4.161
3	_	_	5.469	5.362	5.542	_	_	_
4	6.53	6.52	6.445	6.414	6.416	6.548	6.58	6.542
5	8.27	8.27	8.268	8.088	8.24	_	_	_
6	8.83	8.84	8.854	8.599	8.848	8.48	8.518	8.544

Table 6-2: Damping ratios of Kouga dam

Mode/Method	RFP	CE	EFDD	CFDD	SSI-UPC	SSI-PC	SSI-CVA
1	1.51	2.36	1.245	0.985	0.796	1.524	1.21
2	1.04	2.44	0.697	0.673	4.139	2.367	3.759
3	-	-	0.662	0.695	-	-	-
4	0.739	1.72	0.672	0.556	1.196	1.333	1.105
5	0.455	0.887	0.256	0.257	-	-	-
6	0.676	0.687	0.351	0.321	3.319	3.239	2.975

Table 6-3: Natural Frequencies of Roode Elsberg dam

Mode/Method	RFP	CE	FDD	EFDD	CFDD	SSI-UPC	SSI-PC	SSI-CVA
1	3.54	3.44	3.52	3.38	3.49	3.53	3.53	3.50
2	_	_	3.91	3.59	3.86	3.92	3.99	3.91
3	4.82	4.84	4.88	4.74	4.84	4.83	4.86	4.69
4	6.42	6.52	6.06	5.99	6.09	_	_	_
5	7.59	7.2	7.62	7.53	7.62	7.99	8.05	7.99
6	8.24	8.33	8.59	8.42	8.63	_	_	_

Table 6-4: Damping ratios of Roode Elsberg dam

Mode/Method	RFP	CE	EFDD	CFDD	SSI-UPC	SSI-PC	SSI-CVA
1	0.449	0.823	0.617	0.938	1.467	1.966	1.444
2	_	_	0.575	0.819	1.416	2.099	2.572
3	0.496	0.794	0.470	0.7	1.459	1.416	2.923
4	0.381	1.84	0.519	0.490	_	_	_
5	0.439	1.18	0.351	0.335	0.208	3.305	1.961
6	0.433	0.578	0.075	0.245	_	_	_

The estimates of the damping ratios shown in tables 6.2 and 6.4 show a more significant variation. This does not come unexpectedly, as estimating damping parameters is the most difficult part of modal identification. The advantages and disadvantages of different techniques have the most significant effect onto this parameter: If the enhanced frequency domain decomposition technique cannot create a high quality correlation function out of the selected frequency band, curve fitting a logarithmic decay yields a low quality damping ratio. That was the case in several modes. Similarly, the Curve-fit FDD estimation algorithm had difficulties to fit a spectral bell for close modes and modes that are not well excited. SSI based methods seem to estimate high damping ratios.

Estimated damping ratios vary not only across the employed identification algorithms but also vary significantly across different modes and even for the same mode in different measurement setups. Reasons for a divergence from theory presumably are that the sensors, connector lines, and the adhesive tape for fixation contribute significantly to the structural damping.

6.1.2 Mode shapes

Modes shapes of Kouga dam were estimated using all the methods. Figures 6.2-6.6 and 6.7-6.11 show selected modes shapes of Kouga dam estimated using rational fractional polynomial method and frequency domain decomposition method. Note that the mode shapes of the two different methods differ because they were created in different commercial software. The mode

shapes of Roode Elsberg dam are not reported as during the time for testing it was impossible to access the spillway area.

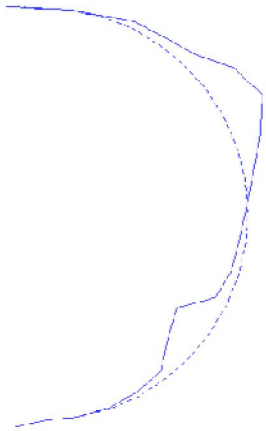

Figure 6.2: Kouga dam mode shape at 3.78 Hz

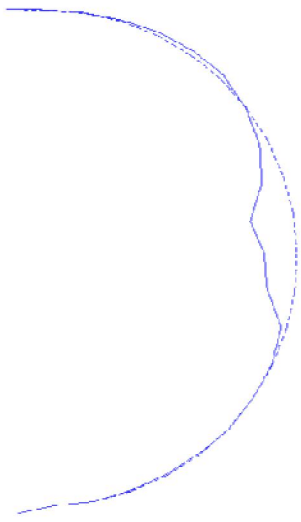

Figure 6.3: Kouga dam mode shape at 4.09 Hz

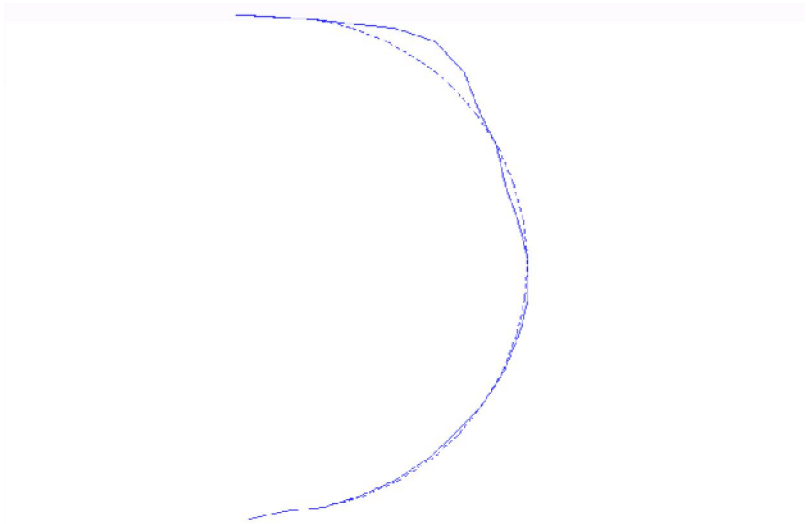

Figure 6.4: Kouga dam mode shape at 6.53 Hz

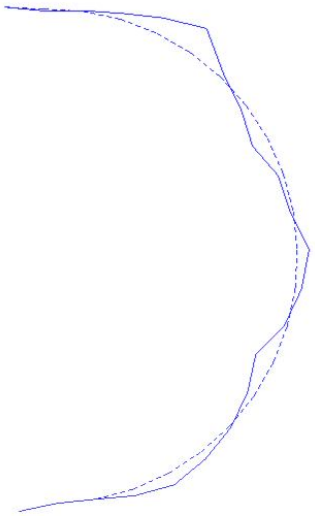

Figure 6.5: Kouga dam mode shape at 8.27 Hz

Figure 6.6: Kouga dam mode shape at 8.57 Hz

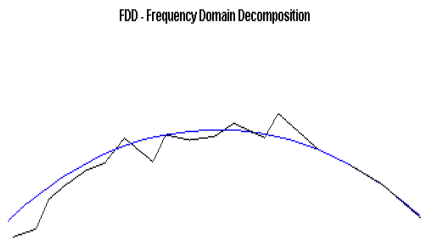

Figure 6.7: Kouga dam mode shape at 3.776 Hz

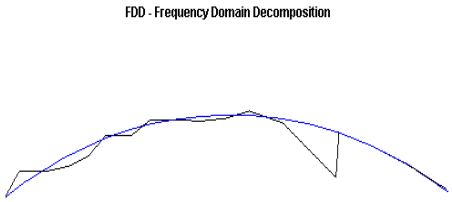

Figure 6.8: Kouga dam mode shape at 4.232 Hz

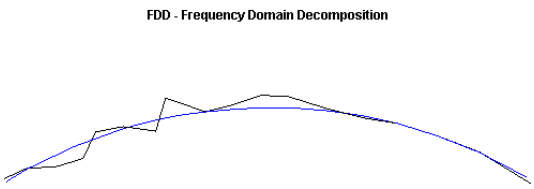

Figure 6.9: Kouga dam mode shape at 6.445 Hz

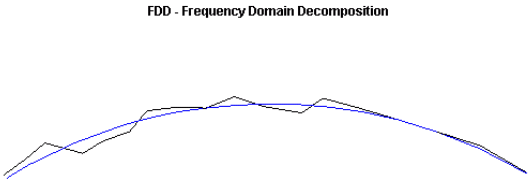

Figure 6.10: Kouga dam mode shape at 8.268 Hz

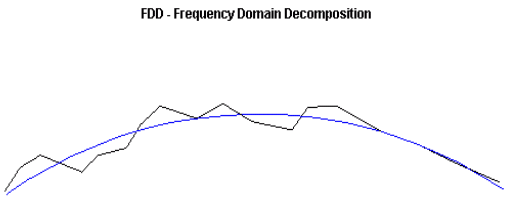

Figure 6.11: Kouga dam Mode shape at 8.854 Hz

6.2 Analysis of Results

6.2.1 Overview of analysis of results and experiences with the methods

6.2.1.1 Frequency domain decomposition based methods

These methods are the most simple and straight forward to use. The selection of the modes from the plot of the average SVDs (Figure. 6.12) of the response spectral density was done after validation of the average spectra of the spectral signals. Three methods namely FDD, EFDD and CFDD were used in the estimation of modes from the ambient data of the dam. Figures. 6.12 and 6.13 show the modes picked from the peaks of the average SVDs of the measurements of the responses from the dam using FDD and CFDD respectively. Note that the CFDD uses curve fitting in the estimation of modes.

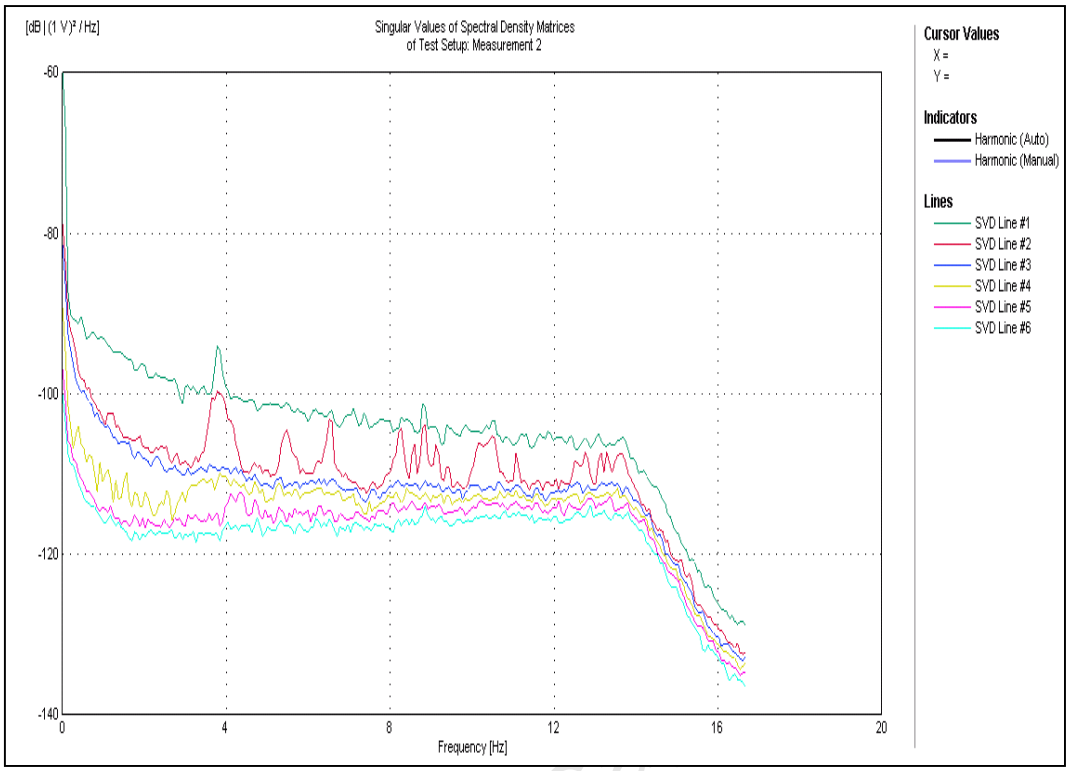

Figure 6.12: Average SVD plot from the test of Kouga dam

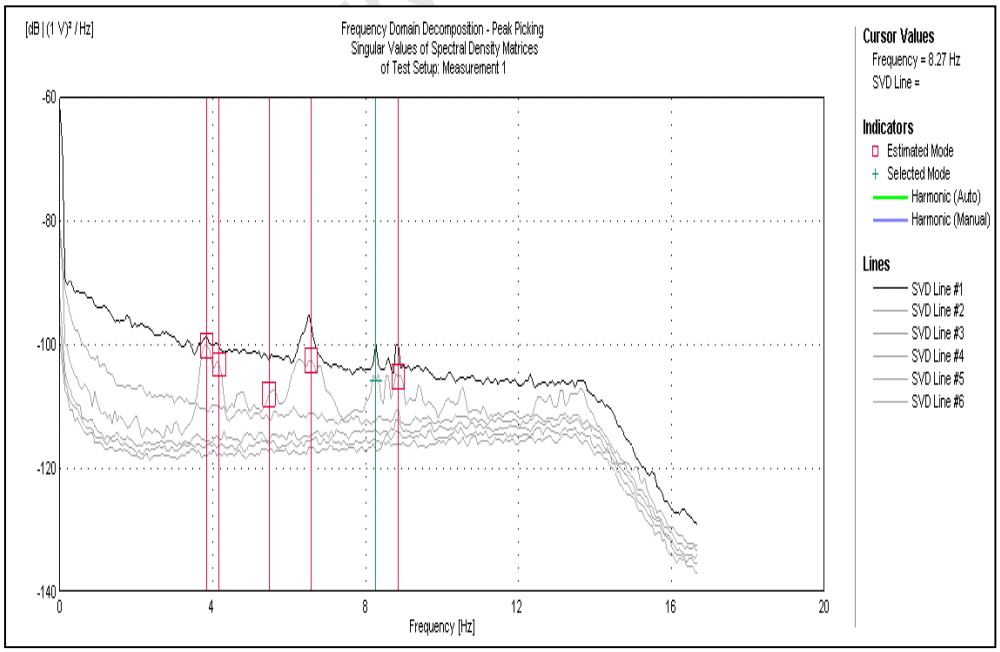

Figure 6.13: Peak picking in the FDD method

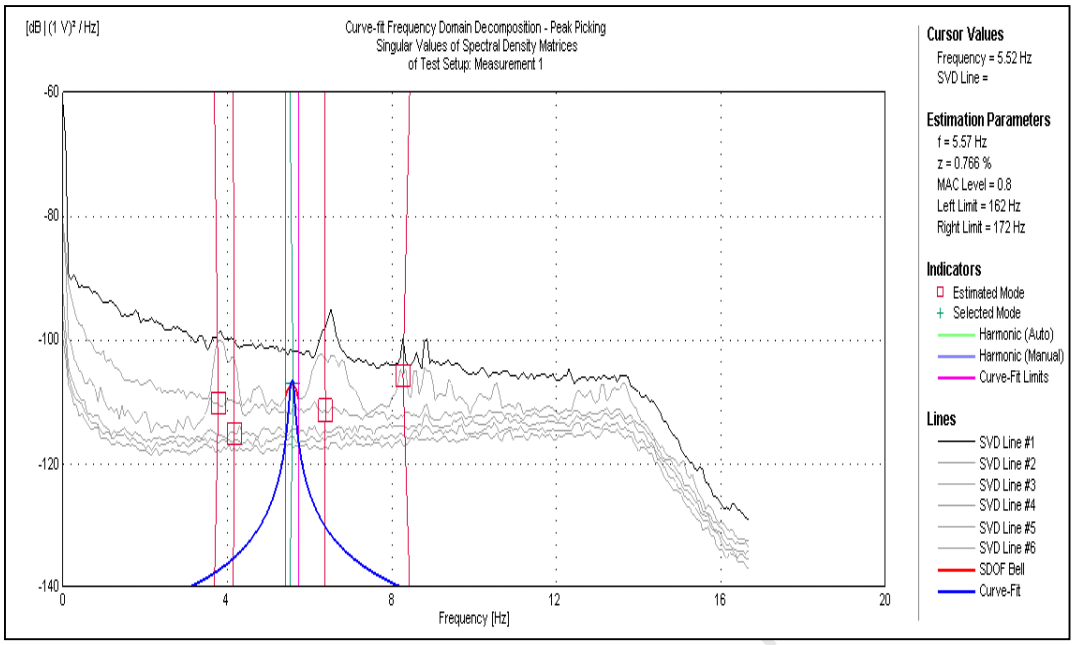

Figure 6.14: CFDD method showing a peak being curve-fit

The number of peaks appears in the SVD specifically in the lower frequency range below 10Hz. Six modes were detected. EFDD and CFDD estimated frequency and damping ratios using a SDOF model in a user definable frequency band and the peak. The mode shapes are determined from the singular vectors weighted by singular values in the frequency band. Two close modes between 3.8 Hz and 4.2 Hz were detected in the frequency domain decomposition confirming the advantage of these methods mentioned in section 3.2.1.

6.2.1.2 Least square complex frequency based procedure

The RFP method used in the analysis of the results uses orthogonal polynomials in the estimation of modes. Figure shows the stabilization diagram with stable and unstable modes. To obtain a clear stabilization diagram, a certain criterion based on frequency resolution, maximum damping ratio and minimum number of poles. This is such a tiresome procedure and also some modes may appear strong in one criterion and then disappear in the other. In the analysis of the results, a frequency resolution of 0.065Hz, maximum damping ratio of 5 Hz and 20 minimum number of poles were used.

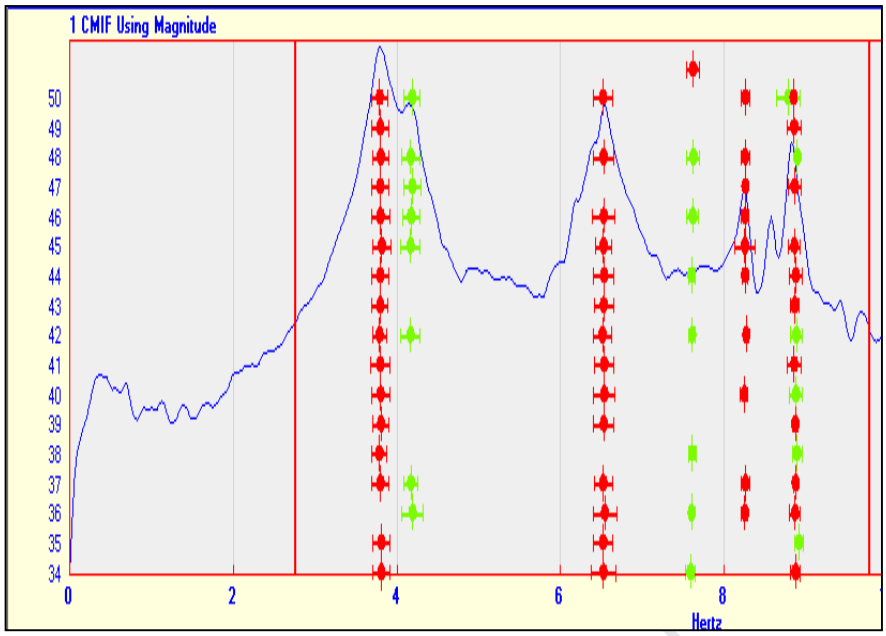

Figure 6.15: Stabilization diagram based on RFP method

6.2.1.3 Stochastic subspace identification method

Three SSI methods namely UPC, PC and CVA were used to estimate the modal parameters of the dams. These methods are based on stabilization diagram criterion; Modes below 10 Hz were obtained after low-pass filtering and decimation to 16.67Hz and the use of six projection channels. Projection channels decreased the amount of redundant information and the estimated models stabilized faster, i.e. at lower state space dimensions.

Figures. 6.16, 6.17, and 6.18 show stabilization diagrams of UPC, PC and CVA algorithms respectively in the frequency band up to 10 Hz with a maximum state space dimension of 80. The SSI techniques showed also the ability of estimating closely coupled modes illustrated in figures below

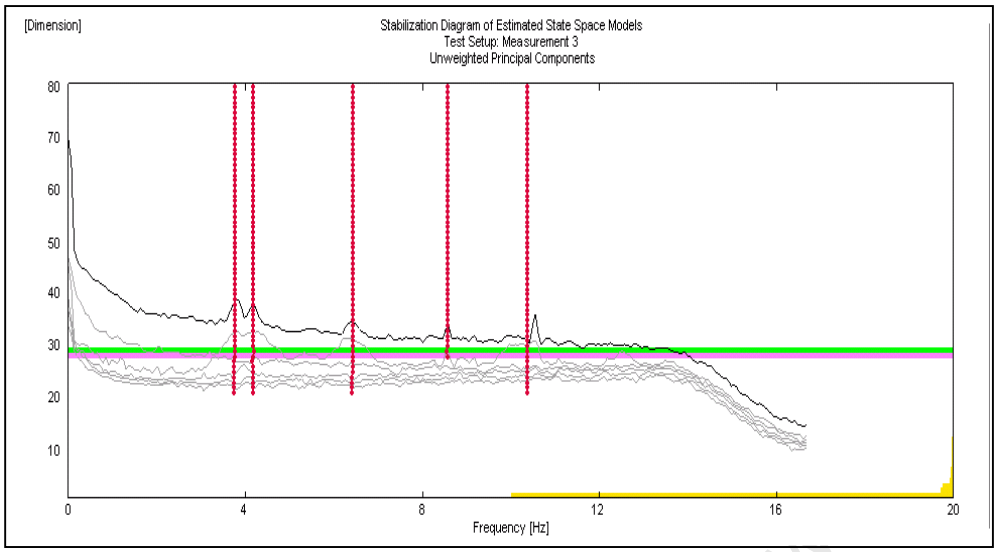

Figure 6.16: Stabilization diagram based on UPC algorithm

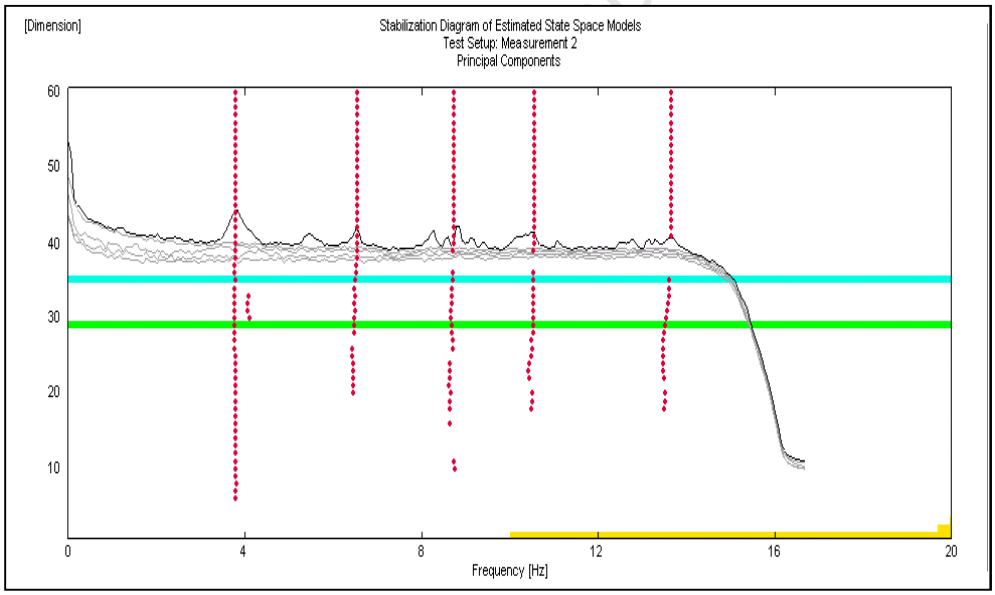

Figure 6.17: Stabilization diagram based on PC algorithm

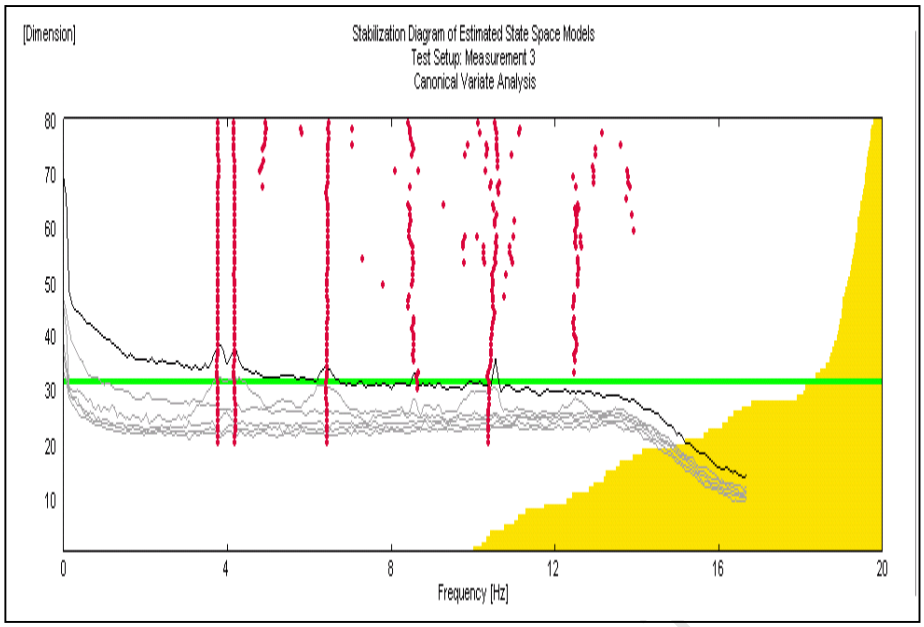

Figure 6.18: Stabilization diagram based on CVA algorithm

The three SSI algorithms gave almost similar results and the selected state space followed the general trend namely UPC< CVA< PC.

6.2.1.4 Complex Exponential

The CE algorithm utilizes the IRFs which are obtained after inverse FFT of the FRFs of the measurements. The method also utilizes the stabilization diagram criterion as the RFP method. However it has disadvantages in that the residual effects of the modes outside the frequency band of analysis are kept outside of this band hence non linear effects of aliasing (Figure. 6.19)

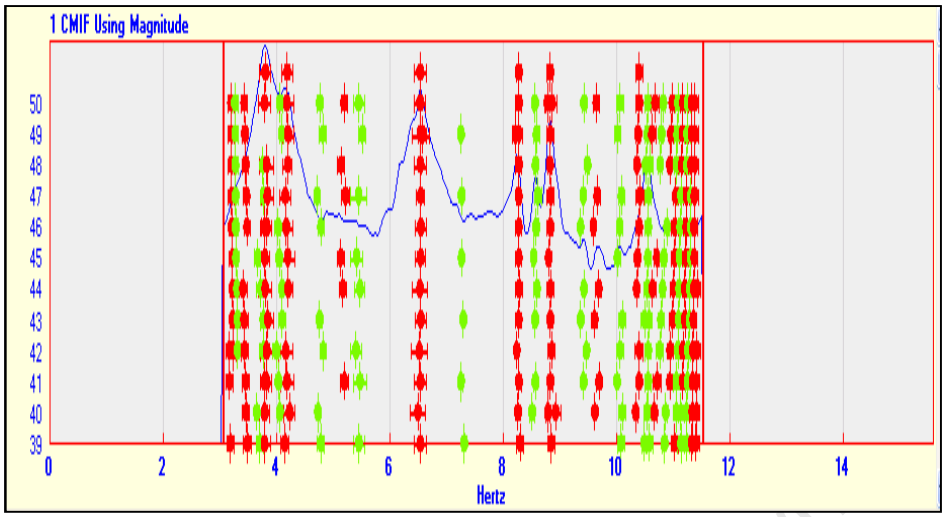

Figure 6.19: Stabilization diagram based on CE algorithm

6.2.2 Detection of Harmonics

Kurtosis and Short time Fourier transform (STFT) methods were used to detect any harmonics at Kouga dam. From the results there were no harmonics detected. This is shown in the spectrogram (Figure 6.20) as there are no “saw tooth” shapes and the PDF shapes (Figure. 6.21).

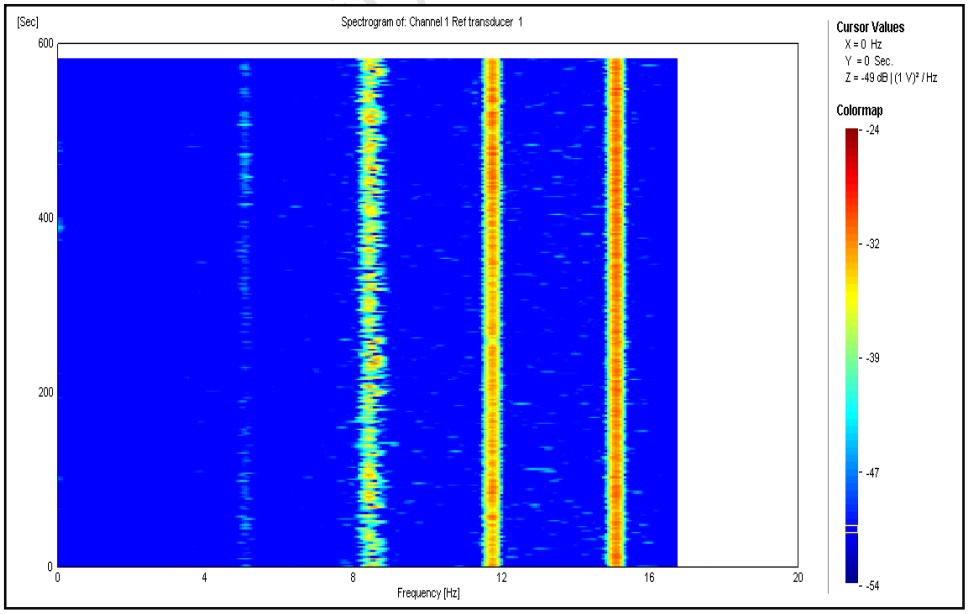

Figure 6.20: STFT method used for harmonic detection

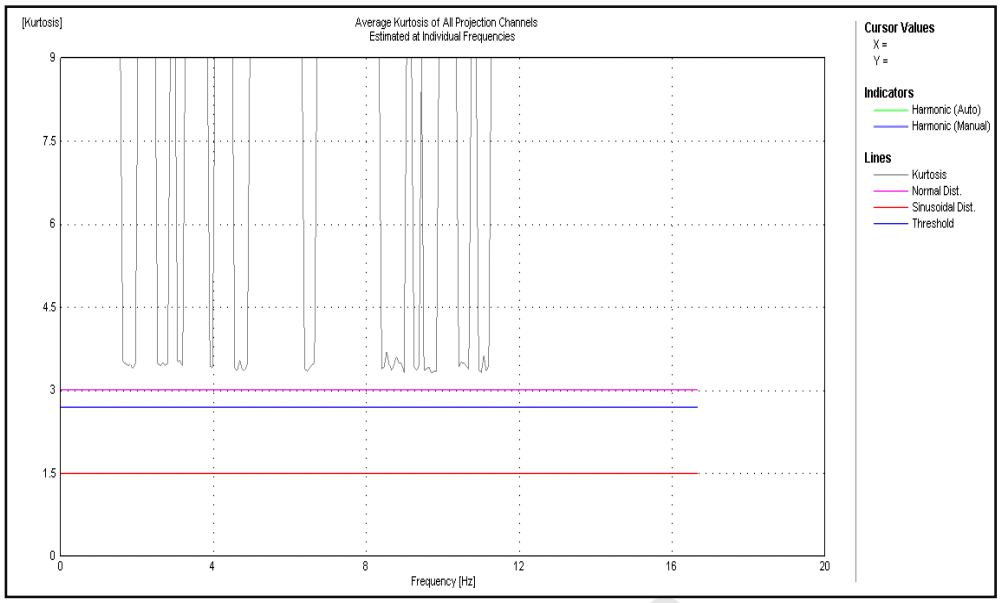

Figure 6.21: Kurtosis method used for harmonic detection

6.2.3 Comparison of Results

6.2.3.1 Comparison of natural frequencies of Kouga dam

Natural frequencies are recognized very consistently among the different techniques. Figure 6.22 below illustrates the estimates for natural frequencies using all methods. The fact that the difference of bar lengths in that diagram can barely be detected shows that the standard deviation of the estimates is usually less than one Hertz. As the frequency resolution used for the Fourier transform was only 0.067 Hz, the variation of the estimates can be considered close to optimal.

All the methods seem to estimate the first three and seventh modes. RFP and CE did not pick the fifth mode while SSI based methods did not pick the fourth and sixth mode. FDD based procedures estimate all the seven modes. This is because they are not based on use of stabilization charts as compared to rest of the methods.

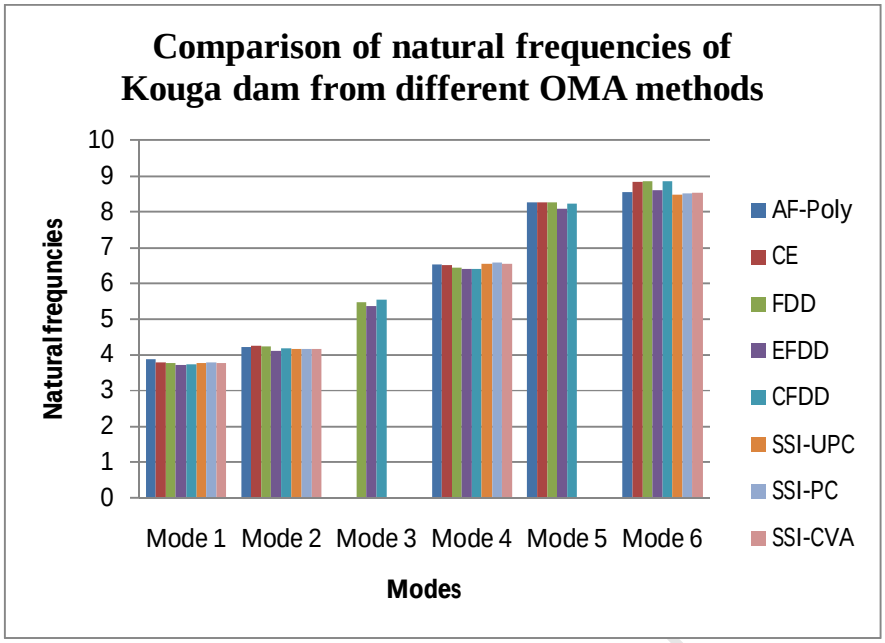

Figure 6.22: Comparison of natural frequencies from the various OMA methods

6.2.3.2 Comparison of natural frequencies Roode Elsberg dam

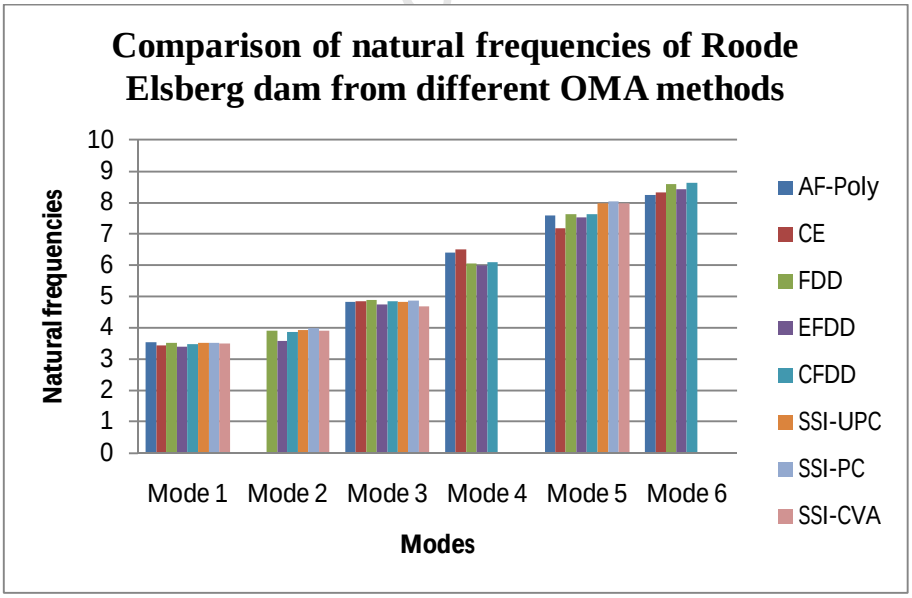

Figure 6.23: Comparison of natural frequencies of Roode Elsberg dam from various OMA techniques.

Natural frequencies estimated of Roode Elsberg dam are recognized very consistently among the different techniques as shown in figure 6.23. All methods picked up modes 1, 3 and 5 with AF-Poly and CE not picking up mode 2. The SSI- based procedures did not pick up modes 4 and 6 while FDD based procedures picked up all the modes. The fact that the difference of bar lengths in that diagram can barely be detected shows that the standard deviation of the estimates is usually less than one Hertz. As the frequency resolution used for the Fourier transform was only 0.067 Hz, the variation of the estimates can be considered close to optimal. This can be explained to the fact that FDD based procedures are based on peak-picking while AF-Poly, CE and SSI use of stabilization charts in determining the modal parameters. Stabilization diagrams are controlled by frequency resolution, damping tolerance and roots so in the approximation of the modal parameters some modes are not picked up.

Table 6-5: Summary of mean and variance of all the methods

OMA Methods	Count	Sum	Average	Variance
RFP	5	30.61	6.122	3.77292
CE	5	30.33	6.066	3.75418
FDD	6	34.58	5.763333	4.154587
EFDD	6	33.65	5.608333	4.307417
CFDD	6	34.53	5.755	4.28291
SSI-UPC	4	20.27	5.0675	4.092692
SSI-PC	4	20.43	5.1075	4.152292
SSI-CVA	4	20.09	5.0225	4.157425

The analysis of variance was carried out on the natural frequencies from Kouga dam to determine where there is a significant difference in the variance of the means. Table 6-5 shows the average and variance of the different methods. There seem to be no significant difference between variances FDD and SSI based procedures although there is a slight difference with the RFP and CE methods.

Table 6-6 shows a summary of ANOVA with a P value of 0.979 which is greater than 0.05. This means that there is no significant difference in the variance of the methods. This however does not tell us which methods are best.

Table 6-6: Summary of ANOVA results

Source of Variation	*SS*	*df*	*MS*	*F*	*P-value*	*F crit*
Between Groups	6.185306	7	0.883615	0.215779	0.979097	2.312741
Within Groups	131.0402	32	4.095006			
Total	137.2255	39				

6.2.4 Comparison of mode shapes

Modal assurance criterion was used in comparing the mode shapes of Kouga dam across all methods. Table 6-7 represent MAC values between rational fractional polynomial and complex exponential methods which are incorporated in ME' scope ves 5.0 software. The MAC values are all greater than one which means that the mode shapes are similar.

Table 6-8 shows a summary of MAC values for mode 1 across FDD and SSI based methods which are incorporated in ARTeMIS Extractor Pro 2010. These MAC values are the same across all the modes. There is no correlation between frequency domain and stochastic subspace methods as the MAC values are too low.

Table 6-7: MAC values between RFP and Complex Exponential for five modes

Mode	**RFP**	**CE**	**MAC**
1	3.78	3.8	0.97
2	4.09	4.18	0.93
3	6.53	6.52	0.97
4	8.27	8.27	0.94
5	8.83	8.84	0.93

Table 6-8: MAC values across FDD and SSI methods

	FDD	EFDD	CFDD	SSI-UPC	SSI-PC	SSI-CVA
FDD	1	0.8834	0.8834	0.1499	0.1499	0.1362
EFDD	0.8834	1	1	0.2964	0.296	0.2556
CFDD	0.8834	1	1	0.2964	0.296	0.2556
SSI-UPC	0.1499	0.2964	0.2964	1	0.9884	0.8832
SSI-PC	0.1499	0.296	0.296	0.9864	1	0.8882
SSI-CVA	0.1362	0.2556	0.2556	0.8832	0.8882	1

6.2.5 Validation of experimental results with FEM results

Table 6-9 shows measured natural frequencies of the Roode Elsberg dam and for finite element model. Tables 6-10 to 6-12 represent errors between the experimental results of different methods and numerical results.

Table 6-9: Measured natural frequencies of the Roode Elsberg dam and for FE- model

Mode/Method	FE-model	RFP	CE	FDD	EFDD	CFDD	SSI-UPC	SSI-PC	SSI-CVA
1	3.36	3.54	3.44	3.52	3.38	3.49	3.53	3.53	3.50
2	3.52	_	_	3.91	3.59	3.86	3.92	3.99	3.91
3	5.03	4.82	4.84	4.88	4.74	4.84	4.83	4.86	4.69
4	6.39	6.42	6.52	6.06	5.99	6.09	_	_	_
5	7.63	7.59	7.2	7.62	7.53	7.62	7.99	8.05	7.99

Table 6-10: Error between FEM and RFP and CE methods

FE-model	RFP	Error	CE	Error
3.36	3.54	0.18	3.44	0.08
3.52	–	–	–	–
5.03	4.82	0.21	4.84	0.19
6.39	6.42	0.03	6.52	0.13
7.63	7.59	0.04	7.2	0.43

Table 6-11: Error between FEM and FDD based methods

FE-model	FDD	Error	EFDD	Error	CFDD	Error
3.36	3.52	0.16	3.38	0.02	3.49	0.13
3.52	3.91	0.39	3.59	0.07	3.86	0.34
5.03	4.88	0.15	4.74	0.29	4.84	0.19
6.39	6.06	0.33	5.99	0.4	6.09	0.3
7.63	7.62	0.01	7.53	0.1	7.62	0.01

Table 6-12: Error between FEM and SSI based methods

FE-model	SSI-UPC	Error	SSI-PC	Error	SSI-CVA	Error
3.36	3.53	0.17	3.53	0.17	3.5	0.14
3.52	3.92	0.4	3.99	0.47	3.91	0.39
5.03	4.83	0.2	4.86	0.17	4.69	0.34
6.39	–	–	–	–	–	–
7.63	7.99	0.36	8.05	0.42	7.99	0.36

There is a good agreement between results obtained from the FE- model and those from the OMA methods for modes 1, 3 and 5 because of the small errors. All the FDD based procedures picked up mode 2 and 4 while the SSI-based methods did not pick up mode 4. This still shows that the FDD-based procedures performed better than the rest of the modal parameter estimation methods as they correlated well with the finite element model results.

6.3 Chapter Summary

The chapter presents analysis and discussion of experimental results obtained from ambient vibration testing of Kouga and Roode Elsberg dams. Natural frequencies and damping ratios of the dams determined by the seven methods are also presented. Validation of the results from the different methods has been done by comparing experimental natural frequencies with those from the FE-model.

Results suggest that however much there is a good correlation between the FE- model and the experimental results from all the methods, frequency domain decomposition, enhanced frequency domain decomposition and curve-fitting domain decomposition had an advantage as over other methods in terms of modal parameter estimation.

7 CONCLUSIONS AND RECOMMENDATIONS

7.1 General Summary

Ambient vibration testing or operational modal analysis is a fast and inexpensive way to identify the dynamic properties of dams for structural health monitoring and calibration of mathematical models. This is because dams are large civil engineering structures that are difficult to mechanically excite and also the expenses involved in carrying out forced vibration tests are too significant. In the last 20 years, a number of publications in ambient vibration testing of dams have been reported by several researchers. The main reasons for carrying out these tests were to determine the modal parameters (natural frequencies, damping ratios and mode shapes) of the dams and to calibrate of mathematical models. See chapter 2 for further information.

In the extraction of the modal parameters from ambient test data from reported dams, frequency domain based procedures (peak picking and frequency domain decomposition) were used. However, the methods reported are not the OMA techniques used in the field of vibration testing of civil engineering structures. Modal parameter estimation techniques in operational modal analysis have been developed in the 20 years and are classified by either parametric methods in time domain, non-parametric methods in frequency domain or wavelet transform in time-frequency domain. The performance of these methods has been studied on flexible structures such as bridges and building but has not been systematically studied on rigid structures such as dams. The primary objective of this research study has been to fill the gap by studying the performance of the different modal parameter identification techniques namely; rational fractional polynomial, frequency domain decomposition, enhanced frequency domain decomposition, curve-fitting frequency domain decomposition, complex exponential and stochastic subspace identification algorithms on dams. This objective has been achieved by applying these methods on ambient test data from tests carried out on two arch dams (Kouga and Roode Elseberg dams) located in South Africa. The following conclusions can be made as a result of the present study:-

Modal parameter estimation techniques in out-put only modal analysis have been categorized into frequency domain, time domain and time-frequency domain methods. Under frequency domain, there are FDD based procedures and LSCF based procedures. Frequency domain

decomposition based procedures (FDD, EFDD, and CFDD) are based on singular value decomposition in the estimation of modal parameters. They share the same advantages of being simple to use, and can be used also as indicators of harmonics (Brincker et al., 2000). However, these methods are disadvantageous in such a way that the estimates relying on heavily the observation of the analyst to detect modes and have problems with estimating modes with high damping. The RFP method is based on a common denominator model in the estimation of modal parameters has advantages of handling noisy measurements and allows the use of additional numerator polynomial terms as a means of compensating for the effects of out-of-band mode. It has disadvantages of mode shapes and modal participation factor are difficult to obtain via reduction of the residues to a rank-one matrix using SVD (2) closely spaced modes show up as a single pole. Operational polymax on the other hand is based on modal decomposition of half PSD, computed from FFT of the COR with positive time lags. It has advantages of (1) yielding extremely clear stabilization diagrams (2) suitable for systems with high modal density and both high and low damping (3) does not suffer from numerical problems as it is formulated in the Z-domain.

The time domain based methods (CE, ARMA, SSI, and ERA) share advantages of being fully parametric implying that they do not rely heavily on the observation of the analyst to detect modes and that stabilization diagrams can be constructed by identifying parametric models of increasing order. These diagrams are very valuable in separating the true system poles from the spurious numerical poles. The disadvantage of these methods is that with heavily damped systems, modal parameters tend to suffer and the computation time is high.

The wavelet transform is a time-frequency method which has an advantage of allowing for the adoption of both traditional time and frequency domain system identification approaches to examine non-linear and non-stationary data. This method has not been fully exploited in civil engineering.

It has been observed that if certain practical issues in OMA are not taken into considerations, erroneous results can be obtained. Practical issues such as instrumentation (data acquisition system), data preprocessing can affect the quality signals if not carefully chosen. Harmonics is the last issue that has been mentioned as if not detected can be mistaken to be structural modes (see chapter 4).

7.2 Conclusions

Ambient vibration tests of two arch dams namely; Roode Elsberg and Kouga dams have been reported. High quality instrumentation manufactured by National Instruments was used to obtain signals from both dams. Issues of signal resolution, bandwidth, sensitivity and dynamic range of accelerometers were taken into consideration while using the instruments. Modal parameters of the dams were extracted using the mentioned methods incorporated in commercial software, namely: ME' Scope Ves 5.0 and ARTeMIS Extractor 2010.

The first six natural frequencies of both Kouga and Roode Elsberg dams have been determined using time and frequency domain based methods. Natural frequencies of Kouga dam and Roode Elsberg dam were in the range of 3.7-8.9 Hz and 3.3-8.7Hz respectively.

Comparison of natural frequencies estimated from all the methods of Kouga dam was done using analysis of variance which gave a P value of 0.975. This implied that there was no significant difference in the natural frequencies.

Modal assurance criterion was used to compare mode shapes of Kouga dam. Rational fractional polynomial and complex exponential showed a good correlation in the mode shapes. There was no correlation between the family of frequency domain decomposition technique and stochastic subspace identification technique.

Validation of experimental results has been done by comparing experimental natural frequencies with numerical natural frequencies of Kouga dam. Absolute errors calculated were in the range of 0.01- 0.4 with modes 1, 3 and 5 having the smallest error.

The FDD-based procedures were the simplest and straight forward amongst all the methods when SVD reveals isolated peaks caused by resonances. The simple peak picking technique gives frequency and mode shape at selected frequencies.

The time domain methods have the advantages of operating directly on the measured time signals. However, they are a bit more complicated to use and time consuming. Different model

orders have to be evaluated in order to determine the optimal one. However, stabilization diagrams give good guidance.

The use of projection channels was essential in signal processing as it reduced the calculation time. Band pass filtering and decimation gave better results and faster stabilization. The modal damping ratios are very sensitive and difficult to measure. There were no harmonics detected in the signals from the dams using kurtosis and short time Fourier transform.

Another observation is that the stabilization diagram is a very powerful tool and it generally does not get the attention it deserves. It is a classical tool in input–output modal analysis that is easily ported to output-only modal analysis as long as a method is used in which a parametric model is fitted to the data. The main benefit of the stabilization diagram is that it allowed the analyst to objectively select the eigen frequencies, without having to find often-unclear peaks in spectrum or frequency-domain singular value plots as FDD methods.

7.3 Recommendations

It is recommended that while operational modal analysis in dams, a combination of FDD based methods and SSI based methods should be used. The FDD methods should be used in determining the modal parameters and SSI should be used for confirmation of the modal parameters.

There is a need for further study in performance of all the available methods in operational modal analysis on ambient data from dams.

A finite element model for Kouga dam is needed such that validation of experimental results from the dam can also be done. This is because the conclusions made in this work are only based on results from Roode Elsberg dam for validation purposes.

Finally, a long term continuous monitoring system is required to be installed on the dams such that there is a continuous acquisition of data and then analysis of data using the various methods. The method or combination of methods which shows continuity will be recommended as the best method in the extraction of modal parameters from ambient data of concrete dams. Properly and accurately extracted modal parameters will be useful in monitoring the changes in the behavior

of dams in terms of natural frequencies which are usually used as damage-sensitive features, finite element model updating which will help in conditional assessment of dams.

References

1. Abdelghani,M., Verhaegen, M., Van Overchee, P., and De Moor, B. 1998. Comparison study of subspace identification methods applied to flexible structures. *Mechanical System and signal processing* 12 (5), pp.679-692.
2. Allemang R.J.2002. The Modal Assurance Criterion-twenty years of use and abuse. *Proc. of 20th International modal analysis conference*, Los Angeles, CA Feb 2002.
3. Andersen P. 1997. Identification of Civil engineering structures using Vector ARMAR Model, Ph.D. Thesis, Aalborg University, Denmark, 1997.
4. Andersen. P, 2010. Technical paper on stochastic subspace identification techniques. ARTeMIS Extractor Online Help. Version 2010.
5. Auweraer, H.2001 Structural Dynamics Modelling Using Modal Analysis: Application, Trends and Challenges. *Proc.of IEEE Instrumentation and Measurement Technology Conference. Budapest, Hungray, 2001*.
6. Batel M, 2002. Operational Modal Analysis- another way of doing modal testing. *Sound and Vibration, 2002*
7. Bendat, J. and Piersiol, A., 1993. Random Data, Analysis and Measurement Procedures, John Wiley 7 Son, New York, USA,
8. Brincker R, and Andersen P.2006. Understanding Stochastic Subspace Identification. In *Proceedings of the 24th International Modal Analysis Conference (IMAC)*, St. Louis, Missouri USA, 2006.
9. Brincker, R., De Stefano, A., and Pambo 1996. Ambient data to analyze the dynamic behavior of bridges. *Proceeding of the 14th International Modal Analysis Conference*, SEM, Dearborn, Mich.
10. Brincker, R.; Zhang, L.; and Anderson, P. 2000. Modal identification from ambient responses using frequency domain decomposition. *Proceeding of the 18th International Modal Analysis Conference (IMAC-XVIII)*.Kissimme, Florida USA, 2000.
11. Brincker R., Ventura C., and Andersen P. 2001. Damping Estimation by Frequency Domain Decomposition. *Proceedings of the 19th International Modal Analysis Conference (IMAC)*, San Antonio, Texas USA 2001.

12. Brownjohn JMW et al, 2010. Ambient vibration re-testing and operational modal analysis of the Humber Bridge. *Engineering Structures*, (2010), doi:10.1016/j.engstruct.2010.02.034
13. Brownjohn, J.M.W. Severn, R.T., and Taylor C.A 1986. Ambient vibration survey of Contra dam. Research Report University of Bristol Department of Civil Engineering.
14. Brownjohn, J. M. W.1990. Dynamic investigation of Hermitage Dam, Jamaica. Report UBCE-EE-90-13 University of Bristol Department of Civil Engineering, 1990.
15. Browjohn J.M.W. 2003. Ambient vibration studies for system identification of a tall building. *Earthquake Engineering and Structural Dynamics* 32(4), pp71-95.
16. Brown et al. 1979. Parameter Estimation Techniques for Modal analysis. SAE Paper No. 790221.
17. Cantieni R.2001. Assessing a dam's structural properties using forced vibration testing. *Proceedings of International Conference on Safety, Risk and Reliability-Trends in Engineering IABSE,* Malta, 2001.
18. Cantieni R.2004. Experimental Methods used in System Identification of Civil Engineering Structures. 2nd Workshop: Problemi di vibrazioni nelle strutture civili e nelle costruzioni meccaniche Perugia, 10-11 Giugno 2004.
19. Chopra N.K. 1995. Dynamics of structures: Theory and application to Earthquake engineering. Prentice-Hall Inc. A Simon & Schuster Company, Eaglewood Cliffs, New Jersey.
20. Chui C. 1992.An introduction to wavelets. New York: Academic Press,1992.
21. Cunha et al., 2006. From input-output to output-only modal identification of civil engineering structures. SAMCO Final report, 2006.
22. Danielle, W.E and Taylor, C.A. 1999. Effective ambient vibration testing for validating numerical models of concrete dams. *Earthquake Engineering and Structural Dynamic*s, 28(11) pp.1327-1344.
23. Darbre G.R, De Smet CAM, Kraemer C.2000. Natural frequencies measured from ambient vibration response of the arch dam of Mauvoisin. *Earthquake Engineering and Structural Dynamics*, 29(5) pp 577–58.
24. Darbre,G.R., and Proulx,J. 2002. Continuous ambient vibration monitoring of the arch dam of Mauvoisin. *Earthquake Engineering and Structural Dynamics* 2002, 31(2) pp 475–480.

25. Deinum et al., 1982. Vibration tests on Emmoson arch dam, Switzerland. *Earthquake Engineering and Structural dynamics*, 10(3) pp.996
26. Duron Z H and Hall J F.1988. Experimental and finite element studies of the forced vibration response of Morrow Point dam. *Earthquake Engineering and Structural dynamics*, 16(7) pp. 1021-1039.
27. Duron Z.H et al., 2007. Ambient and Forced Vibration survey of San Vicente Dam. A report submitted to Montgomery Watson Harza (MWH) and the San Diego County Water Authority (SDWCA), October 2007.
28. Duron et al., 2005. Dynamic Testing and Numerical correlation studies for Folsom dam. *Tri-service Infrastructure systems conference and Exhibition. St Louis MO-Aug 2-4-2005*
29. Ewins, D.J, 1984. Modal Testing; Theory and Practice. *John Wiley & Sons, New York, USA*, pp 225
30. Fassois S.D. 2001. MIMO LMS-ARMAX identification of vibration structures-part 1: the method. *Mechanical Systems and Signal processing*, 15(4) pp 723-735.
31. Felber, A. 1993. Development of a Hybrid Bridge Evaluation System, Ph.D. thesis, University of British Columbia (UBC), Vancouver, Canada,
32. Formenti, D and Richardson, M.H. 1985. Global curve fitting of Frequency Response Measurements using Rational Fraction Polynomial Method. *Proceedings of the 3rd International Modal Analysis Conference*, Orlando, Florida.
33. Formenti, D and Richardson, M.H. 1986. Global Frequency and Damping from Frequency Response Measurements. *Proceedings of the 4th International Modal Analysis Conference (IMAC),* Los Angeles, CA.
34. Formenti, D and Richardson, M.H. 2002. Parameter Estimation from Frequency Response Measurements using Rational Fraction Polynomial Method (Twenty years of Progress). *Proceedings of the 20th International Modal Analysis Conference (IMAC),* Orlando, Florida.
35. Friswell, M.I, and Penny, P.E.T. 1993. Technical note: The choice of orthogonal polynomials in the rational fractional polynomial method. *The international Journal of Analytical and Experimental Modal Analysis*, 8(3) pp 257-262.
36. Gade et al., 2005. Frequency domain techniques for operational modal analysis. *Proceeding of 1st IOMAC conference, 2005, Copenhagen, Denmark.*

37. Giraldo et al, 2009. Modal identification through Ambient Vibration: Comparative study. *Journal of Engineering Mechanics*,135(8) pp. 759-770
38. Guillaume et al., 2003. A poly-reference implementation of least-squares complex frequency-domain estimator. *Proceedings of the 21st International Modal Analysis Conference,* Kisssimmee, Florida, USA.
39. Goursat M., Mevel L., and Andersen P., 2010. Crystal Clear SSI for operational modal analysis for Aerospace vehicles. *Proceedings of the 27th International Modal Analysis Conference,* Florida, USA.
40. He, J and Fu, Zhi-Fang 2001. Modal analysis. Reed Educational and Professional Publishing Ltd
41. He, X., Moaveni, B., Conte, J.P., and Elgamal, A. 2006. Comparative study of system identification techniques applied to new Caquinez Bridge. *Proceeding of 3rd International Conference on Bridge Maintenance, Safety and Management (IABMAS)*, Porto, Portugal.
42. Jacobsen, N.L, 2006. Separating Structural Modes and Harmonic Components in Operational Modal Analysis. *Proceeding of the 24th International Modal Analysis Conference,* St. Louis, Missouri.
43. Jacobsen, N.L., Andersen, P., Brincker, R. 2008. Application of Frequency Domain curve-fitting in the FDD technique. *Proceeding of 26th International Modal Analysis Conference,* Orlando, Florida.
44. Juang ,J.N., Pappa, R.S. 1985. An eigensystem realization algorithm for modal parameter identification and model reduction. *Journal of Guidance Control Dynamics,* 8(5) pp 620-627.
45. Kailath T. 1980. Linear Systems. Prentice Hall Inc., 1980
46. Kelly,L.G. 1967. Handbook of Numerical Methods and Applications, Chapter 5 curve fitting and Data Smoothing. Addison-Wesley Pub.Co.Inc.1967
47. Kemp B.G.1996 Ambient Vibration Assessment of Ruskin dam Dynamic Properties. M.A, Sc thesis Faculty of Graduate Studies, Department of Civil Engineering, University of British Columbia,1996.
48. Kirkegaard,P.H., and Andersen, P. 1997. State space identification of civil engineering structures from output measurements. *Proceeding of the 15th International Modal Analysis Conference,* Orlando, Florida.

49. Lardies J. and Gouttebroze S. 2002. Identification of modal parameters using wavelet transforms. *International Journal of Mechanical Science,* 44(11), pp 2263-2283.
50. Lew, J.S. Juang, J.N. and Longman, R.W. 1993. Comparison od several system identification methods for flexible structures. *Journal of sound and Vibration*, 167(3), pp.461-480.
51. Ljung, J 2001. A stochastic realization algorithm with application to modal parameter estimation. *Mechanical systems and signal processing,* 15(2) pp275-285.
52. Loh, C.H. and Tsu-Shiu, W. 1996. Identification of Fei-Tsui Arch Dam from both Ambient and Seismic Response Data", *Soil Dynamics and Earthquake Engineering*, 15(7), pp 465-483. 1996.
53. Luz E.1991. Experimental modal analysis using ambient vibration. *The International Journal of Analytical and Experimental modal analysis*, 7(1) pp 29-39.
54. Makha L, 2009. Dynamic behavior of an arch dam under ambient vibrations. BSc (CIV) thesis Faculty of Engineering and Building Environment, Department of Civil Engineering, University of Cape Town,2010.
55. Maybeck P. S.1979. Stochastic models, estimation, and control, volume 1. Academic Press, 1979.
56. Melsa J. L. and Sage A.P. 1973. An Introduction to Probability and Stochastic Processes. Prentice-Hall Inc., 1973.
57. Mendes, P and Oliveira, S. 2009. Influence of the intake tower behavior on modal identification of Cabril dam. *Proceeding of the 3rd International Operational Modal Analysis Conference (IOMAC IX)* Portonovo, Italy.
58. Mivehchi, M.R. Ahmadi, M.T. 2003. Effective Techniques for Arch dam Ambient Vibration Test. Application on Two Iranian Dams, *International Institute of Earthquake and Seismology (IIEES),* 5(2).
59. Mohanty, P. and Rixen, D.J.2004. Operational modal analysis in the presence of harmonic excitation. *Journal of Sound and Vibration,* 270(1-2) pp 93-109
60. Montgometry, D.C., and Runger, G.C. 2002. Applied statistics and probability for engineers (3rd edition). John Wiley & Sons. Inc.
61. Moyo, P and Oosthuizen C. 2010. Ambient Vibration Survey Trials of Two Arch Dams in South Africa. *Proceeding of the 8th ICOLD European Club Symposium,* Innsbruck, Austria

62. Neild S.A, McFadden, P.D, and Williams M.S.2003. A review of time-frequency methods for structural vibration analysis, *Engineering Structures,* 25(6) pp 713-728.
63. Okuma N, Etou Y, Kanzawa K, Hirata K.2008 Evaluation of dynamic properties of an aged large arch dam. Civil Engineering Group, Research Laboratory, Kyushu Electric Power Co. Fukuoka, Japan
64. Peeters.,B.,and De Roeck, G. 2001. Stochastic system identification for operational modal analysis: a review. ASME *Journal for Dynamic Systems, Measurement, and Control,*123(4) pp 659.
65. Peeters, B., and Ventura, C. E. 2003. Comparative study of modal analysis techniques for bridge dynamic characteristics. *Mechanical Systems and Signal Process*, 17(5) pp 965-988.
66. Peeters B.,Van der Auweraer H and Leuridan J. 2004. The PolyMAX frequency-domain method: a new standard for modal parameter estimation, *Shock and Vibration*, 11(3), pp. 395–409.
67. Peeters B.,Van der Auweraer H. PolyMAX: a revolution in Operational Modal Analysis. *Proceedings of the 1st International Operational Modal Analysis Conference*, Copenhagen, Denmark.
68. Petsounis, K.A and Fassois, S.D.2001. Parametric Time-Domain Methods for the identification of vibration structures-A Critical Comparison and Assessment. *Mechanical System and Signal Processing,* 15(6) pp 1031-1060.
69. Richardson, M.H and Formenti, D. 1982. Parameter Estimation from Frequency Response Measurements using Rational Fraction Polynomial Method. *Proceedings of the 1st International Modal Analysis Conference,* Orlando Florida.
70. Ren Wei-Xin and Zong Zhou-Hong. 2004. Output-only modal parameter identification of civil engineering structures. *Structural Engineering and Mechanics,17(3-4)* pp. 429–444
71. Severn R.T. Brownjohn J M W, Taylor C.A.1986. Ambient Vibration survey of Contra dam. Research report, Dept of University of Bristol,1986
72. Severn, R.T., Jeary A.P., and Ellis B.R.1980. Forced vibration tests and theoretical studies on dams. *Proceedings, Institution of Civil Engineers, Part 2,* Vol 69 and 71,ICE London, UK, 1980.

73. Sheulen, F, Ellis, E and Duron, Z.H. 2009. Experimental and Finite Element Studies of the Forced Vibration Response of Big Creek Dam No.7. Submitted to Southern Califonia Edison, Octobber 2009.
74. Siringoringo D and Fujino Y. 2007. System identification of suspension bridge from ambient vibration response. *Engineering structures,* 30(2) pp 462-477.
75. Smail M and Thomas M. 1999. ARMA models for modal analysis: Effect of mode orders and sampling frequency. *Mechanical Systems and Signal Processing,* 13(6) pp.925-941.
76. Staszewski W.J.1997. Identification of damping in MDOF systems using time-scale decomposition. *Journal of Sound and Vibration*, 203(2) pp. 283–305
77. Takahashi, T. 1964. Results of vibration tests and earthquake observations on concrete dams and their considerations. *Proceedings of International Conference on Large dams.* Einburgh Scotland.
78. Tilly G.P.1986. Dynamic behavior of concrete structures, Report of the RILEM 65 MDB Committee. Developments in Civil Engineering 13.Elsevier Science Publishers B.V., Amsterdam, 1986.
79. Van Overschee,P. and De Moor, B. 1996. Subspace Identification for linear systems: theory-implementation and applications, Dordrecht, The Netherlands: Kluwer Academic Publishers.
80. Ventura,C. E. and Tomas H. 1997. Structural Assessment by Modal Analysis in Western Canada. *Proceeding of the 15th International Modal Assurance Conference,* Orlando, Florida.
81. Vold H. 2007. Aliasing in modal parameter estimation: An historical Look and New innovations. *Proceeding of 25th International Modal Analysis conference.* Orlando, Florida.
82. Wang, D and Haldan, A. 1994. Element level system identification with unknown input. *Journal of Engineering Mechanics,* 120(1) pp. 159-176.
83. Wei-Xin R Zong, Z. 2004. Output only modal parameter identification of civil engineering structures. *Structural Engineering and mechanics,* 17(3-4) pp. 429–444.
84. Yan B.F., Miyamoto A, and Bruehwiler E. 2005. Wavelet transform-based modal parameter identification considering uncertainty. *Journal of sound and Vibration*, 291(1-2) pp 285-301.

85. Zhang, L, M, Brinker, R. Andersen, P. 2005. An overview of operational of modal analysis: Major developments and issues. *Proceeding of International Operational Modal Analysis Conference*, Copenhagen, Denmark.
86. Zhou W., Chelidze D. 2008. Generalized Eigenvalue Decomposition in Time Domain Modal Parameter Identification. *Journal of Vibration and Acoustics ASME*, 30(1) pp.1-6.

APPENDICES

A1. CONFIGURATION FILE FOR GEOMETRY INPUT

```
Ambient vibration testing of Kouga dam 15th September,2010

Header
     Kouga dam

T
    1.00000E-03

Nodes
    105-8.0000E-01 3.9200E+00 0.0000E+00
    106-6.0000E-01 3.9500E+00 0.0000E+00
    107-4.0000E-01 3.9800E+00 0.0000E+00
    108-2.0000E-01 3.9900E+00 0.0000E+00
    109 0.0000E+00 4.0000E+00 0.0000E+00
    110 2.0000E-01 3.9900E+00 0.0000E+00
    111 4.0000E-01 3.9800E+00 0.0000E+00
    112 6.0000E-01 3.9500E+00 0.0000E+00
    113 8.0000E-01 3.9200E+00 0.0000E+00
    114 1.0000E+00 3.8700E+00 0.0000E+00
    115 1.2000E+00 3.8200E+00 0.0000E+00
    116 1.4000E+00 3.7500E+00 0.0000E+00
    117 1.6000E+00 3.6700E+00 0.0000E+00
    118 1.8000E+00 3.5700E+00 0.0000E+00
    119 2.0000E+00 3.4600E+00 0.0000E+00
    120 2.2000E+00 3.3400E+00 0.0000E+00
    121 2.4000E+00 3.2000E+00 0.0000E+00
    122 2.6000E+00 3.0400E+00 0.0000E+00
    123 2.8000E+00 2.8600E+00 0.0000E+00
    124 3.0000E+00 2.6500E+00 0.0000E+00
    125 3.2000E+00 2.4000E+00 0.0000E+00
    126 3.4000E+00 2.1100E+00 0.0000E+00
    127 3.6000E+00 1.7400E+00 0.0000E+00

Lines
    105 106
    106 107
    107 108
    108 109
    109 110
    110 111
    111 112
    112 113
    113 114
    114 115
    115 116
    116 117
    117 118
    118 119
    119 120
    120 121
    121 122
    122 123
    123 124
```

```
Setups
  Measurement 1
   110-111.txt /ASCII
   0
  119  0.00000E+00  0.00000E+00  1.00000E+00  0.00000E+00  acceleration m/s^2 Channel 1 Ref transducer  1
  119  1.00000E+00  1.00000E+00  0.00000E+00  0.00000E+00  acceleration m/s^2 Channel 2 Ref transducer  2
  119  1.00000E+00  0.00000E+00  0.00000E+00  0.00000E+00  acceleration m/s^2 Channel 3 Ref transducer  3
  110  0.00000E+00  0.00000E+00  1.00000E+00  0.00000E+00  acceleration m/s^2 Channel 4 Free transducer 1
  110  0.00000E+00  1.00000E+00  0.00000E+00  0.00000E+00  acceleration m/s^2 Channel 5 Free transducer 2
  110  1.00000E+00  0.00000E+00  0.00000E+00  0.00000E+00  acceleration m/s^2 Channel 6 Free transducer 3
  111  0.00000E+00  0.00000E+00  1.00000E+00  0.00000E+00  acceleration m/s^2 Channel 7 Free transducer 4
  111  0.00000E+00  1.00000E+00  0.00000E+00  0.00000E+00  acceleration m/s^2 Channel 8 Free transducer 5
  Measurement 2
   112-113.txt /ASCII
   0
  119  0.00000E+00  0.00000E+00  1.00000E+00  0.00000E+00  acceleration m/s^2 Channel 1 Ref transducer  1
  119  1.00000E+00  1.00000E+00  0.00000E+00  0.00000E+00  acceleration m/s^2 Channel 2 Ref transducer  2
  119  1.00000E+00  0.00000E+00  0.00000E+00  0.00000E+00  acceleration m/s^2 Channel 3 Ref transducer  3
  112  0.00000E+00  0.00000E+00  1.00000E+00  0.00000E+00  acceleration m/s^2 Channel 4 Free transducer 1
  112  0.00000E+00  1.00000E+00  0.00000E+00  0.00000E+00  acceleration m/s^2 Channel 5 Free transducer 2
  112  1.00000E+00  0.00000E+00  0.00000E+00  0.00000E+00  acceleration m/s^2 Channel 6 Free transducer 3
  113  0.00000E+00  0.00000E+00  1.00000E+00  0.00000E+00  acceleration m/s^2 Channel 7 Free transducer 4
  113  0.00000E+00  1.00000E+00  0.00000E+00  0.00000E+00  acceleration m/s^2 Channel 8 Free transducer 5
  Measurement 3
   114-115.txt /ASCII
   0
  119  0.00000E+00  0.00000E+00  1.00000E+00  0.00000E+00  acceleration m/s^2 Channel 1 Ref transducer  1
  119  1.00000E+00  1.00000E+00  0.00000E+00  0.00000E+00  acceleration m/s^2 Channel 2 Ref transducer  2
  119  1.00000E+00  0.00000E+00  0.00000E+00  0.00000E+00  acceleration m/s^2 Channel 3 Ref transducer  3
  114  0.00000E+00  0.00000E+00  1.00000E+00  0.00000E+00  acceleration m/s^2 Channel 4 Free transducer 1
  114  0.00000E+00  1.00000E+00  0.00000E+00  0.00000E+00  acceleration m/s^2 Channel 5 Free transducer 2
  114  1.00000E+00  0.00000E+00  0.00000E+00  0.00000E+00  acceleration m/s^2 Channel 6 Free transducer 3
  115  0.00000E+00  0.00000E+00  1.00000E+00  0.00000E+00  acceleration m/s^2 Channel 7 Free transducer 4
  115  0.00000E+00  1.00000E+00  0.00000E+00  0.00000E+00  acceleration m/s^2 Channel 8 Free transducer 5
  Measurement 4
   116-117.txt /ASCII
   0
  119  0.00000E+00  0.00000E+00  1.00000E+00  0.00000E+00  acceleration m/s^2 Channel 1 Ref transducer  1
  119  1.00000E+00  1.00000E+00  0.00000E+00  0.00000E+00  acceleration m/s^2 Channel 2 Ref transducer  2
  119  1.00000E+00  0.00000E+00  0.00000E+00  0.00000E+00  acceleration m/s^2 Channel 3 Ref transducer  3
  116  0.00000E+00  0.00000E+00  1.00000E+00  0.00000E+00  acceleration m/s^2 Channel 4 Free transducer 1
  116  0.00000E+00  1.00000E+00  0.00000E+00  0.00000E+00  acceleration m/s^2 Channel 5 Free transducer 2
  116  1.00000E+00  0.00000E+00  0.00000E+00  0.00000E+00  acceleration m/s^2 Channel 6 Free transducer 3
  117  0.00000E+00  0.00000E+00  1.00000E+00  0.00000E+00  acceleration m/s^2 Channel 7 Free transducer 4
  117  0.00000E+00  1.00000E+00  0.00000E+00  0.00000E+00  acceleration m/s^2 Channel 8 Free transducer 5
  Measurement 5
   118-119.txt /ASCII
   0
  119  0.00000E+00  0.00000E+00  1.00000E+00  0.00000E+00  acceleration m/s^2 Channel 1 Ref transducer  1
  119  1.00000E+00  1.00000E+00  0.00000E+00  0.00000E+00  acceleration m/s^2 Channel 2 Ref transducer  2
  119  1.00000E+00  0.00000E+00  0.00000E+00  0.00000E+00  acceleration m/s^2 Channel 3 Ref transducer  3
  118  0.00000E+00  0.00000E+00  1.00000E+00  0.00000E+00  acceleration m/s^2 Channel 4 Free transducer 1
  118  0.00000E+00  1.00000E+00  0.00000E+00  0.00000E+00  acceleration m/s^2 Channel 5 Free transducer 2
```